# A Grid-Level Alkali Liquid Metal Battery Recycling Process: Design, Implementation, and Characterization



By

Dale Arlington Thomas III
B.S. Marine Systems Engineering (2013)
Maine Maritime Academy

Submitted to the Department of Mechanical Engineering
in partial fulfillment of the requirements for the degree of
Masters of Engineering in Manufacturing

at the

MASSACHUSETTS INSTITUTE OF TECHNOLOGY
September 2014



Signature redacted

Author .....
Dale Arlington Thomas III
Department of Mechanical Engineering
August 7, 2014

Signature redacted

Certified by .....
Timothy G. Gutowski
Department of Mechanical Engineering
Thesis Supervisor

Signature redacted

Accepted by .....
David E. Hardt
Ralph E. & Eloise F. Cross Professor of Mechanical Engineering Chairman,
Department Committee on Graduate Students

This page intentionally left blank.

# A Grid-Level Alkali Liquid Metal Battery Recycling Process: Design, Implementation, and Characterization

By

Dale Arlington Thomas III
B.S. Marine Systems Engineering (2013)
Maine Maritime Academy

Submitted to the Department of Mechanical Engineering on August 7, 2014
in partial fulfillment of the requirements for the degree of
Masters of Engineering in Manufacturing

Abstract:

The application of liquid metal batteries for large scale grid-level energy storage is being enabled through the development of research conducted at the Massachusetts Institute of Technology (MIT) in 2006. A recycling process to facilitate the end-of-life cycle for alkali or alkaline earth liquid metal batteries was designed, implemented, and characterized through a collaboration between MIT and a battery company. The process developed utilizes recycling methodologies developed and successfully implemented for the recycling of lead-acid and lithium ion batteries. The two methodologies selected for implementation were physical separation and hydrometallurgical material separation. The combination of these two methods results in the liquid metal battery process being carried out at near room temperature and atmospheric pressure. The characterization conducted demonstrated that the developed recycling process is feasible and scalable for future development.

Thesis Supervisor: Dr. Timothy G. Gutowski
Title: Professor of Mechanical Engineering

This page intentionally left blank.

## Acknowledgements:

I would like to first thank our advisor, Prof. Timothy Gutowski, for his latitude in the development of the recycling process which allowed for the full application of the team's knowledge and academic knowledge. Prof. Gutowski was always available to meet, and he provided valuable feedback about our progress and ideas and insured a fundamental understanding of the implemented process.

In addition, I would like to express my appreciation for all the great work my team member, Martin Christopher Feldmann, did during the course of the project. Martin is a great friend, resource for technical design critics, and a very logical and motivated person. Working with Martin was nothing short of the best team experience, I have had during my academic career.

Next, I would like to thank all the people we worked with at Ambri. I appreciate David Bardwell's support of this recycling project and allowing the publication of our work during the collaboration. I would especially like to thank, Shazad Butt and Isha Gujarati, whom we worked closely on all aspects of the process with. Isha Gujaratti was an amazing resource who was always very responsive.

Furthermore, I would like to thank Prof. David Hardt who during the entire length of the MEngM program was always available to meet where he provided encouragement and guidance. Last but not least, I would like to thank Dr. Jose Pacheco who provided the coordination of the MEngM program.

This page intentionally left blank.

# Table of Contents

## List of Figures

## List of Tables

# 1. Introduction

Grid-level energy storage (GLES) is vital for enabling the widespread use of renewable energy, such as tidal, wind, and solar. Due to the cyclic energy patterns of nature, the world's current energy grid has struggled to install large-scale renewable energy projects. The ability to store renewable energy at a grid level will enable the cyclic effect of green energy to be dampened out and easily accepted by the current grid structure [1].

Grid-level energy storage systems are either mechanical or electrochemical installations capable of storing large amounts of energy. They are charged during off-peak or high production hours and discharged during high demand hours. The main requirements for the development of GLES are high energy capacity, long operation life, and low amortized cost [2]. Ambri, formerly Liquid Metal Battery Corporation, is developing a unique liquid metal battery technology that is focused on developing grid level electrical storage solutions.

The electrical grid is the largest and most critical supply chain in the world, affecting billions of people each second. Like any critical supply chain, it is built to withstand peak demand, which requires excess generation capacity that comes at a high cost. Also, the supply chain requires local production, or large transmission losses are experienced. In 2005, the United States (US) electrical grid had a 6.1% net generation (239 million MWh) loss due to transmission and distribution losses [3]. ABB, under contract by the Department of Energy, pinpointed the inefficiency of the grid to several areas: lack of smart distribution systems, non-local distribution/micro grids, and lack of grid level energy storage. The ability to store energy allows the electrical grid to generate energy during off-peak hours and deposit it during times of peak demand, allowing for lower capital expenses in power generation and decreasing transmission losses of off-peak excess power. If electrical power is not consumed moments after it is produced, the energy is consumed within the electrical distribution and transmission systems.

The ability to store excess energy contained in the electrical grid using batteries allows it to be released when required. However, these battery technologies will consume a large amount of the world's strategic resources. Additionally, if the battery components are not recyclable, then those resources must be disposed of as hazardous material, resulting in the components being landfilled or incinerated. Both of those options are not environmentally sustainable for grid level batteries.

Ambri, in order to have an environmentally sustainable grid level technology, has invested in the development of an end-of-life cycle recycling process. The process was developed in collaboration with the Massachusetts Institute of Technology.

## 1.1 Background and Research Motivation

### 1.1.1 Current Grid Level Storage Systems

The current grid level energy storage in the US has a cumulative operation capacity of 24.6 GW (2.3% of current energy production) [2] and the world's operation capacity is 130 GW (6% of current world energy production) [4]. The current predominate storage technology is pumped hydro, which represents 95% of the capacity. The reason for its dominance can be attributed to its high reliability, large storage capacity, and long operational life; however, the technology has several large drawbacks, such as environmental permitting, long term operation costs, and large capital expenditures.

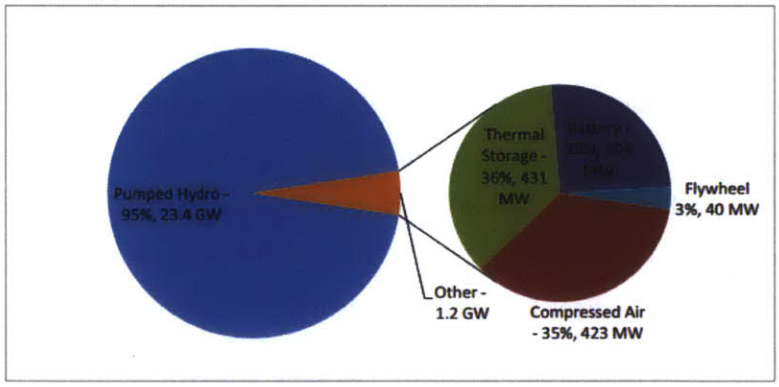


*Figure 1 - Rated Power of US Grid Storage Projects (includes announced projects) [2]*

To meet the renewable profile standards (accepted by 30 out of 50 states), a 20% increase in renewable energy on the grid is expected by 2020 [2]. This is anticipated to result in an additional 18.6 GW of intra-hour balancing to maintain grid stability. The intra-hour technologies that can be developed are additional energy storage systems (ESS), demand response, and fast gas turbines. These energy systems are required in order to dampen the cyclical effects that result from harvesting of energy from nature. Pike Research has estimated that an additional 14 GW (10.7% increase) will be developed worldwide by 2022 [5].

Due to anticipated increase in demand, the electrical storage capacity market is fragmented, with the current leader being pumped hydro due to its reliability, robustness, and industry acceptance. Several startups and research institutions have demonstrated grid level technologies that will compete with currently deployed technologies on reliability, longevity, permitting, and cost.

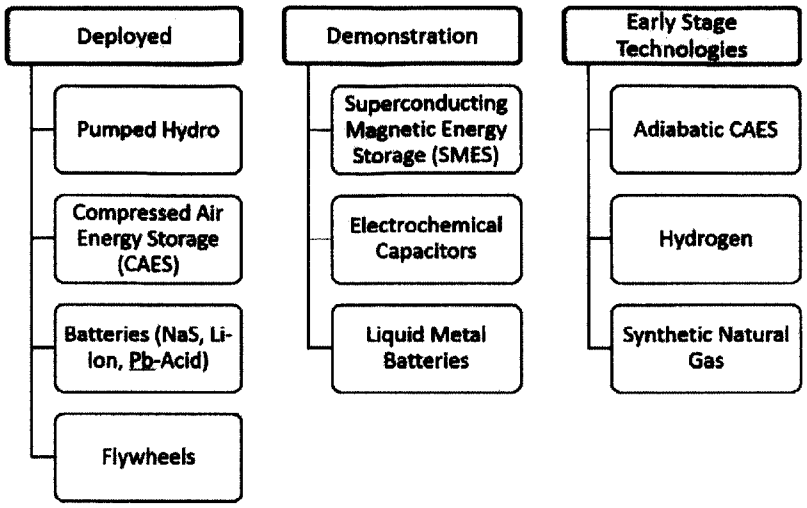


*Figure 2 – Maturity of Electricity Storage Technologies [4]*

The currently deployed battery systems are Pb-acid, NaS, and Li-ion. Li-ion battery characteristics are best suited for frequency regulation and uninterruptible power supplies [4]. NaS batteries have longer discharge cycles and appear to have better discharge characteristics than Li-ion for load leveling and price arbitrage operations. Lead-acid batteries have a mature battery chemistry, which has not taken hold in grid level ESS due to their low energy density and short cycle time. Despite the short comings of the current technologies, the deployment of 1MW+ grid level battery storage systems have not realized widespread deployment. The number of deployments for each type of battery is in

Table 1.

*Table 1 - Installations of Batteries [4]*

| Battery Type | 1 MW + Deployments |
|---|---|
| Lithium Ion | 15 |
| Sodium Sulfur | 11 |
| Lead Acid | 9 |

Through the analysis of the cost of power and the cost of energy, it can be shown which types of batteries and energy storage systems are the most attractive to further development and deployment. In

Figure 3, it is clear that Li-ion batteries are the most expensive option as well as quickest to discharge. Lead-acid, Na-S, and flow batteries all have around the same power cost and energy cost. The outlier is the liquid metal battery, which is shown to be the most economical option for grid level storage when compared to the current battery technologies and other energy storage systems. From an economic perspective, liquid metal batteries appear to be the grid level battery technology of the future.

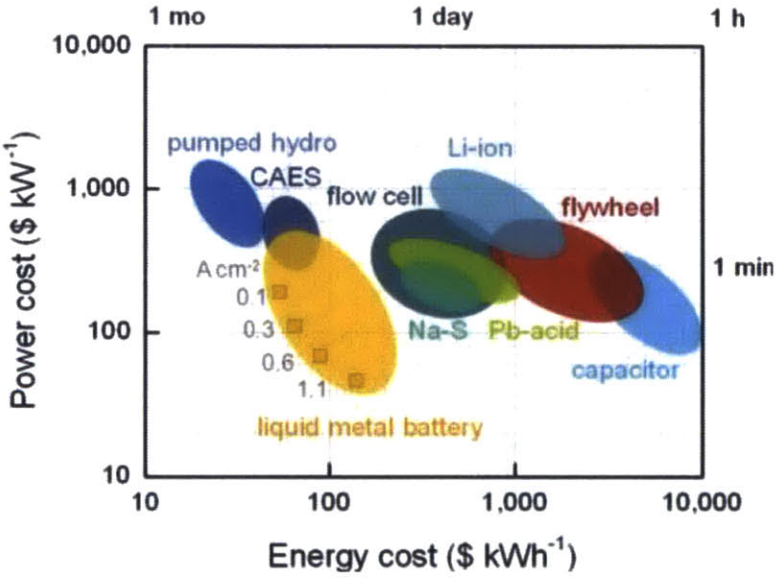


*Figure 3 - Cost of Energy versus Power Plot [6]*

### 1.1.2 Market for Grid Level Storage Systems

The global high-technology market for industrial batteries in 2013 was $16.32 billion market with only 2.7% coming from grid level storage systems [2]. In this market, US battery companies captured $6 billion of the total global revenue. The top four main industries that consume industrial battery technology are telecom and communication (31.5%), industrial equipment (20.1%), UPS/backup application (17.9%), and aerospace and defense (12.7%), which combined represented 82.2% of the 2014 market. The anticipated growth rate of the industrial battery market for the next three years is expected to between 8% and 9%.

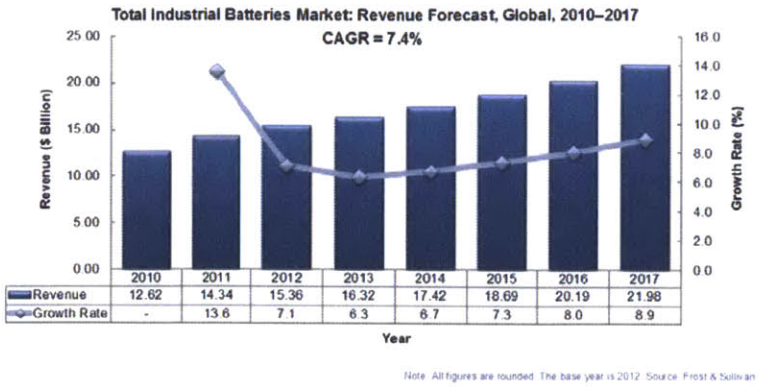


*Figure 4 - The Global Industrial Batteries Market [2]*

## 1.2 Battery End of Life Disposal

Current battery technologies have a finite cycle life, which results in all batteries becoming unserviceable as energy storage devices at the end of their lives. The end-of-life disposal of batteries presents a threat to the environment because of the hazardous materials used to construct them. There are several means of disposal which include:

- Landfill: the disposal of primary batteries in sanitary landfills
- Stabilization: the disposal of batteries which have been treated to prevent the leaching of metals into the landfill
- Incineration: the disposal of batteries through combusting them at a municipal waste combustion facility, which can result in mercury, cadmium, lead, and dioxins emissions
- Recycling: the disposal of batteries through a process which recovers part or all of the batteries components for reuse

Recycling is the only sustainable and environmentally friendly process for batteries due to their precious and strategic metal components as all other end-of-life methods do not reuse those componets.

## 1.3 Liquid Metal Batteries

The development of the thermal battery happened during World War II when the German scientist Dr. Ing Georg Otto Erb developed the first practical cell. The liquid metal battery is comprised of two liquid metal electrodes which are separated by a molten salt electrolyte. Further research was

completed during the Cold War because of the battle for technological supremacy, especially in the areas of thermally and electrically rechargeable all-liquid energy storage cells. The key breakthrough came in 2009 when Donald Sadoway and David Bradwell demonstrated the Mg-salt-Sb battery technology. These technological advancements have been driven by the rapid growth of renewable energy, which has in turn driven the demand for low-cost, long-life, large-scale energy storage systems [6].

The unique battery technology that Ambri is developing came from the idea of running an aluminum electrolysis cell in reverse to produce a battery. The Hoopes aluminum electrolysis process is very energy intensive and uses high temperatures and electrical energy to turn a metal oxide into aluminum. This is the same electrochemical process as charging a battery.

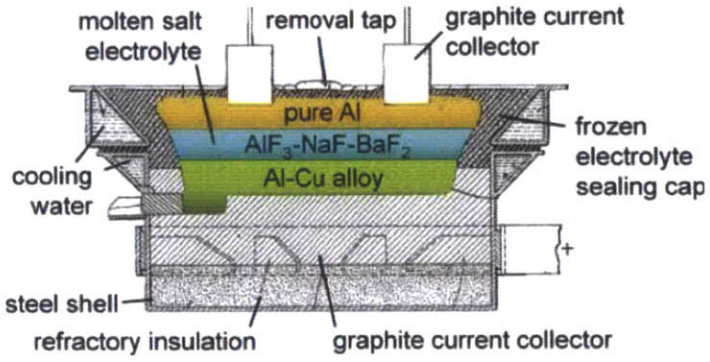


*Figure 5 - Diagram of Hoopes Cell Describing Three-Liquid-Layer Electrolytic Cell [6]*

The liquid metal battery technology has also taken inspiration from molten electrolysis for extracting oxygen from lunar regolith and lithium polymer batteries.

### 1.3.1 Ambri's Design and Chemistry

The main components of liquid metal batteries are the metal electrodes and molten salt electrolyte, [6]. The layers of the liquid metal battery are self-segregating because of the different material densities. When a liquid metal battery is operational, the battery is typically operating at temperatures greater than 200 degrees °C. That elevated temperature results in high liquidity of the metals, which aids in the kinetic and transport properties being superior to current technologies. Liquid metal batteries have the potential of being low cost – less than \$100 $kWh^{-1}$ – because the electrode materials are earth-abundant [5].

A major advantage of liquid metal battery technology is an almost zero (0.0002%) cycle-to-cycle capacity fade, resulting in batteries that can work efficiently for years [6]. Ambri has demonstrated this capability for cells cycled over 1,000 times. A graph of the discharge capacity versus cycles is produced below. Lead-acid batteries typically see a capacity fade around 0.1% per cycle.

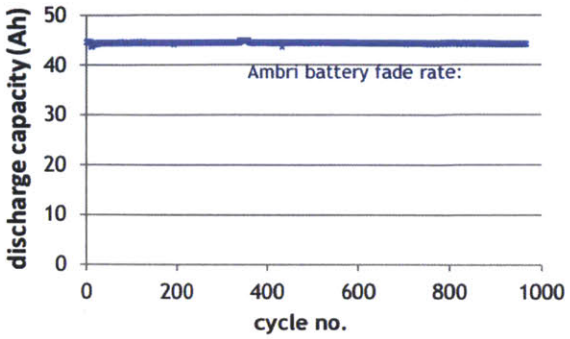


*Figure 6 - Ambri Battery Fade Rate [6]*

David Bradwell first demonstrated the concept of a liquid metal battery with Mg||Sb in 2007 and published his success in 2009 [6]. The work was carried out at MIT under Donald Sadoway from 2005-2010 and focused on exploring cell chemistries which could meet the performance and cost targets required for commercialization. Ambri has developed its proprietary chemistry based off of this MIT research. The chemistry is no longer Mg||Sb; however, the commercial cell chemistry is comprised of a reactive metal alkali or alkaline earth metal as the anode, and a higher density bottom metal as the cathode.

Liquid metal battery chemistries vary in operational temperature, energy density, electric potential, and operational life; however, the operational principles are very similar. This allows for the published Mg||Sb battery to provide the required insight for this thesis. A Mg||Sb cell operates at 700°C. The battery can maintain its molten state once operational through the thermal losses of charging and discharging given adequate insulation. The electrochemistry of the battery uses densities and the kinetics of the atoms to store energy. The charging cycle is when electrons are added to the battery, resulting in the magnesium being electrochemically extracted from the cathode of the Mg||Sb electrode and deposited as pure Mg in the anode,

Figure 7. This is called dealloying. During the discharge cycle, the magnesium is oxidized causing the release of two electrons. This change in charge causes the migration of the magnesium across the salt electrolyte to form a Mg||Sb alloy.

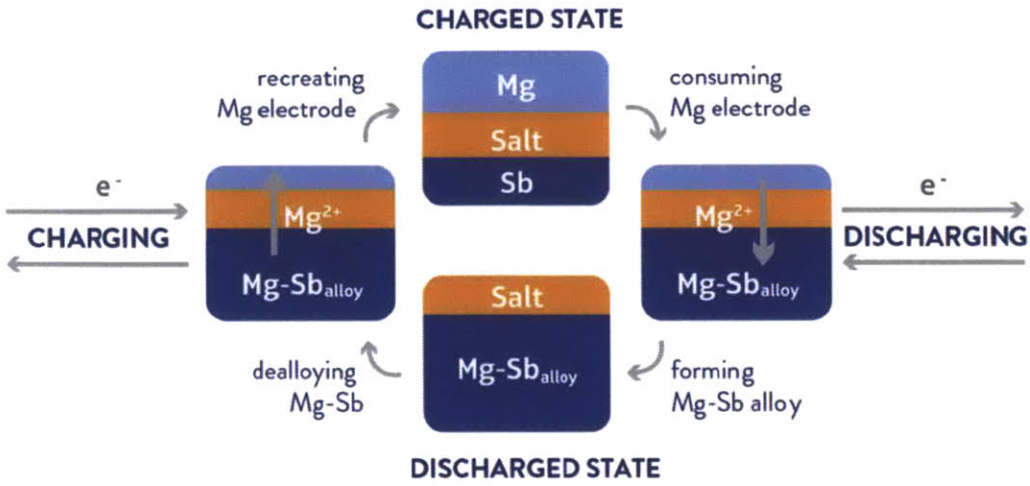


*Figure 7 - Mg||Sb Liquid Metal Battery Reaction [1]*

The Mg||Sb battery technology and Ambri's current battery chemistry are both stored inside a stainless steel canister in which the main parts are the negative current collector or stem, seal, liner, and positive current collector or canister. The stem or current collector is made from 304 stainless steel. The seal is a ceramic capable of withstanding the difference in thermal expansions between the metals. Due to Ambri's intellectual proprietary, the battery schematics and drawings have been generalized and should be considered graphical representations of the battery in order to provide the necessary information required to understand the design challenges and decisions. The liquid metal battery representations can be found in Figure 8.

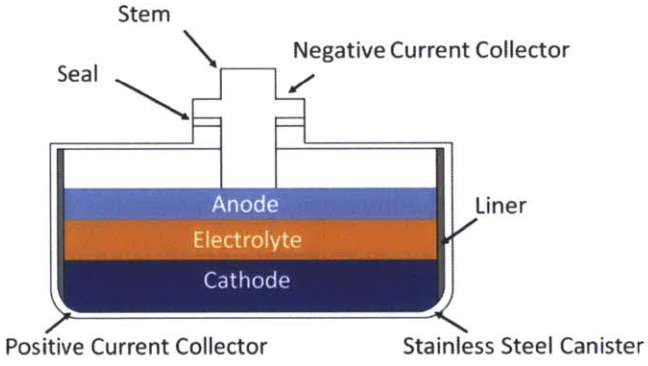

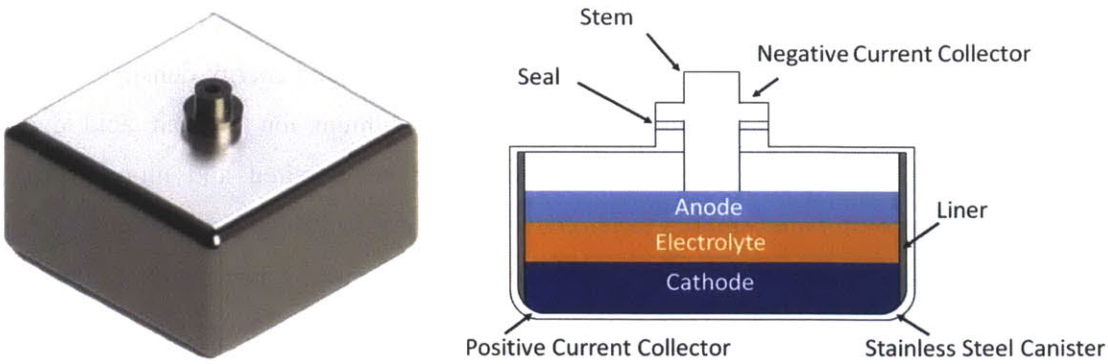


*Figure 8 - Liquid Metal Battery Diagram*

The cell design, which is currently being commercialized by Ambri, is 4 inches long, 4 inches wide and 2 inches high. The ceramic seal plays a significant role in maintaining the long lifetime of Ambri's liquid metal batteries because it provides a hermetic seal that prevents secondary reactions and corrosion caused by oxygen, nitrogen, and moisture in the cell. Another role of the seal is to provide electrical insulation between the anode and cathode while joining materials of different thermal coefficient of expansion. Ambri has adopted adhesive seals which joins the different materials together using a metal joining material between the steel and ceramic.

## 1.4 Research Motivation

To implement grid level storage technologies, the world is investing valuable time, resources, and capital. In light of this fact, both useful service life and end-of-life are important to consider due to the substantial strategic metal resources batteries utilize (e.g., lead, lithium, nickel, aluminum, and copper). These resources have a substantial environmental impact when mined and refined, but if not recycled at the end-of-life the replacement materials have an equal or worse environmental impact.

Ambri's current technology utilizes several metals, ceramics, and salts. The combinations of metals, salts, and ceramics will consume approximately 700 kg of strategic earth metals for every 20 KWh of installed capacity [6]. This means that the full size deployment of 2 MWh storage capacity will utilize approximately 70 tons of metals, ceramics, and salts. Since the materials used in the construction of Ambri's batteries are in large quantities, separable, and valuable, the technology is positioned to be one of the only economical recyclable battery technologies.

Ambri's technology was founded on using common metals and substances to lower the cost of grid level storage. This resulted in using materials that optimize cost and energy density. The resulting battery technology requires more material compared to lithium ion or lead acid due to the electrochemical composition; however, the batteries are better-suited and more economically feasible for grid level storage. Ambri's technology is suited for recycling due to its large amounts of relatively separated metals. Nevertheless, the innovative chemical composition cannot utilize a developed recycling process due to its unique metal and salt composition. The result is that the batteries can only be disposed of through incineration. Incineration is costly and increases the batteries environmental impact. Also, the incineration process does not fit the company's policy for being environmentally conscious. Furthermore, Ambri needs to have a recycling process in order to have a destructive quality control process at their factory for legal and economic reasons.

### 1.4.1 Problem Statement

The problem statement defined for the collaboration between Ambri and MIT was the development of a recycling process for the current battery design and chemistry. The timeline specified for the development was between January and August 2014, as required for Ambri's production throughput to increase.

The objective developed during the industrial process design, implementation, and characterization of a grid level liquid metal battery recycling process was to meet or exceed current environmental regulations, optimize recyclable outputs, and minimize unrecoverable waste streams. In order for the process to be serviceable as Ambri's recycling strategy, the process developed needs to meet the company's rigorous safety policies, be economically sustainable, and have the flexibility to recycle Ambri's developing battery technology for a period of no less than one year.

The objective of the designs evolved to include plans for process automation, full process containments, quality control measurements, and upgradeability to future process advancements. This thesis outlines the approach to design, implementation, and characterization of the liquid metal battery recycling process developed for Ambri's specific battery chemistry.

### 1.4.2 Methods

The design, implementation, and characterization of the novel recycling process for liquid metal batteries used a three phase approach, as shown in

Figure 9. The phases were broken down into understanding the current disposal processes, development of a safe, stable, and economical recycling process, and then development of a scalable recycling process.

The first phase was the understanding of the current process employed by Ambri to do their postmortem analysis of the cells. This consisted of first hand observations through involvement in the process, and then interviewing the operators and designers. Careful documentation of the observations was made in the form of photographs and notes.

The next phase was to develop the recycling process where the design circle process was used to minimize the environmental impact, cost of operation, cycle time, and maximize process stability and safety. The design circle was an iterative process completed for each of the process steps. After a process was designed, the team constructively criticized the design until the best possible design was agreed upon.

The third phase was to develop a scalable process which was safe, stable, environmentally feasible, and economical. The scalability of the process is the focus of future improvements. Due to time constraints, this thesis' main focus is on the development of a stable liquid metal battery recycling process.

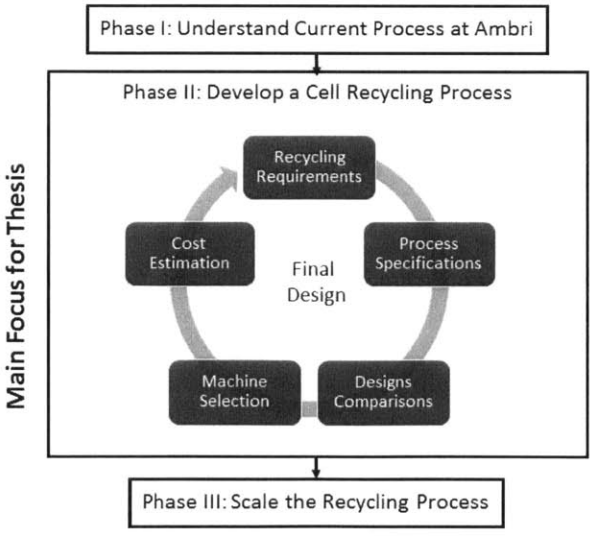


*Figure 9 – Design Circle Approach*

# 2. Current Battery Technology Literature Review

The basic principles of all battery technologies are based on the formation of an electrochemical device that converts stored chemical energy into electrical energy. The most basic batteries utilize an anode, cathode, electrolyte, external cans, and a separator to create the electrochemical cell [7]. The differences in batteries come from the section of electrodes and electrolytes. Because grid level battery technologies are a new scale of electrochemical cells that, have not yet been iterated through years of use, the study of, widely used, mass-produced technologies will speed development by lowering the learning curve. Lead-acid and lithium ion battery recycling technologies are examined here due to the similar recycling needs of the liquid metal battery technology developed by Ambri. Both lead-acid and lithium ion batteries have significant hazards which have been overcome to result in safe, efficient, and economically feasible recycling processes.

## 2.1 Recycling

There are three main types of recycling: physical separation, hydrometallurgy, and pyrometallurgical separation [8]. The process of physical separation uses a pretreatment method, which enables material classification as metallic or non-metallic. The other two processes are either used together or separately to achieve efficient separation and purification of battery components.

### 2.1.1 Physical Separation

Physical separation is the use of mechanical processes, thermal treatment, and mechanochemical processes. These processes utilize machinery that crush, screen, magnetically separate, and gravity separate battery components. The components are typically divided into metallic and non-metallic components. The non-metallic organic components are separated from the inorganic components with the organic components either being disposed of by landfilling or recycling through mechanical, biological, or thermo-chemical means.

### 2.1.2 Pyrometallurgical Separation

Pyrometallurgical separation is the use of thermal treatments to cause chemical and physical changes in the elements, allowing for their separation [8]. This treatment enables recovery of metals

and minerals that, can then be sold as pure metals or alloys. The process is generally grouped into the following categories:

- Calcining
- Roasting
- Smelting
- Refining

Most pryometallurgical processes need energy input to get the chemical and physical separation; however, the process can be autogenous if the feed material reacts exothermically enough to maintain reaction temperature.

### 2.1.3 Hydrometallurgical Separation

Hydrometallugical separation is the acid or base leaching of metal followed by a metal recovery step, such as: solvent extraction and precipitation or electrolysis [8]. This process separates the organics and inorganics using the different solubility's of elements. This process has been deployed for the separation of lithium batteries, Ni-Cd batteries, and alkaline and zinc batteries.

## 2.2 Lead Acid Batteries

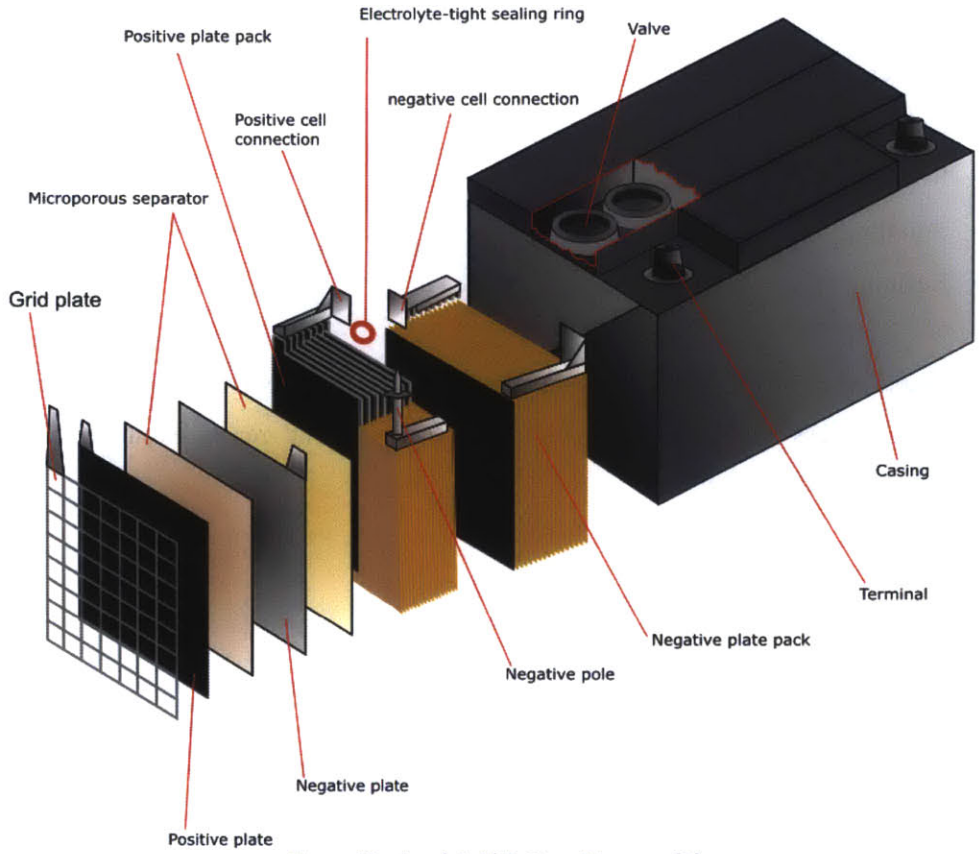


*Figure 10 – Lead-Acid Battery Diagram [9]*

Lead-acid batteries have a mature battery chemistry that was discovered in 1859 by a French physicist, Gaston Plate, and is considered the oldest type of rechargeable battery. The lead-acid battery has a low energy-to-weight ratio and low energy-to-volume ratio but provides a relatively high surge current which results in its power-to-weight ratio being large. Lead-acid batteries are mainly used in the automobile industry and in large battery backups. A graphical representation of the common automobile lead-acid battery if found in Figure 10. Lead-acid batteries account for 40-45% of worldwide battery sales.

### 2.2.1 Design and Chemistry

The lead-acid battery consists of several designs, including: Plate, Faure, and tubular electrodes. The typical automotive battery has the Faure pasted-plate design. In this construction, the rectangular grids of lead plates are alloyed with antimony or calcium to improve mechanical characteristics. The gird holes are filled with a lead paste. The paste increases the surface area that the sulfuric acid can interact with, which results in better battery performance.

The lead-acid batteries' electrode reaction is unusual in that both the positive and negative electrode reactants are the same elements. The anode reaction is where the lead is oxidized by the sulfate ion to form lead sulfate [13].

$$Pb(s) + HSO_4^-(aq) \leftrightarrow PbSO_4(s) + H^+(aq) + 2e^- \qquad (1)$$

The cathode reaction is the reduction of the lead dioxide with sulfuric acid to form lead sulfate and water.

$$PbO_2(s) + HSO_4^-(aq) + 3H^+(aq) + 2e^- \leftrightarrow PbSO_4 + 2H_2O(l) \qquad (2)$$

The net electrochemical reaction is a double sulfate reaction.

$$Pb + PbO_2(s) + 2H_2SO_4 \leftrightarrow 2PbSO_4 + 2H_2O(l) \qquad (3)$$

The reaction mechanism is a dissolution/precipitation where the $Pb^{2+}$ ion dissolves and precipitates on the surface of the electrode; however, the porosity of the cell tends to be maintained through charging and discharging.

While lead-acid batteries are a mature technology, the batteries have a limited cycle life because of several failure modes, which are as follows [13]:

- Shorting
- Sheading of lead oxide
- Loss of surface area, porosity, or chemical conductivity
- Contamination of lead/electrode
- Corrosion of the positive plate current collector

As the result of these failure modes, the batteries need to be recaptured and disposed of because of the hazardous materials that can leach into the environment if not disposed of properly.

### 2.2.2 Recycling

The recovery of lead-acid batteries has been driven by economic and environmental concerns. Governments around the world have enacted policies to establish a collection and recycling network for lead-acid batteries. Because of the material economics and composition of lead-acid batteries, they are readily recycled through pyrometalurgical processes. In the U.S., 96% of lead-acid batteries are recycled back into the material supply chain which makes it the most recycled consumer product [14].

The lead-acid battery recycling process has evolved over the years to become efficient and account for the hazards of lead-acid battery recycling. The general processes for the recycling of lead-acid batteries are very similar to the primary lead production process as seen in Figure 11. The main difference is in the material preparation before reduction because there is no need for sintering [10]. The recycling process starts with the batteries being retired from service due to a failure, maintenance, or a number of other reasons. The battery is then returned to a recycling center which can be a scrap metal yard, or any retailer who sells lead-acid batteries.

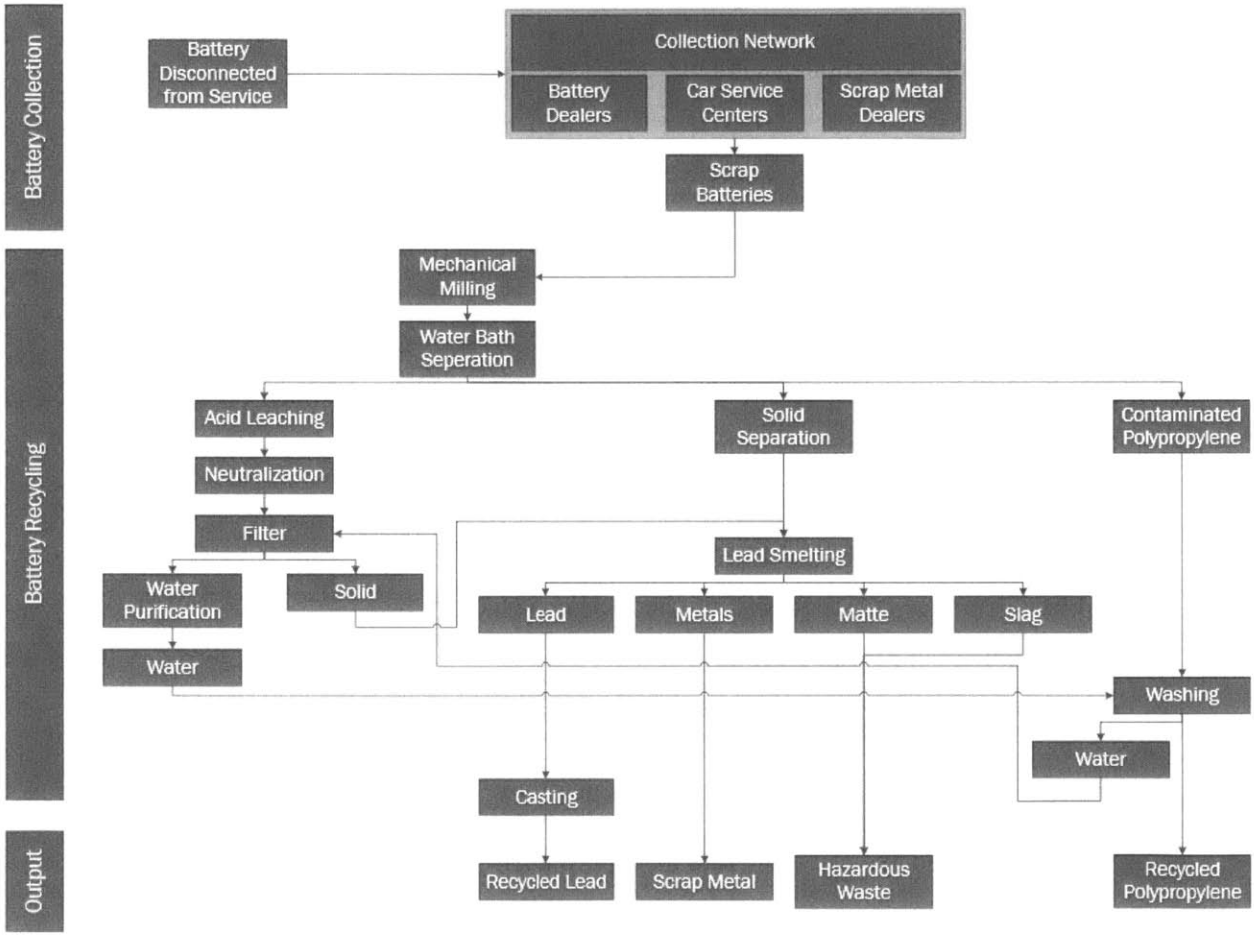


*Figure 11 - Lead Acid Battery Collection, Recycling, and Output Flowchart*

Once the battery is delivered to the battery recycling facility, the individual batteries are dismantled into their component parts. Because the batteries being made of low yield strength materials they can be pulverized and separated. The low yield strength also allows for high throughput. This is usually accomplished by either hammer mills or spreaders [10]. Typically the pieces fall or are taken by conveyor belt to a water bath separator where the acid is carried away by the water and the

solids are separated by density. The lead sinks to the bottom of the separator and the polypropylene is buoyant. At this point, the components are subjected to different recycling processes [15].

The acid solution is typically processed with a carbonate salt to form a neutral solution. The solution, which contains suspended and precipitated particle from the milling and neutralization, are then removed in a filtration step. Those particles are sent to the lead smelter in order to recover as much material as possible. The water is then further purified in order to allow it to be reused and in other section of the process. It is also possible to convert the sulfuric acid into sodium sulfate which can be used in different industries.

The solids that sunk to the bottom of the water bath are then mixed with reducing agents such as coal, iron hydroxide or sodium hydroxide. The reagents are mixed and then are typically smelted in a rotary furnace. The furnace temperature is between 300 and 400 °Celsius in order to melt the lead but not the other metals contained within the material placed in the furnace [10]. Using temperature to separate the material allows for easy separation and reclamation of the other metals. From the furnace, the lead is cast into pure ingots that then enter back into the supply chain

Lead-acid recyclers take precautions to insure operators do not come into contact with the hazardous gasses and materials produced and used during the process steps through personal protective equipment, process, and building design. The typical personal protective equipment worn is respirators, acid resistant clothing, gloves, and safety glasses. Lead-acid recyclers have the process contained in well ventilated buildings with proper air filtration. The design of the processes allows for proper handling of hazardous chemicals and protects the operator from the hazardous output.

Lead-acid battery recycling is done through a number of processes which utilize the basic recycling processes of mechanical separation and pyrometallurgical. Lead-acid battery recycling has the benefit of a well-implemented and regulated collection network. The batteries' chemistry is well suited for recycling due low variability, melting points, yield strength, and large quantities. The implemented supply chain and recycling processes have resulted in efficient re-entry into the market

## 2.3 Lithium Ion Batteries

Lithium battery technology was first demonstrated by J. O. Besenhard at TU Munich in the 1970s. The initial problems of electrolyte decomposition and graphite intercalation have been resolved to a commercial level. Currently, lithium-ion batteries are the main type of battery used in consumer electronics. Lithium ion batteries currently account for 63% of the worldwide sale of portable batteries [16]. The reason for the mass acceptance for lithium ion batteries is their high energy density and flexible design.

### 2.3.1 Design and Chemistry

Lithium batteries have an important difference between the primary and secondary batteries. The primary cells (single use) use metallic lithium as the cathode. The secondary cells (rechargeable) use materials, such as: $LiXMA_2$ for the positive electrode and graphite for the negative electrode. Lithium ion batteries are usually produced in the prismatic geometry, which produces a thinner geometry. Li-ion polymer chemistry uses exclusively prismatic geometry.

The typical lithium ion battery is comprised of a cathode, an anode, organic electrolyte, and a separator. The Li-ion battery's layers are laminated together with the cathode and anode on either side of the separator. The separator contains the electrolyte. The cathode is usually a thin aluminum foil with the electrode material, and the anode is a thin copper foil with the electrode material, Figure 12.

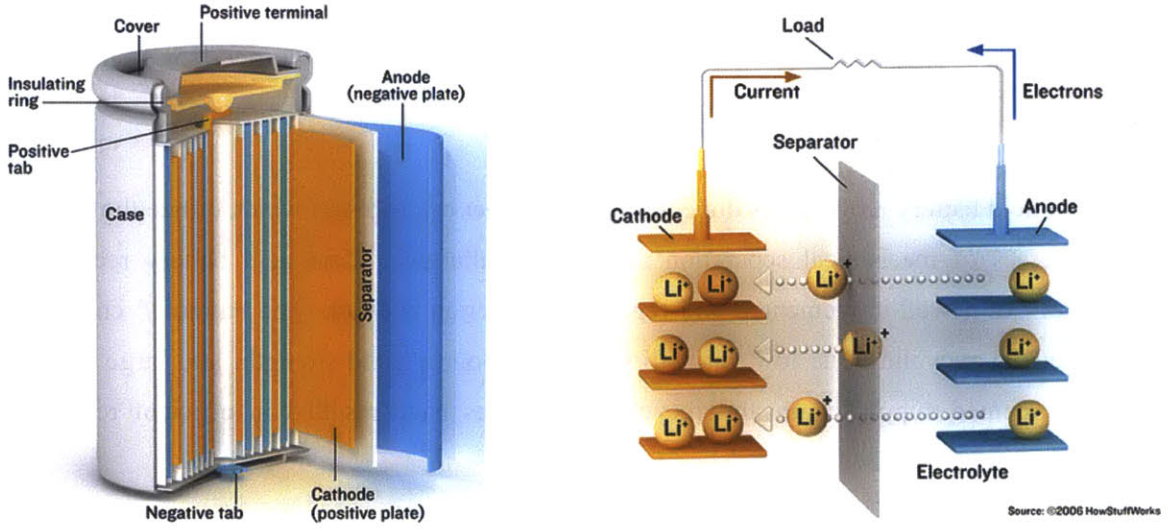


*Figure 12 - Lithium Ion Battery Diagram [17]*

Lithium cobalt oxide is typically used as the cathodic material. Carbon is typically selected as the anodic material.

The reaction at the cathode is the intercalation of the lithium into the graphite anode. The chemical reaction is expressed below [11]:

$$xLi^+ + xe^- + 6C \leftrightarrow x\,Li^+ + x\,e^- \qquad (4)$$

The reaction at the anode is the production of Li from $LiCoO_2$.

$$LiCoO_2 \leftrightarrow Li_{1-n}CoO_2 + xLi^+ + e^- \qquad (5)$$

where the charging direction is the forward direction and the discharging direction is reverse [12].

Lithium ion batteries under certain conditions (short circuit, excessive heating, etc.) can be dangerous due to the production of hydrogen gas when exposed to water. Lithium ion battery technology has advanced quickly over the last 4 decades; however, the batteries still have short cycle life, which is the result of the natural interface between the electrode and the electrolyte. The result of the capacity fade from this interaction is that most industrial batteries are specified to have better than 80% capacity at 500 cycles. The capacity fade of the lithium ion batteries results in the disposal of nearly all batteries produced within two years. Recapturing and disposing of battery waste is important to protect the environment from the leaching of metals and electrolytes into the environment.

### 2.3.2 Recycling

The recycling of current lithium ion battery technologies is dependent on if it is a primary or secondary battery. The current portable electronics' market uses secondary batteries, which is resulting in a growing amount of lithium ion battery waste. This waste is not uniform in composition, which has made it hard to develop a robust recycling process. Also lithium is very reactive when exposed to air, which causes an industrial safety hazard.

There are currently several processes that recycle lithium ion batteries. The Toxco process, which is a hydrometallurgical process, processes secondary lithium ion batteries[18]. Recupyl Battery Solutions also has a hydrometallurgical solution, for which the inventors Farouk Tedjar and Jean-Claude Foudraz received the Eurpoean Inventor Award in 2012[19]. The process is fast, efficient, and inexpensive, and is able to recover 98% of valuable metals. Inmetco and Umicore have

developed pyrometallurgical processes that are capable of recycling spent NiCd, NiMH, and Li-ion batteries. Sony also has developed a process that through incineration captures the cobalt from the Li-ion battery cathode material [20].

The general process flow for hydrometallurgical recycling of lithium ion batteries is discussed because of its relevance to the developed recycling process for liquid metal batteries, Figure 4. The other type of lithium ion battery recycling, pyrometallurgical and incineration, were not seen as viable options, the reason for which will be discussed in more detail in Chapter 4, Design Consideration.

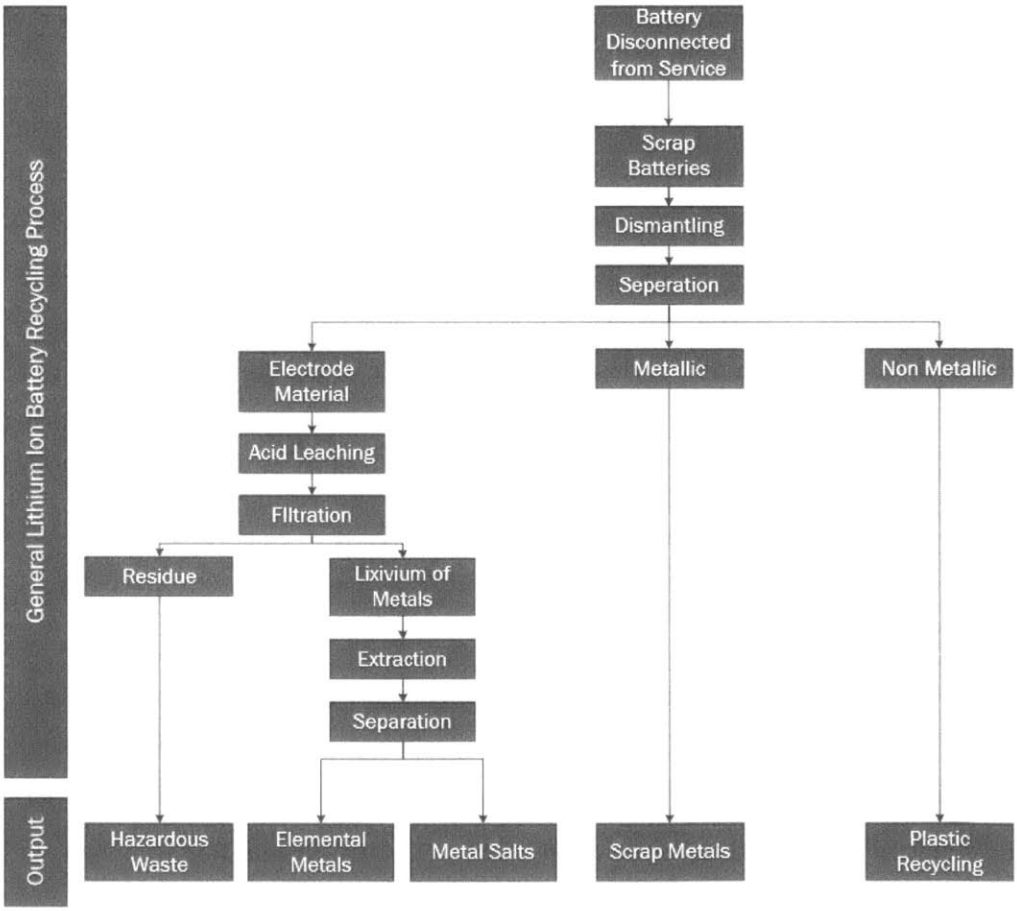


*Figure 13 - General Hydrometallurgical Lithium Ion Battery Recycling [12]*

The first step in the lithium-ion battery recycling process is the disconnection of the battery from its current application due to a failure, preventative maintenance, or other requirement that results in discontinued use of the battery. The batteries then need to be turned into a battery recycling service

for collection. The battery collection services send the batteries to a battery recycler which accepts the scrap batteries as feedstock for their recycling process.

In a hydrometallurgy process, the first step is to dismantle the batteries resulting in higher efficiency separation of component parts [12]. The dismantling can be accomplished in several ways. Typically components are disassembled in an inert atmosphere or cryogenically cooled to inhibit the reaction of lithium with the humidity in the air [12]. Lithium becomes more reactive as temperature rises which is the reason for cooling the lithium during dismantling. The dismantling process is either accomplished through crushing with a mechanical mill or shredding the batteries.

Once the battery is divided into smaller parts, the particles are separated through sieving and magnetic separation. This allows for the separation of iron, aluminum, copper, and plastics. Some processes will repeat the dismantling and separation steps more than once to increase effectiveness of the separation step. Separation also consists of an acid leaching step that causes the lithium and cobalt to dissolve into solution. The acid leaching agents that have been used are 4.0 $molL^{-1}$ HCl, 2.0 $molL^{-1}$ $HNO_3$, and 1.0 $molL^{-1}$ $HNO_3$ solutions at temperatures between 75$^{o}$C and 100 $^{o}$C [12]. The metallic and non-metallic materials are then processed as scrap metal and plastics.

The hydrometallurgical separation starts with the dissolved metal solution going through a filtration step to insure that fine particles from dismantling do not interfere with the extraction of the metals from the solution. Particles of concern are the undissolved PVDF and PVC from the electrolyte and binder [12]. These particles, if not dissolved, will leach chlorine and fluorine into the solution and can cause problems with the extraction of the metals. The metals can now be extracted from the lixivium of metals through chemical precipitation by changing the pH. Also, extraction using organic solvents can be utilized, followed by separation of the metals through electrolysis or chemical precipitation. Depending on the chemical processing steps used, either a metal or metal salt will be recovered from the solution.

Over the past several years, the drop in price of lithium ion battery production costs has resulted in an increased demand for the lightweight, energy dense battery technology; however, the lack of standardized chemistry ($LiCO_2O_4$, $LiMn_2O_4$, $LiFePO_4$) [21], [22] within lithium ion batteries has inhibited investment in recycling plants/processes due to unknown profitability. Lithium ion batteries within consumer electronics have not been widely recycled and do not have a well-developed recycling network, mainly due to lack of legal requirements and the recycling capacity of

current technology. The European Union is stimulating innovation in the area of battery recycling with the directive 2006/66/EC which requires "battery and electric vehicle producers to conceive and establish effective collection and recycling solutions before market penetration." [23]

## 3. Research and Development Disposal Process

Waste from an industrial process or product is considered hazardous if it exhibits one or more of the following characteristics: ignitability, corrosivity, reactivity, and toxicity [24]. Due to the reactive metal component, salts, and toxic metals, expended liquid metal batteries are classified as hazardous waste resulting in the only EPA approved disposal process being incineration. The ability to separate the batteries into principal components results in the ability to recycle the principal components for reuse in other industrial processes. The advances in Ambri's liquid metal battery technology are making the use of grid level liquid metal battery farms feasible. Due to this success, Ambri has the potential to produce large quantities of batteries that can only be disposed of through incineration. The best way to deal with the creation of hazardous waste, is to develop technologies that recycle the batteries principal components.

The disposal path of Ambri's liquid metal battery waste has three different steps: processing, transportation, and incineration. In an attempt to reduce the amount of hazardous waste disposed of, Ambri separates the active, corrosive, and toxic materials from the research and development cells. Then it has a hazardous waste transporter remove the waste from the facility and transport it to the incinerator. In order to develop a process that improves the recycling capabilities of the Ambri process, the current process disposal process map was made, Figure 14.

It is not sustainable to economically dispose of the batteries using incineration because it cost $125 for each cell.

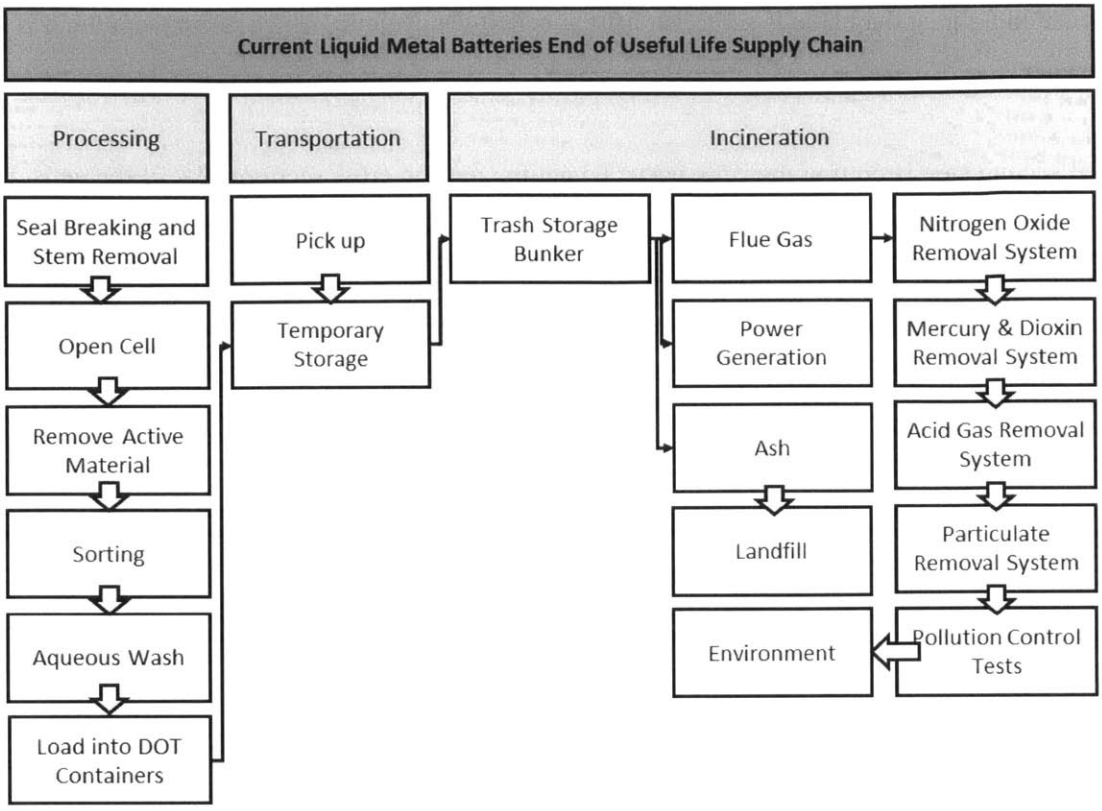


*Figure 14 - Current Liquid Metal Batteries End of Useful Life Supply Chain [25]*

## 3.1 Processing

Ambri currently needs to perform a post mortem analysis on all of its cells in order to understand the chemistry and modes of cell failure. The analysis that is conducted allows Ambri to process its waste in a manner that allows for the separation of the hazardous waste and stainless steel. This allows them to dispose of the contaminated stainless steel as a toxic metal waste instead of a hazardous waste stream. The reactive material is separated and placed in DOT approved 5 gallon buckets, which each contain 30 pounds of reactive, corrosive, and toxic material.

The first step in the processing and analysis of the cells starts with using a Clausing Industrial bandsaw model KC812W with a 6-10 LENOX blade to cut the seal. The blade is run at 65 m/s with a feed rate of 5 ipm. Oil coolant is used, reducing the amount of particulates introduced into the air, coating the active material to prevent its reaction with the environment, and providing a longer blade life. reducing the amount of particulates introduced into the air, coats the active material which prevents its reaction with the environment, and provides a longer blade life. The seal is

placed in a jig, and a blade is set to cut off the cell at the ceramic, which is between the cell and the canister.

The second step is cutting the cells open. To get the desired cross section view of the cells, they are cut at a 45 degree angle; however, cutting the cells in this manner results in the cell being cut into two pieces: one with a negative current collector and one without the negative current collector, Figure 15. This produces a technical challenge when removing the battery material within the cell.

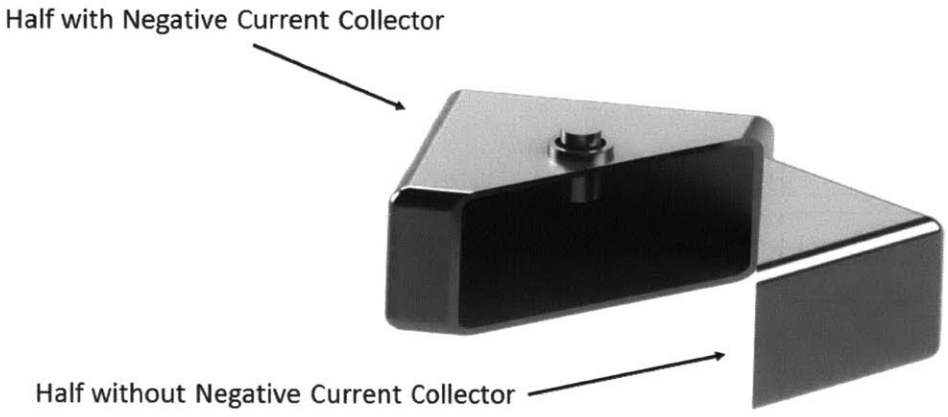


*Figure 15 - Output from R & D Sawing Process*

The third step is the accomplished using a 30-ton press. The press has two round dies which are used to deform the steel canister. The dies are also used to push the seal into the active material to separate the remaining connection between the canister and the stem. The deformation of the canister causes the active material, liner, and cathode material to become separated from the sides; however, not all the material can be removed due to the strong adhesive force between the liner and steel. This means that the press operator has to use a screwdriver to remove the material from the canister. Once the materials have been removed, they are placed in one common stack.

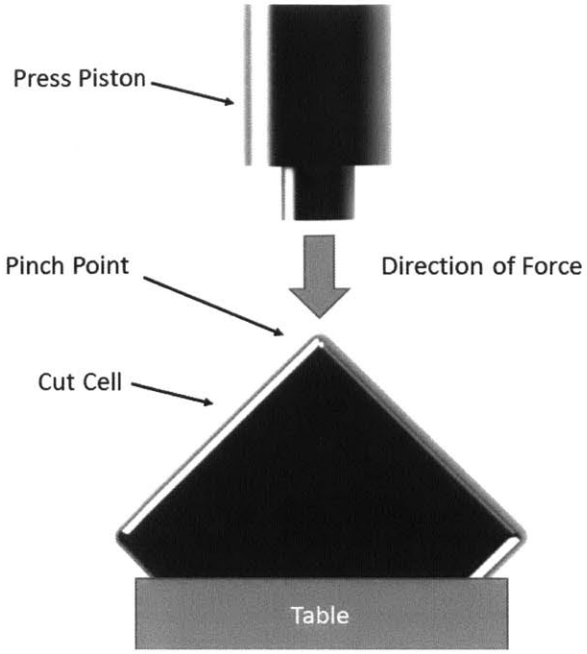


*Figure 16 - R & D Process for Content Removal*

The fourth step is the separation of the active material and stainless steel canisters. The active material is placed in steel canisters, which are then closed and placed into department of transportation (DOT) approved 5 gallon buckets with no more than 30 pounds of material. The steel canisters are assumed to have reactive material remaining on them, which means that they need to be further processed in order to dispose of a contaminated metal.

The fifth step is the placement of the stainless steel canisters into the aqueous wash, which uses water to react off all the remaining reactive metal. The water is stagnated within the steel containment, which results in a slow reaction rate. The containment is ventilated into lab heating, ventilation, and air conditioning (HVAC) system. The process has no monitoring system for the reaction rate and is allowed an adequate amount of time for the reaction to take place. The cells are then removed from the aqueous wash and placed in a contaminated waste 55 gallon drum for disposal.

### 3.1.1 Time Study

A time study of the current process was completed to understand the current throughput, and labor costs. The cutting of the stem, opening of the cell, and aqueous wash were determined through direct observation to have very low variability in processing time due to the time being controlled

by the machine or standard operating procedure. The processing time of the content removal process step has large processing time variability, which resulted in the need to do a time study over a large sample set. The variability is due to the differences in adhesion of salts, liner, and active material to the stainless steel canister. The current process utilized a mechanical press and operator to account for this variability in cells, which causes high variability in process time.

The time study examined the four major process steps of the research and development process, which are as follows: seal removal, cell cutting, content removal, and aqueous wash. From the time study data, the average time and standard deviation were calculated for each process step.

*Table 2 - Time Study*

| Process Steps | Average Time | Standard Deviation | Units |
|---|---|---|---|
| **Seal Removal** | 20 | | Seconds |
| **Cell opening** | 430 | | Seconds |
| **Content Removal** | 138 | 103 | Seconds |
| **Aqueous Wash** | 20 | 0 | Seconds |

The time study that was completed followed 65 cells without seals and 12 with stems. The difference in the number of cells with seals and without is due to the date of time study. The variability of the R&D system is shown in a Shewart chart of the processing time. The upper and lower control limit is set to one standard deviation [41]. The processing time for cells without seals is above or below the control limits 15 times, which indicates an out of control process. The average processing for cells without seals is 14 seconds with a standard deviation of 6.2 seconds. The standard deviation is 44% of the average indicating high process variability.

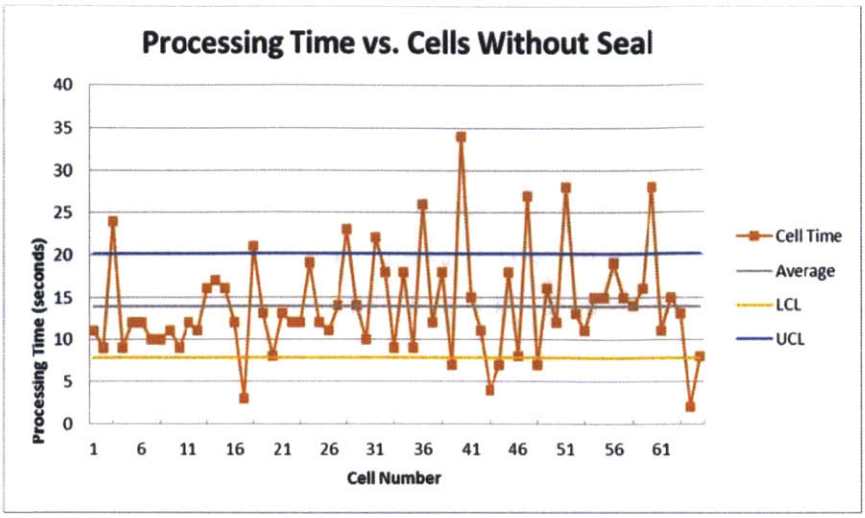


*Figure 17 - Time Study Run Chart for Cells without a Seal*

The processing time for cells with seals had an average processing time of 124.6 seconds with a standard deviation of 103.0 seconds. The standard deviation is 83% of the average, which means the process is highly variable. The run chart shows one point, which is 2.67 standard deviations from the mean. The Western Electric Rules do not indicate this process step is out of control, but the sample size is small [41]. The standard deviation was not taken during a time of statistical control, which means the control limits are not properly set indicating the process is not a statically controllable process.

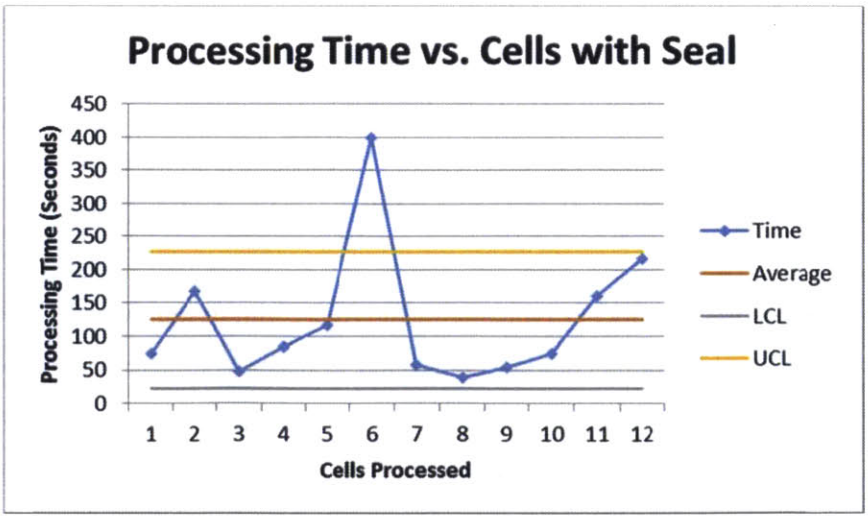


*Figure 18 - Time Study Run Chart for Cells with a Seal*

## 3.2 Transportation

Once the cells are placed in the appropriate containers, the contracted DOT certified waste transporter, such as Clean Harbors or Triumvirate Environmental, picks up the hazardous waste buckets and contaminated metal waste. The transporter brings the waste to a certified waste holding facility for no more than ten days. The contaminated metal waste is transported to a scrap metal yard. The hazardous waste is transported to the contracted environmental protection agency (EPA) certified incinerator, such as Clean Harbors or Ross Environmental Services.

## 3.3 Hazardous Waste Incineration

Hazardous waste incineration is an ultimate disposal method that is used for waste streams that cannot be recycled, reduced, or safely disposed of in a secure landfill site [24]. This thermal treatment process converts the hazardous wastes into gases and solid residues through oxidation of the waste material. There are three main types of incineration: high temperature, low temperature, and co-incineration. In order to oxidize the reactive metals within liquid metal batteries, high temperature incineration is used. All incineration processes consist of the process steps of volume and weight reduction, detoxification, and energy recovery. This process is carried out in a combustion chamber that can handle hazardous solids, liquids, and gases. Incineration is capable of destroying solvents, and polychlorinated biphenyls (PCB), but it does not destroy metals such as lead and chromium.

In the United States, there are 164 hazardous waste incineration facilities [26]. Of these only about 30 waste incineration facilities accept off-site waste streams. These 30 waste incineration facilities service 95% of all hazardous waste generators, because it is more effective and economical then disposing of the waste in hazardous waste landfills or on-site incineration.

The first combustion chamber is typically of the rotary kiln design, which slowly rotates about the vertical axis to tumble solids components around to insure complete combustion. The incineration process is typically operated between 900 ° C to 1,400 °C [25]. These temperatures are sufficiently high to vaporize hazardous material, preventing the release of toxic material into the environment upon disposal into a landfill. However, the gases then travel though a secondary combustion chamber which is operated at 1,200 °C or higher. The high temperature causes the breakdown of the gaseous vapors into atoms which then recombine with oxygen to form predominantly non-hazardous chemicals.

The rate of combustion within the plant is also controlled through the amount of air present within the combustion chambers. The greater the turbulence, the more air is allowed into the chamber. The duration of time that the waste spends in the combustion chamber is between 30 and 90 minutes. Due to the large amount of heat generated during the hazardous waste disposal process, heat recovery systems are typically used to generate electrical power.

The EPA requires that the incinerator be able to destroy and remove 99.99% of each harmful chemical present. The residual materials are tested against EPA standards to insure the ash meets the EPA regulations as safe for landfills. The material is then stabilized to prevent its leaching above the EPA regulations. After stabilization, it is certified as inorganic waste which has completed all treatment requirements for landfilling.

## 4. Recycling Process Design Considerations

Liquid metal batteries are designed to operate at high temperatures with highly active materials contained for 30 years. Those operating conditions have dictated the battery housing to be made of stainless steel with a seal and stainless steel current collector. The active materials inside are housed in an insulting sheath. The active material consists of a reactive metal, reactive salts , and metallic cathode alloy. The batteries when recycled can be in any charge state, which results in different amounts and alloys of the anode, and cathode materials in each battery. To recycle a liquid metal battery, the principal components need to be separated into reusable materials with a salvage value.

Three methods of battery decomposition were considered for use, which were pyrometalurgical separation, initial physical separation with pyrometalurgical separation, and initial physical separation along with hydrometallurgical separation. Each option was researched and considered. Pyrometalurgial separation of the components within the cell required separation processes and techniques that required having active material at temperatures above its melting point, which requires special precautions. The corrosiveness of the salts would have necessitated using exotic metals for the separation process. The EPA also requires the treating and monitoring of the off gassing from the reactor. The throughput of a pyrometalurgical system also would have given more throughput than required. Given the restriction of time, budget, and need for a safe and stable physical separation, hydrometallurgical separation was pursued.

The physical separation step is broken up into three different operations: seal breaking, cell opening, and content removal. The first of these three operations separate the stainless steel canister and stem from the active, corrosive, and toxic materials. The active, corrosive, and toxic materials then go through an aqueous wash process. At the output of this process, there is not any hazardous waste and metals that can be recycled. The process flow is found in Figure 19.

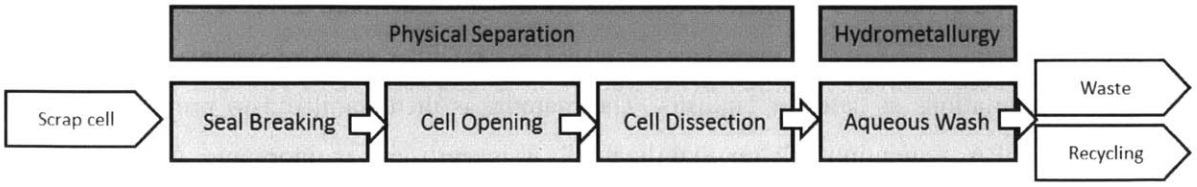


*Figure 19 - Process Flowchart*

## 4.1 Seal Breaking and Removal

Seal breaking and removal is the first physical separation process step. Due to this being the first process step, there is a chance that a pocket of flammable gas could have formed within the cell; therefore, special care needs to be taken. In order to breach the cell, the seal needs to be broken, and then the stem removed from the cell. Those two steps can be classified as two different operations within the process.

Presently liquid metal battery seal technologies are changing rapidly. This requires that the seal breaking and removal step to be highly configurable to cope with the changing of the seal technology over time. The breaking and removal of the seal requires a safe, stable, configurable, and robust process.

### 4.1.1 Seal Breaking Process Selection

The seal is a sintered ceramic (alumina) which is joined to the stainless steel stem and case. A representation of the cell required to be processed in the seal breaking step is provided in Figure 20. The ceramic seal is susceptible to impact or tensile force. The stem needs to be disconnected from the anode material and seal, and must be pulled through the hole in the cell made for the seal and stem. Both operations can be accomplished with the application of a tensile force in one process step.

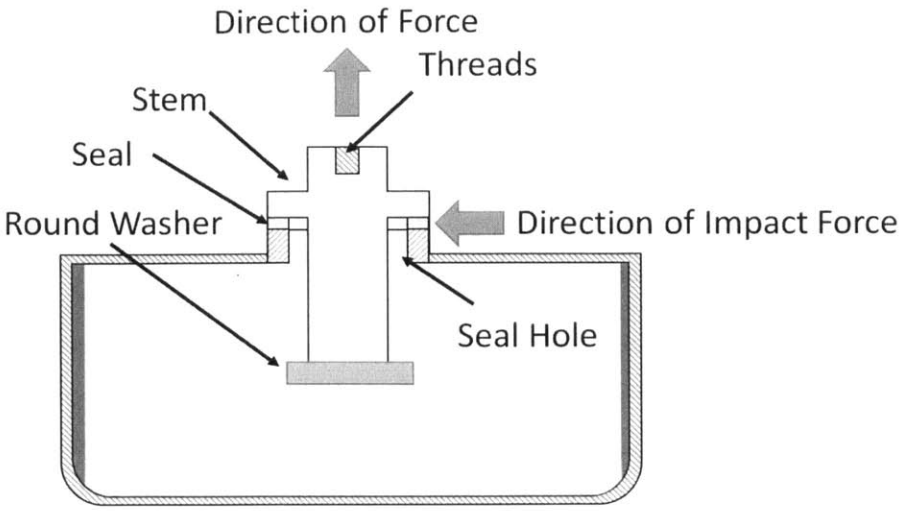


*Figure 20 - Representative Diagram of Cell Requiring Stem Removal*

Impact was shown to break the ceramic, but due to the common force requirement between the two operations, the application for a tensile force was decided on. Also, should the seal be moved into the canister, applying an impact force directly to the seal would not have been possible.

The force required to remove the seal from the steel container was calculated using the ultimate tensile strength of the ceramic, which is the highest tensile strength material of the current seal design. The maximum cross sectional area of the seal ceramic is 0.000158 $m^2$. The ultimate tensile strength of the ceramic tends to will vary an order of magnitude due to the wetted surface and differences in thermal coefficients of expansion. The highest ultimate tensile force was used to calculate the breaking force with equation 6 [28]. This resulted in a predicted tensile force which needed to be applied a of 105 kN of force.

$$F = \sigma_u * A \qquad (6)$$

Where $\sigma_u$ is the estimated ultimate tensile strength, $\sigma_u$ is the ultimate tensile strength, A is the cross-sectional area, and F is the shear force.

The seal technology is advancing quickly; however, due to the need for electrical connection to the individual cells, there is always going to be a need for a stem that protrudes above the canister top. This allows for a gripping device to be placed onto the stem to apply the force for removal. Two options to grip the stem were considered: using a collet or wedge action gripers with vee blocks.

The wedge grip action are rated for 100kN which is near the calculated breaking strength, and way two order of magnitudes above the seal force seen in experiments. Due to the cost of the wedge grips, collet grips were used for testing; however, collets provide lower tensile strength force application capabilities.

### 4.1.2 Seal Breaking Experiments

To determine if the seal could be broken in the two ways described above, two experiments were run to determine the breaking strength of the ceramic seal. The first experiment was applying a localized impact force, and the second was applying a tensile force. These experiments provided valuable knowledge before the development of the fully implemented system.

The first experiment used a chisel to apply the localized force to the ceramic seal, and a hammer acted as the impact force. The cell seal was held horizontally in a vise. The vise was set up to insure no deformation of the seal. The chisel was placed on the seal, and the hammer hit the chisel to apply the force. Ten seals were tested. The seal was broken in every case with one or two applied impacts of the seal. Each seal failed along the line of applied force not at a joint between the steel canister and ceramic. It was noted breaking the seal with an impact does not provide any means of removing the seal from the cell. The impact force also must be applied perpendicular to the force required to remove the seal from the cell.

The second experiment was run with a double acting Dake press with the ability to apply 111 kN to the seal, which had a calculated breaking strength of 105 kN. A vise to hold the cell at its edges was developed in order to put the seal in tension. In initial observations, the cell top deformed when the cell was only held at the edges. To minimize the deflection of the cell top, a thick top plate was used to increase the stiffness of the top. Two cells were tested and both seals were successfully removed from the system. A minimal force was required to remove the seal, estimated through video review to be around 300 kg. The force required to completely remove the stem was considerably more due to spherical bending of the washer through the seal hole in the canister. An exact force could not be determined due to a lack of force measurement on the pulling side of the press. These experiments proved the ability to apply the seal breaking force in the same direction as required for the removal of the seal from the cell. This allowed for the combing of the seal breaking and the removal process steps, which reduces the operator interaction with the cell.

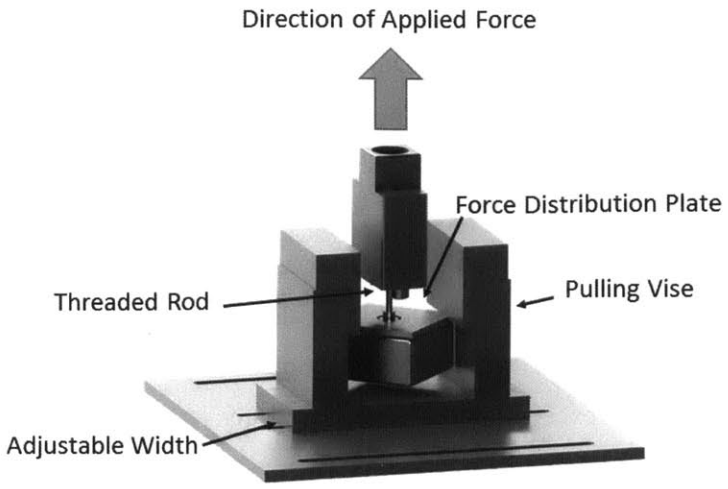


*Figure 21 - Experimental Setup for Removing Seal*

The third experiment completed was with a precision 5-C collet and horizontal/vertical collet fixture. The collet fixture was connected to the press die using an adaptor plate. The application of the clamping force was through the tightening of the collet around the stem. The collet was able to provide enough clamping force to break the seal; however, it was not able to provide enough force to remove the stem from the canister due to the removal force of the washer being greater than the seal breaking.

## 4.2 Cell Dissection

Current liquid metal batteries are contained within a stainless steel container, which needs to be opened in order to get access to the active material. The method of opening the cell is using a cutting method, which allows for the separation of the active material from the stainless steel. The content removal process determines the cut plane for the cell dissection cutting method.

### 4.2.1 Cell Cutting Process Selection

Due to the reactive material within the stainless steel enclosure, extra care is needed to be taken to ensure a safe, stable, and cost effective means to open the battery. The cutting options identified as being possible candidates are as follows: abrasive cut off saw, blade cut off saw, bandsaw, plasma cutting, and water jet. To evaluate the cutting processes, we identified the major cutting process characteristics, such as: cutting time, safety, consumables cost per cut, automation, containment number of cuts before service, cutting fluid, and capital cost. Many machines per category were

considered, but only one machine per category was selected for analysis. The machines selected are , as follows: abrasive cut-off saw was Dewalt 14 inch cut-off saw, cold saw was D350, bandsaw was Baileigh BS-260SA, plasma cutter was Hypertherm Powermax 65, laser was the Hypertherm fiber laser, and water jet was the OMAX 2626.

The safety rating was based of the vapors produced, heat generated, and the risk of cutting was to the operator. The containment was evaluated on the manufacturability and cost of the enclosure to protect the user from the toxic material being handled. The cutting times were obtained through test cuts for every process, except for the laser and water jet. The laser was estimated based off of videos of the process cutting 4 inch by 4 inch stainless steel tubing, but due to the high capital cost, no further characterization was carried out. The water jet cutting time was estimated based off of the cutting speed per minute of an Omax 2626 for .125 inch 316 stainless steel. Due to the reactivity of the metals within the cells to water, no experiments were carried out with the water jet. The cut quality was based on test cuts made by each method, except for the laser and water jet due to the reasons stated above. The number of cuts was based on experiments conducted by the manufacturers, except for the laser and water jet for reasons previously mentioned. For the laser and water jet cut, quality was assessed based on conversations with the manufacturers. The capital costs of the system are based off of quotes from either the manufacturer or distributor. Cutting fluid was based off of the manufacturer specifications.

The selection criteria were evaluated to ensure the most cost effective, stable, safe design was selected. A safety level of low or high* was considered acceptable. All cut times were found to be acceptable, because the sawing process was not the bottleneck of the process. The cut quality needed to be at an acceptable level for the process to be considered. The consumable cost and capital costs were used to select the lowest possible option. Automation needed to be either semi or fully automated. The containment was not used for selection of a cutting method but was researched to provide additional information. The cutting process needed to have no cutting fluid. The capital cost was considered acceptable up to $40,000. Through the analysis, it can be shown that either a bandsaw or plasma cutter is acceptable for opening the cells.

*Table 3- Cutting Method Decision Matrix, High* = Acceptable Safety Level with Proper Precautions*

| Process | Cut Quality 1-3 | Cut Time Seconds | Safety 1-3 | Consumables Dollars | Automation 1-3 | Containment 1-3/1-3 | Number of Cuts | Cutting Fluid 1-3 | Capital Cost Dollars |
|---|---|---|---|---|---|---|---|---|---|
| Cutoff Saw | Not Acceptable | 60 | High | 3.28 | None | Hard/Cheap | 80 | None | 435.00 |
| Cold Saw | Marginal | 22 | Low | 10.00 | None | Hard/Medium | 10 | Water Soluble | 5,995.00 |
| Band Saw | Acceptable | 240 | Low | 0.18 | Semi | Hard/Medium | 320 | None | 7,995.00 |
| Plasma Cutter | Acceptable | 60 | High* | 0.50 | Full | Medium/Medium | No Quantifiable | None | 35,000.00 |
| Laser | Acceptable | 45 | High* | 0.07 | Full | Hard/Expensive | No Quantifiable | None | 400,000.00 |
| Water Jet | Acceptable | 60 | Very High | 0.54 | Full | Hard/Expensive | No Quantifiable | Water | 300,000.00 |

### 4.2.2 Plasma Cutting

Plasma arc cutting is the process of using a transferred electric arc between the negative electrode of the plasma cutting torch and the positive work piece. The process cuts the work piece through the dual action of melting and vaporizing the material. The material is removed along the plasma jet. The plasma operates at a temperature between 5-30K [29]. Once the molten and vaporized metal leaves the plasma jet, it reacts with air and forms the metal oxides.

To test the plasma arc cutting, a Hypertherm PowerMax 65 was used to cut open a test cell. When the Hypertherm Massachusetts sale representative, demonstrated the plasma cutter, he said "the PowerMax 65 uses 65 amps to cut the stainless steel at 25K." The test piece was hand cut with a beveled angle to prevent the metal particles from being forced into the cell. A full cell was not cut because of the reactive material and the risk of cutting posed too large of a fire hazard.

The picture below shows that there are metal oxides formed on the inside edge of the cell even when cut at a beveled angle. There is also a substantial amount of metal dust made up of the metal oxides created from the cut. The amount of slag produced remaining on the surface of the cell container was acceptable.

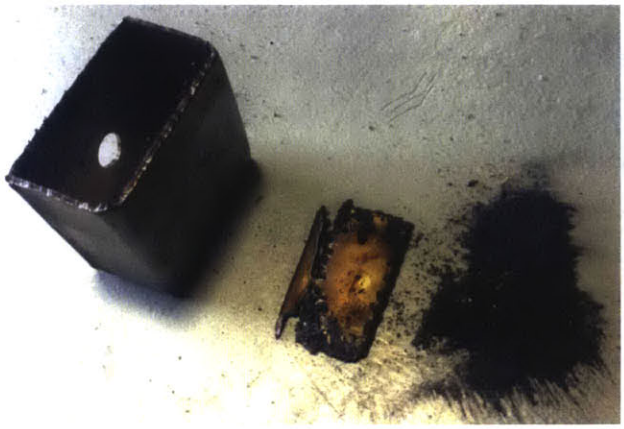

*Figure 22 - Plasma Cutting Experiment*

The main concern with plasma cutting is the risk of fire with a gaseous heat source close to the reactive material. The plasma arc will also cut through toxic material, which when vaporized is harmful to humans [30]. An automated plasma cutting system could mitigate these safety concerns when deployed in an inert atmosphere with proper material handling equipment. Due to the inability to deploy plasma cutting safely at atmospheric pressure and without custom designed enclosure and material handling equipment, the implementation will be prohibitively expensive.

### 4.2.3 Bandsaws

Horizontal bandsaws have a continuous cutting blade which is driven at a constant cutting speed. This enables a thrust load to be applied between the blade and the workpiece [31]. The cutting performance is affected by the blade selection, blade speed, and thrust load. To extend the blade life, either oil-based or water based lubricants are used. It is possible through proper blade selection and cutting characteristics to not use lubricants; however, the blade life will be typically reduced by as much as 50% according to Joe Maiolo at LENOX. The bandsaw produces a clean, straight cut that is predictable and easily controlled.

Bandsaws cause heat through the shear created by the blade's cutting teeth. The heat is then absorbed and increases the temperature of the steel. Since the active material is isolated from the steel, the active material is not directly exposed to the heat generated by this cutting process. The bandsaw does cut through toxic metal, but the risk to humans is minimized because the toxic metal does not change phase. The particulate sizes are large, which prevents them from becoming airborne.

To optimize the bandsaw's cutting performance, the blade manufacturer, LENOX, was contacted for their engineering expertise. Our point of contact at LENOX was Joe Maiolo, an engineer in the Research and Development Tools Business Segment. In order to optimize the blade performance a 4 foot 4 inch square by 0.125 inch 304 stainless steel tubing was sent to LENOX for testing. The test cuts were performed without lubricant in a Daito GA-330. The blade selected for the test cutting was the LENOX Rx+ length 13'6" x 1-1/4"x .042" x 5/8 TPI. The blade was optimized to have a band feed rate of 70FPM and a feed rate of 1.01 imp. The blade performed 337 cuts with an average cut time of 4 minutes 5 seconds.

The bandsaw blade optimization collaboration showed adequate blade life could be achieved while cutting dry. The cut upon examination had little bur and was straight. The cut time was long; however, the recycling process system optimization should be able to compensate for the cut time. The kerf of .042 inches also allows for the blade to have minimal contact with the material within the cell. The slow speed of the blade results in less heat generation. The slow speed does not cause any airborne material. The material deposited close to where the blade teeth exited the side of the cell. The material removed is also not a fine dust but large particles.

## 4.3 Content Removal

The liquid metal battery cell's internal material needs to be removed in order to separate the stainless steel canister from the active material contained within the liner. Once the stainless steel is separated from active material, it is ready to be recycled as scrap metal. The active material once separated is ready to be further separated in the aqueous wash system. The cell dissection process needs to be stable, robust, safe, and cost effective. The process needs to be stable and robust in order to maintain process flow within the recycling system. The safety concerns are because there is active material being handled.

### 4.3.1 Content Removal Process

Content removal could have been accomplished in three different ways: cutting one side off and crushing/scraping the material from the cell containment, removing the top and bottom and pushing it out, or removing two sides and pushing it out. The three possible different canister outputs can be seen in Figure 23.

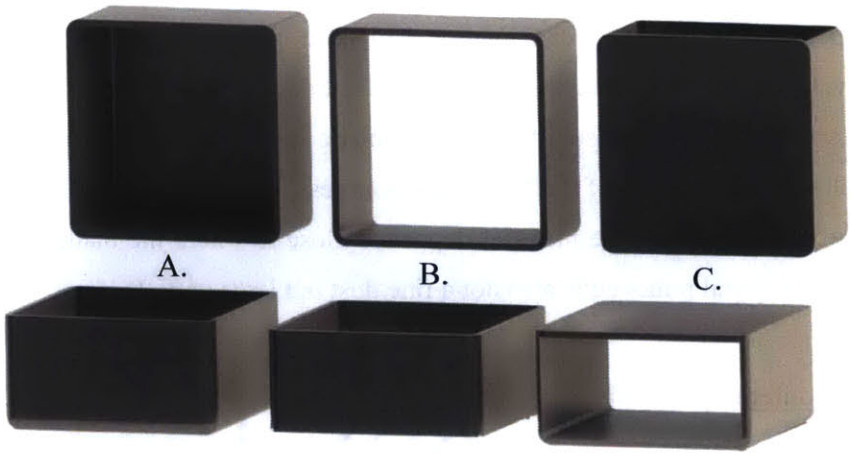


*Figure 23 - Three Possible Cell Content Removal Directions. A. Removal of the Front, B. Removal of the Front and Back, and C. Removal of Two Sides*

The electrolyte material when solidified forms a polycrystalline structure, which has an increasing shear stress with increased pressure [35]. The material is not isotropic, which means the forces on the die when crushing the active materials are not uniform. Input cells can also be in different charge states, causing the batteries to be processed to have chemical composition causing a variation in the shear force required. Due to the problems stated above, the removal of the front or back and crushing the material was not chosen.

The decision to push the internal material out through the back or side was considered. The direction of material removal was evaluated on the desired process characteristics. Safety was evaluated by the risk of toxic metal contamination, risk of flammable gas, and ability to use shield gas. The stability and robustness was evaluated on the process ability to be repeated reliably with cell-to-cell variation. The cost was evaluated on the amount of time required to cut open the cell, which is assumed to be related to the length of cut. The decision matrix can be seen in Table 4. Due to the two side removal process having a smaller cut length and the ability to use a shield gas, the two side removal process was selected.

*Table 4 - Decision Matrix for Content Removal*

| Process | Length of Cut<br>Inches | Safety<br>Safe(5)-Unsafe(1) | Stability<br>Stable(5) - Unstable(1) | Robustness<br>Robust(5) - Not Robust(1) |
|---|---|---|---|---|
| Front/Back Removal | 32 | 3 | 5 | 5 |
| Two Side Removal | 24 | 5 | 5 | 5 |

The force required to push the active material out of the steel container was calculated using the ultimate tensile strength of the material that bonds the liner and the steel. Since the material that connects the two is ductile, it is a good estimation of the shear stress to use the tensile strength. The maximum adhesive area that the material can cover is 75% of the two sides and back of the cell. This gives an estimated area of 0.01633 $m^2$. The highest ultimate shear strength relationship to ultimate shear strength for ductile material was used in order to calculate the shear. To calculate the tensile force equation (8) was used. The ultimate tensile strength of the binding material is around 12 mpa. In order to calculate the shear force, equation 7 was used [28]. This resulted in a predicted shear force of 196 kN of force.

$$F_{us} = \tau * A \qquad (7)$$
$$\tau = .8 * \sigma_u \qquad (8)$$

Where $\tau$ is the ultimate shear strength, $\sigma_u$ is the ultimate tensile strength, A is the cross-sectional area, and $F_{us}$ is the estimated shear force required.

### 4.3.2 Experiment

An experiment was run to insure the removal of the content from the inside of the cell. The experiment utilized the double acting Dake press which can apply 111 kN. A precision die and vise was made to hold the cell. The experimental set up can be seen in Figure 24.

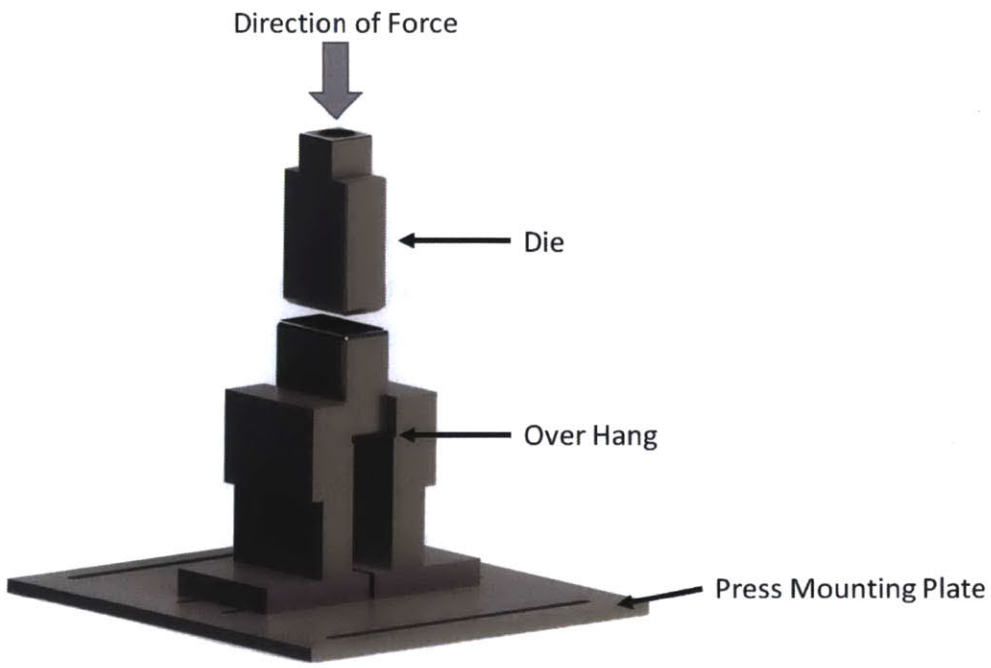


*Figure 24 – Experimental Test Setup for Content Removal*

The die developed for the testing was a modular design which allowed for multiple iterations of the die in order to get proper geometry, Figure 25. The die was split into multiple sections: press mount, spacers, and nose. The press mount is the piece that allows the connection of the press and the die and where the bolts that hold the spacers and nose together are threaded. The spacers were designed to be smaller than the nose because this would have caused increased friction force. The spacers and press mount were made of carbon steel. The nose piece was designed to be the piece which interfaces with the cell. To prevent the bolt from interfacing with cell before the nose, a counter-bore hole was used to recess the bolts into the nose piece. All the nose pieces have a 45 degree chamfer to allow the die to do fine alignment with the cell before it contacts the sides of the cell. The nose pieces were made of A2 tool steel.

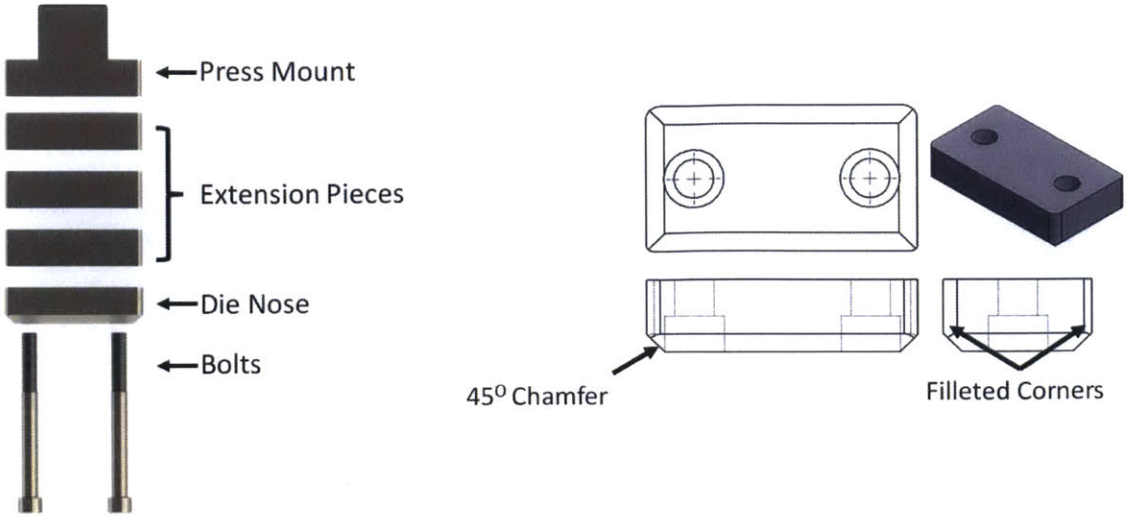


*Figure 25 - Best Experimental Die Design*

The four nose pieces were made to determine which die provides the most reliable removal of the material from the cell. The first die made has a nose piece oversized by 50 thousandths from max cell specification. The oversized die was not hard enough to deform the stainless steel canister, resulting in the die not entering the can. The second die was the largest specification. This nose piece also did not fit into the cell due to the cell not being at the larger specification. The third nose piece was at the lower specification limit. This nose piece fit into the cell and removed the cell content; however, the two non-radius corners needed to be rounded in order to compensate for the weld penetration into the top corners of the cell. The fourth nose piece developed was 50 thousandths smaller than minimum specifications. This removed the content; however, it left too much residual connecting material.

## 4.4 Aqueous Wash

The aqueous wash system is the last step in the recycling process. This step neutralizes all the reactive and corrosive materials in an aqueous solution where they can be reconstituted as usable salts. The reactive and corrosive material are all contained within the liner; however, when the seal is removed there is a chance that it will have active material attached to the stem mandating it be processed in the aqueous wash system as well. The reduction of active metals into an aqueous process is an industrial chemical process.

The reaction of active metals with in an aqueous solution has three significant parameters: molarity of the solution, temperature, and flow rate. The aqueous reactor must have the ability to control all

three of the significant factors in order to have a controlled, stable process. The relationship the different paramerters have on the reaction rate are seen through the Arrhenius equation (10) and linear relationship between the metal dissolution rate and corrosion current (13) [32]. The design of the aqueous wash system needed to be safe, stable, and cost efficient.

$$v_f = k_f[Metal][H_2O] \qquad (9)$$

$$k_f = Ae^{\frac{-E_{act,r}}{RT}} \qquad (10)$$

Where $k_f$ is the rate constant, $E_{act,r}$ is the activation energy, $A$ is the effective surface area, $R$ is the universal gas constant, and $T$ is the temperature.

The linear plot of logarithmic corrosion rate has shown that the Arrhenius equation is obeyed for the aqueous corrosion.

$$Metal + OH^- \longleftrightarrow MetalOH_{(aq)} + e^- \qquad (11)$$

$$e^- + H_20 \longleftrightarrow OH^- + \frac{1}{2}H_2 \qquad (12)$$

The electrochemical reduction of active material is defined by equation 13 [32].

$$R_M = \frac{M}{nF\rho} i_{corr} \qquad (13)$$

Where $R_M$ is the corrosion rate, $i_{corr}$ is the corrosion current, M is the atomic weight of the metal, $\rho$ is the density, $n$ is the charge number, and $F$ is the Faraday constant.

### 4.4.1 Material Selection

The aqueous wash system contains reactive metal salts and needs to operate with high hydroxide concentration. Due to the caustic and corrosive environment that results from processing the batteries, materials that withstand this battery environment needed to be selected.

The polymers selected for the aqueous wash system had a high chemical resistivity to concentrated basic solutions and high concentrations of active metal salts. To determine the stability of the plastics in different solutions, the Cole-Parmer chemical compatibility database and the IPEX chemical resistance guide were used [36], [37]. Only polymers that had a rating of excellent and high resistance were considered. A rating of excellent and high resistance means the solutions had little to no effect on the polymer, resulting in the polymer acting inert at the specified temperature and pressures. The plastics that were found to meet the requirements of the system were fluorocarbon polymers (PTFE, PFA, PVDF), polypropylene (PP), and high-density polyethylene

(HDPE). Poly vinyl chloride (PVC) was found to have acceptable characteristics but was used only in non-wetted areas of the reactor.

The consideration to the types of metals used in the system was important as well. Alloys were evaluated using the Uhlig's Corrosion Handbook [33]. Both 304 and 316 stainless steel were found to have acceptable resistance to high concentrations of the active metal solutions when compared to the anticipated operating temperature below 50 ° C. 316 stainless steel has better resistance to the salt corrosion. This resulted in the steel selected for use in the system being 316. Also nickel 200 was found to be suitable for use in the basic and salt solutions .

### 4.4.2 Molarity

The reactive material within the cell is highly reactive with water where it reduces to form a base. It can be seen from the rate equation, equation 12, that molarity has a negative linear relationship with the kinetics of the reaction. If a basic aqueous solution is used instead of pure water, the reaction is slowed.

### 4.4.3 Temperature

The dissolution of the active metal and salts into the aqueous solution is very exothermic. This exothermic reaction is important to understand in order to prevent thermal run away. A thermal run away could occur if too many cells were placed into the reactor and the reaction was allowed to the heat up. This heating would drive the reaction forward even faster causing the reactive metal to heat up. This could lead to an explosion when hydrogen is above the auto-ignition temperature of 500-571 °C[38]. To calculate the amount of energy released, the enthalpy of the reaction in water was found for salts and metals [32].

$$\Delta H^{0}_{reaction} = \sum \Delta H^{0}_{f}(Products) - \sum \Delta H^{0}_{f}(Reactants) \qquad (14)$$

The heat of reaction for a complete cell is around 700 kJ/cell (683.85 kJ/cell).

Due to the exponential increase in reaction rate with respect to temperature of the reactive metal solution, a temperature of 60 °C was decided on. This corresponds to a 10-fold increase in the reactivity of the active material within the cell.

### 4.4.4 Flow Analysis

Active metal corrosion rate can be linearly correlated to the flow rate of the solution across the metal. This correlation is due to the mass transport limit that results in a slowing of the reaction due to diffusion. If the flow is not controlled within the system, stagnation of the boundary layer will happen causing the mass transport limit to be reached and the system to become diffusion dependent, causing a significant slowing of the reaction. To avoid a diffusion dependent system, the stagnation of the boundary layers on the cells needs to be prevented, and a flow established within the system. Flow within the system also allows for mixing to occur, which keeps the system homogeneous with respect molarity and temperature.

To establish a flow within the system, two types of processes were considered: mechanical pumping of the fluid and mechanical agitation. The options were examined for their ability to withstand a caustic environment and the formation of hydrogen gas, which is flammable and causes a slight pressure within the system. Due to this requirement, magnetic coupled stirrer drives were considered and positive displacement air pumps. An agitator provides good mixing characteristics, predictable flow patterns, and adequate flow rates and control. Many agitators were looked at, but the Büchiglasuster Cyclone 250 was considered the best for the application; however, due to its high cost and lack of less expensive alternatives, an agitator was not included in the system. A positive displacement pump creates flow within the reactor by pumping liquid from the bottom of the tank to the top of the tank. This movement of the fluid creates Using a pump to flow the solution over the reactive material provides a cost effective design but careful design of the reactor is required to get the desired flow profile.

In order to insure the proper flow was developed in the reactor, a computational fluid dynamic model was created using Solidworks Flow Simulation, Figure 26. The simulation was completed with three boundary conditions: inlet flow rate, outlet flow rate, and environmental pressure. The simulations were run using a mesh size adequate to develop the flow characteristics required as well as make the simulation run in less than 8 CPU hours. The simulation was run at two different flow rates: 3.5 gallons/minute and 5 gallons/minute. The strainer was included with a porosity of 50%. The simulations can be seen below.

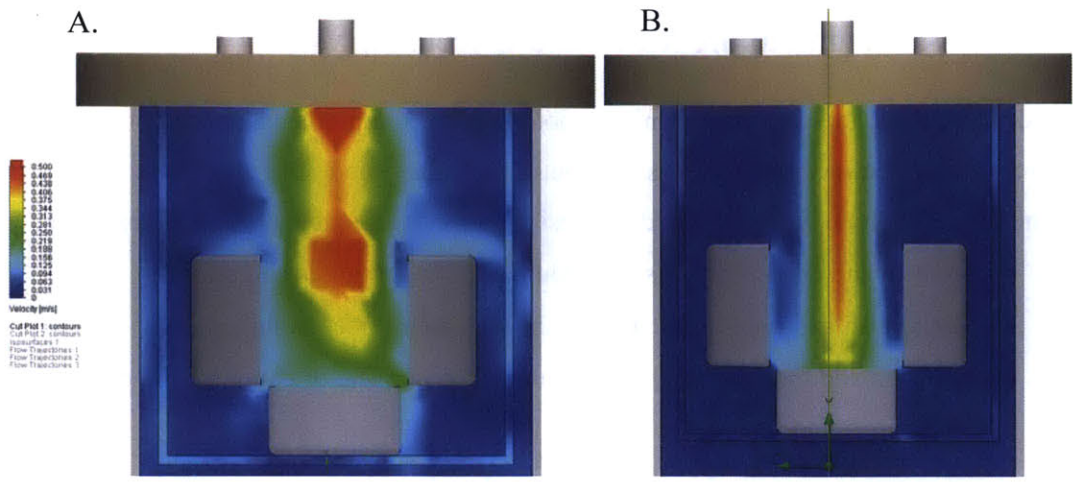


*Figure 26 - Velocity Field Plot of Reactor Design A. Simulation flow rate 5 gpm B. Simulation flow rate 3.5 gpm*

The simulations provided insight on the flow profiles within the reactor. From the simulation, it was clear that the placement of the inflow needs to be at the center of the reactor to produce symmetric flow. The simulation also showed the importance of placing the active material contained within the liners be uniformly and symmetrically in the reactor to get the uniform flow and the desired flow rates. The shape selected has one cell facing up at the bottom of the cell container, and the other cells are elevated to the upper edge of the bottom cell and placed around the perimeter. This configuration causes the inlet stream to be redirected towards the bottom cell's perimeter. The cells on the perimeter then redirect the flow shed off the bottom cell over their face. This cell configuration causes high uniformity of flow over the cells' faces, which is desired to control the mass transfer limit of the reaction.

### 4.4.5 Gas Production

During the reaction of the active material to form the alkaline metal solution, there is a generation of $H_2$. The amount of hydrogen gas was calculated for each cell under standard temperature and pressure, and assumed 100% reaction. Each cell is capable of producing 40 L of hydrogen. The stoichiometry of this reaction is found in equation 11. The amount of hydrogen produced per cell if oxygen is introduced could cause an explosion if the hydrogen concentration is allowed above the 4% lower explosive limit but below the upper explosive limit of 76% [38].

## 5. Process Design Failure Mode and Effect Analysis

In order to define, identify, and eliminate potential process problems, and errors, a process design failure mode and effect analysis was conducted. A failure mode and effect analysis is a systematic engineering technique intended to aid the design process through the following exercise:

- Analyze and determine possible failures with their causes and effects
- Distinguish and rank failure modes through their effect on the process
- Redesign and improve the process in order to mitigate or eliminate the potential failure from happening

In order to distinguish the modes of failure that have the greatest effect on the system, process knowledge and data are utilized to rate each failure mode and effect on the following three factors [39]:

- Severity: the effect a failure has when it occurs
- Occurrence: the frequency or probability of a failure happening
- Detection: the chance of an eminent failure being detected before it impacts the process

The severity ratings for the analysis are broken down into a ranking from 1-10; however, only eight levels were used. By not using all rankings, the levels are weighted when assigning the risk priority number (RPN). The RPN value combines the different factors and allows for the failure modes to be compared. In the developed of a safe process all steps were required to have an RPN number below 200 because this was declared to be a safe operating point. When a process step has an RPN number above 200, additional engineering and design was done to insure a safe process.

The ten rankings were then split into five different categories with three categories assigned with two levels and two categories assigned with one level. The highest category was the "failure to meet safety and/or regulatory requirement" which a failure occurs. The second category was the "loss or degradation of primary function" when a failure occurs. The third category was the "loss of secondary functions" when a failure occurs. The criteria for the different levels can be found in Table 5.

The occurrence ratings for the analysis were broken down into a ranking from 1-10, and only 5 of those rankings were used. The rankings were split up into the likelihood of failure from very high, high, moderate, low, and very low. The frequency of failures is defined by the ratio of failures to

successes. For the very high level, it is less than 1 failure to 10 successes, and the low is less than one failure to 1,000 successes.

The detection ratings for the analysis were ranked from ten to one, with only four levels utilized. The levels were near impossible to detect, difficult to detect, moderately hard to detect, and easy to detect.

Once the severity, occurrence, and detection ratings were assigned, the risk priority number (RPN) value was determined by multiplying the ranking of the three rating factors together, equation 15.

$$\text{Risk Priority Number (RPN)} = Severity * Occurrence * Detection \quad (15)$$

The RPN value combines the different factors and allows for the failure modes to be compared. In the developed of a safe process all steps were required to have an RPN number below 200 because this was declared to be a safe operating point. When a process step has an RPN number above 200, additional engineering and design was done to insure a safe process.

Table 5 - Ambri PFMEA Categories, Criteria and Ranking

Severity

| Effect of Failure | Criteria | Rank |
|---|---|---|
| Failure to meet safety and/or regulatory requirement | Failure mode results in safety event/breach of regulation with NO WARNING PRIOR TO EVENT | 10 |
| | Failure mode results in safety event/breach of regulation with triggerable indicator prior to event | 9 |
| Loss or degredation of primary function | Failure mode results in the inability to operate the device without additional safety event | 8 |
| | Failure mode results in degredation in performance of the device | 7 |
| Loss of secondary functions | Failure mode results in the loss of a secondary function of device. Device is operable, but one or more ancillary functions is lost. | 6 |
| | Failure mode results in the degredation of a secondary function of the device. Device is operable, but one or more ancillary functions are at a reduced level of performance. | 5 |
| Annoyance | Failure mode leads to change in appearance or audible noise, noticed by most operators with no degredation of performance or safety implications | 4 |
| | Currently out of AMBRI resolution. | 3 |
| | Currently out of AMBRI resolution. | 2 |
| No Effect | Failure mode has no discernible Effect | 1 |

Occurrence

| Liklihood of Failure | Criteria | Frequency | Rank |
|---|---|---|---|
| Very High | Failure is almost inevitable | >1 in 10 | 10 |
| | Currently out of AMBRI resolution. | | 9 |
| High | Repeated failure | >1 in 50 | 8 |
| | Currently out of AMBRI resolution | | 7 |
| Moderate | Occasional failures | >1 in 100 | 6 |
| | Currently out of AMBRI resolution | | 5 |
| | Currently out of AMBRI resolution. | | 4 |
| Low | Relatively few failures | >1 in 1000 | 3 |
| | Currently out of AMBRI resolution | | 2 |
| Very Low | Failure is unlikely | Eliminated Through Design Control | 1 |

Detection

| Likelihood for detection | Criteria | Rank |
|---|---|---|
| Near impossible to detect | No obvious design control or requires long term testing | 10 |
| | Currently out of AMBRI resolution. | 9 |
| | Currently out of AMBRI resolution. | 8 |
| Difficult to Detect | Design control implemented, but inadequate to detect cause prior to release for mass production | 7 |
| | Currently out of AMBRI resolution. | 6 |
| Moderately hard to detect | Reasonable confidence that implemented design control will detect cause prior to release for mass production. | 5 |
| | Currently out of AMBRI resolution. | 4 |
| | Currently out of AMBRI resolution. | 3 |
| | Currently out of AMBRI resolution. | 2 |
| Easy to detect | Almost certain that implemented design control will detect cause prior to release for mass production | 1 |

Process design failure mode and effect analysis was completed on all steps of the process to ensure the safety of our process. This resulted in the control loop, PDFMEA, to be utilized as a feedback loop for informed design, Figure 27.

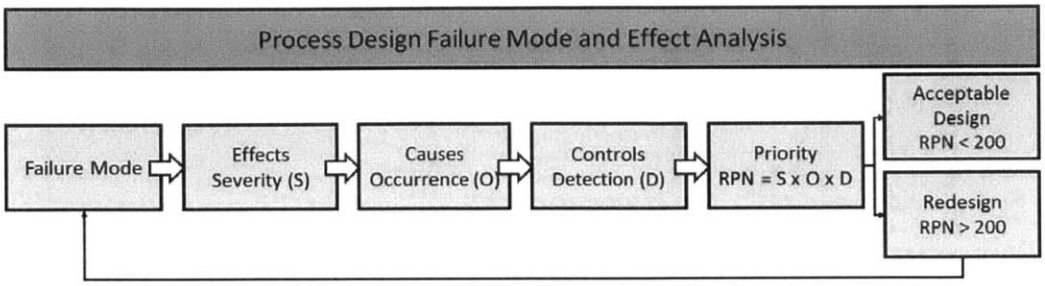


*Figure 27 - Process Design Failure Mode and Effect Analysis*

## 5.1 Current Process

The current process was evaluated using the severity, occurrence, and detection criteria to determine the base line of our process when compared to the developed processes. The analysis showed 27 process steps were required to get the cell ready for disposal. Out of those steps, 15 were considered to be unsafe and required process redesign. The distribution of the percent process steps with respect to the RPN value shows that 50 percent of the process steps are happening above 1,000.

The most unsafe process steps surrounded the removing of the material from within the cell and the containment for the reactor. These steps all have an RPN number of 1,000, which is 5 times higher than the redesign point for the developed system. The other 12 unsafe process steps encompassed varied from 800 to 270. These steps put the operator at risk during every major operation.

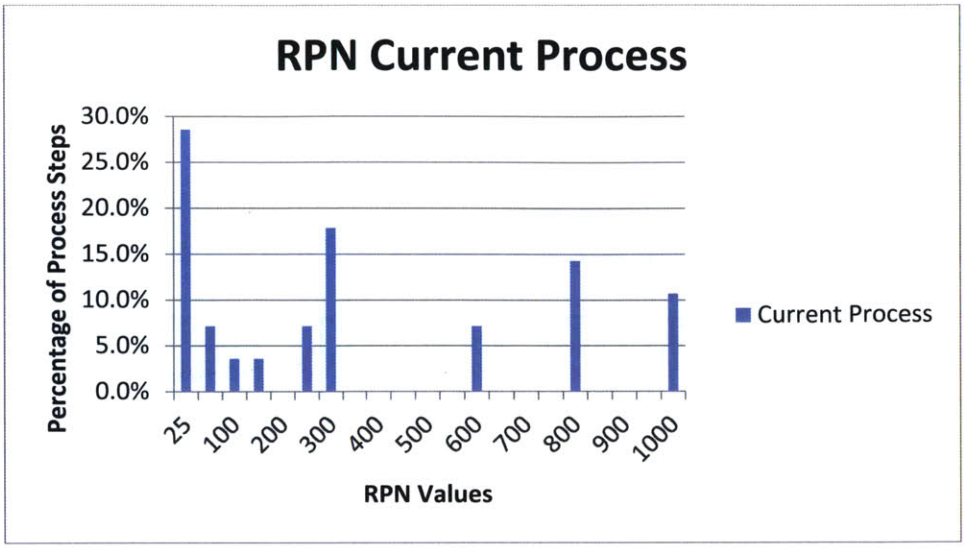


*Figure 28 - RPN Distribution for current process*

The insights from this risk analysis showed that the operator needs to be protected from the hazardous gasses produced from the reactor with process controls and system design. The operator also needs to be able to remove the content with minimal pinch points and be protected from flying debris. Also the operator needs to be protected from the cutting process due to the risk of the blade breaking and getting cut from the moving blade.

## 5.2 Aqueous Wash

The aqueous wash process was evaluated on the severity, occurrence, and detection criteria to determine if the process was designed safely. The analysis covered the 28 process steps, which were required to react the active material. All of the processes were able to be designed with an RPN number of less than 200. The distribution of the percent process steps with respect to the RPN value shows that 50% of the process steps have a value of 25 or less.

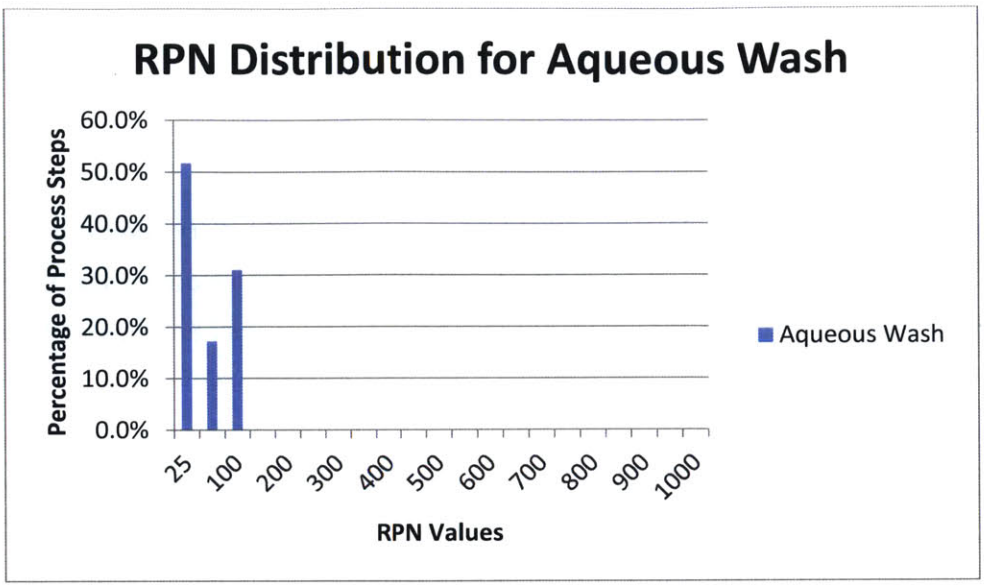


*Figure 29 - RPN Distribution for Aqueous Wash*

The highest risk for potential failures involve when the operator needs to make a visual inspection, opening the containment, and placement of material into the reactor. These risks are mitigated through a user friendly control panel which gives visual cues and is logical to use. The visual cues are in the form of labeled valves, transparent tubing for flow indication, pressure gauges, timer, and temperature read outs. The placement of materials within the reactor was made ergonomic by insuring no sharp edges and designing cell placement within the reactor. Opening the containment was reduced through the utilization of chemically inert materials and properly designed opening mechanism.

The PDFMEA showed that the process needed to utilize chemically inert materials to prevent corrosion and binding issues in the future. Bypass valves were needed to provide a manual override in case of a failure. Easy operation of the valves during a thermal runaway is important to protect the system from failing.

## 6. System Implementation

The first liquid metal battery recycling process was installed at Ambri's Marlborough facility. [1]. This novel approach is able to process the batteries into recyclable stainless steel, toxic metals, and salts. The process was setup to be run by one operator, have minimal work-in-process, and the flexibility to be run as a batch system. The operator is separated from the toxic and reactive

materials through process containments and personal protective equipment, all of which meets OSHA standards. This process was completed on a short timeline with economic and safety considerations in mind.

The ability to produce recyclables from the Ambri's liquid metal battery comes from our process, which combines physical separation and hydrometallurgy to eliminate nonhazardous waste. The processing step of the supply chain now has four principle steps: seal breaking and stem removal, cell dissection, content removal, and aqueous wash. The aqueous wash reacts the active material and the electrolyte to form l salts where they can be crystallized and resold. The crystallization of the salts from the aqueous wash allows that waste to be reused. Once the cells have gone through the aqueous wash, the cathode material and the canister are ready for recycling. The recycler picks up that material from Ambri, which it is taken to a temporary scrap metal facility. From the scrap metal facility, it is brought to a blast furnace or smelter. The metal waste is then further refined and turned into useful metals for manufacturers. The end of life battery cycle can be seen below in Figure 32.

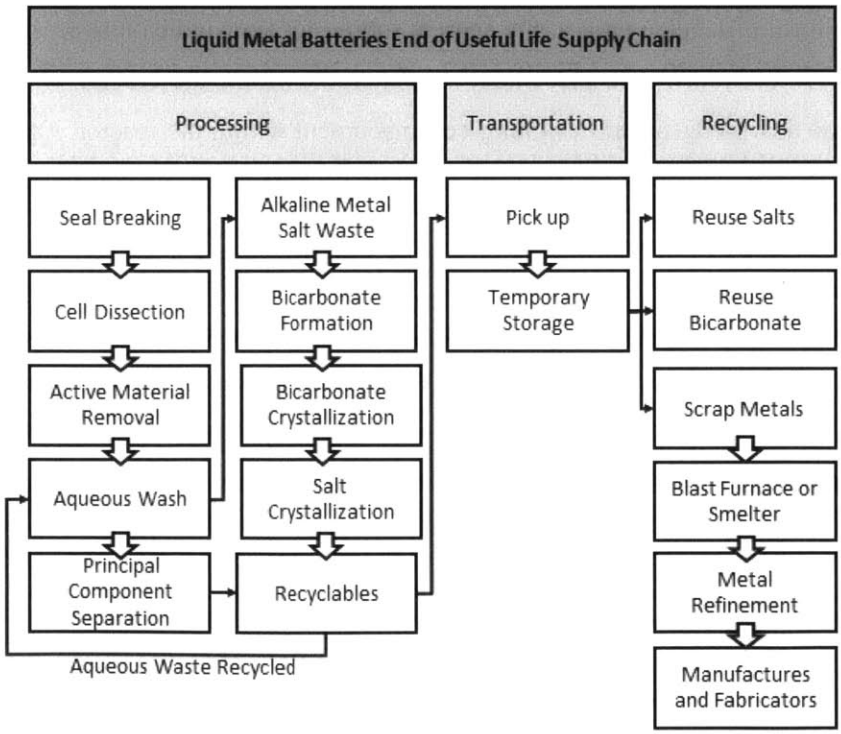


*Figure 30 - Liquid Metal Batteries End of Useful Life Supply Chain[40]*

The processing step is the only part of the battery end-of-life cycle that is carried out by Ambri. The process is configured to operate as either a Toyota production cell or a 5 piece batch, Figure 31.

The Toyota production cell is designed to have one piece work piece flow until it reaches the aqueous wash system where five cells will be processed as a batch. The operator will complete one cutting operation to one seal removal and one active content removal, which results in the bandsaw being utilized twice per process cycle. The buffers are placed in order to have improved flow through the cell.

The throughput of the system was analyzed using the cycle time of the system and operator's time at each step. The limitations of the system are the requirement to react the active material within the aqueous wash and the limitation of one saw for cell opening when the cell requires both sides opened. The recycling cell is optimally operated with one piece flow which is why the analysis was completed for one piece flow. The analysis was also completed for when the recycling cell is operating at a steady state, which is when there is a cell at each of the process steps. The processing times for the analysis are estimated on a study where the operator times were calculated through acting out the process and the cycle times are estimated on the data from real cells.

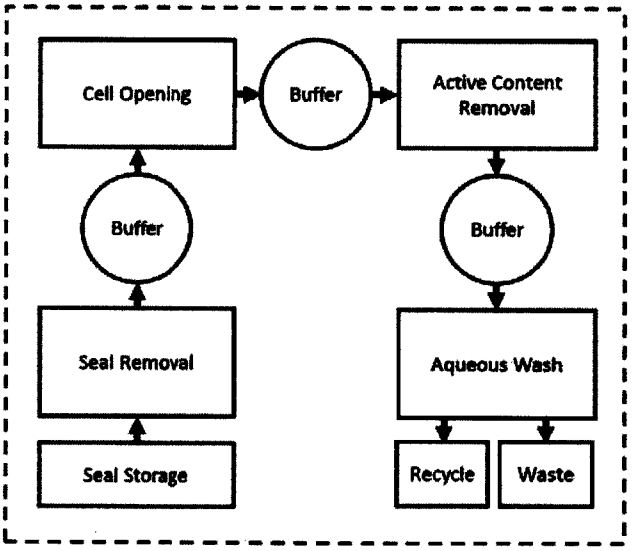


*Figure 31 - Toyota Production Cell Workflow and Setup*

The recycling cell process starts with the operator loading and starting the bandsaw. Once the bandsaw is started, the saw automatically cuts the cell. The operator time at the first cell opening step is 35 seconds. Then the operator places a cell into the seal breaking press and removes the content. The cycle time here is 45 seconds. The operator must then wait for the saw to complete the cell, which is an additional 55 seconds. Once the sawing is completed, the operator spins the cell

and starts the saw cutting the other side, which takes 35 seconds. When the second side is being cut, the operator loads a cell into the content removal press and removes the content. The cell dissection step takes 45 seconds. The operator must then wait an additional 55 seconds for the sawing process to be completed.

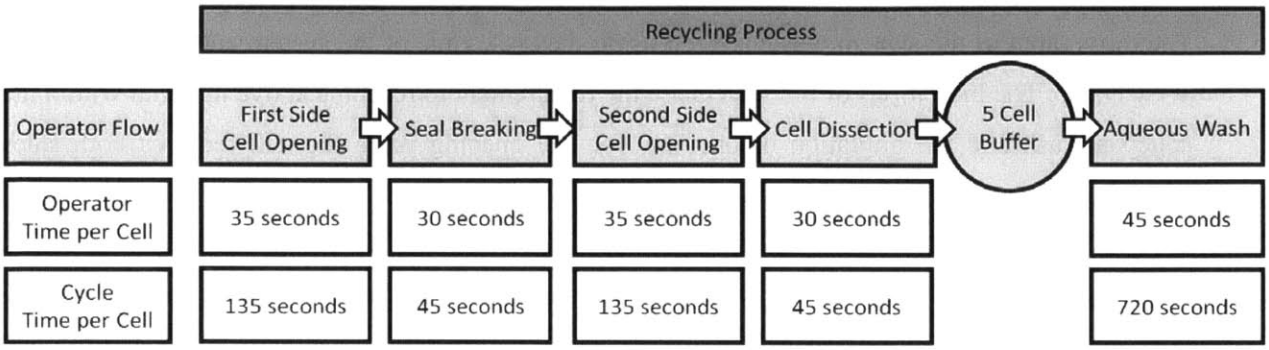

*Figure 32 - Recycling Process Cycle Times*

After careful consideration of the failure modes and selection of the processes to be implemented, the design went through a detailed design process, safety measure development, and characterization.

## 6.1 Detailed Design Seal Breaking and Stem Removal

Once the initial design was tested, the design was updated and implemented at the Marlborough facility. The seal breaking and stem removal step has the whole cell as the input material.

The vise design was updated to only serve as the vise for the removal of the seal, Figure 33. Having a dedicated vise decreases the setup time between the seal breaking and content removal because they share the DAKE 25 DA. The vise is made to have as low a profile as possible to allow easier setup between cells.

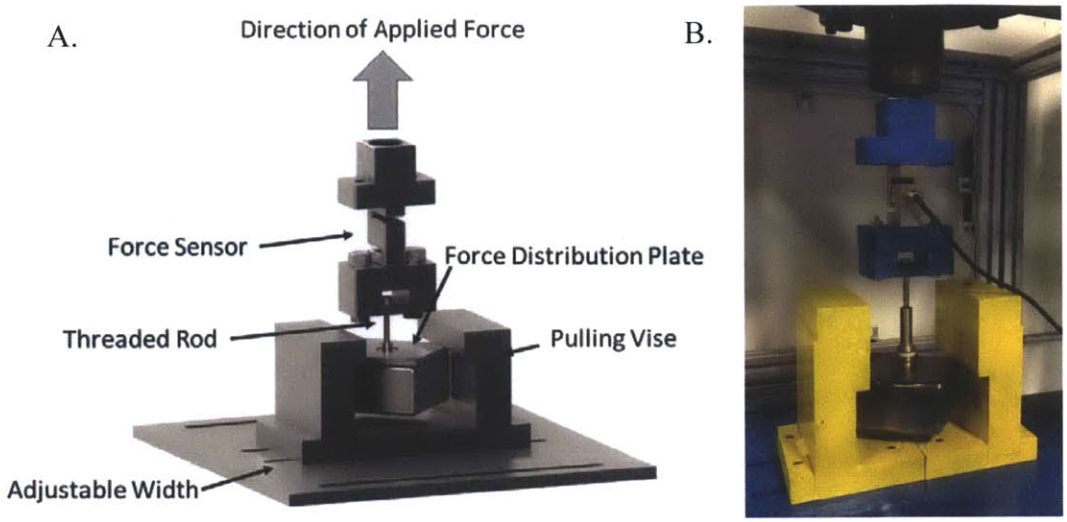


*Figure 33 - Vise and Die Designed for Seal Breaking A. Rendering of optimized design B. Implemented design*

The redesigned die uses the threads machined into the top of the seal to apply the force for the removal and the stem. The updated design, however, uses a through-hole bolt instead of a stud. This allows the bolt to spin separate from the die, enabling easier installation of the bolt into the threaded seal. The updated design also integrates a force measurement device to monitor the differences in seal breaking strength.

The enclosure is made out of impact resistant polycarbonate as seen in Figure 34. The polycarbonate protects the user from debris caused by force applied to the ceramic in order to break it. There are four locking doors on the enclosure, which allows for easy maintenance, easy operation, and placement of the steel container. The door jams have a rubber gasket in order to maintain an inert gas level within the enclosure if required.

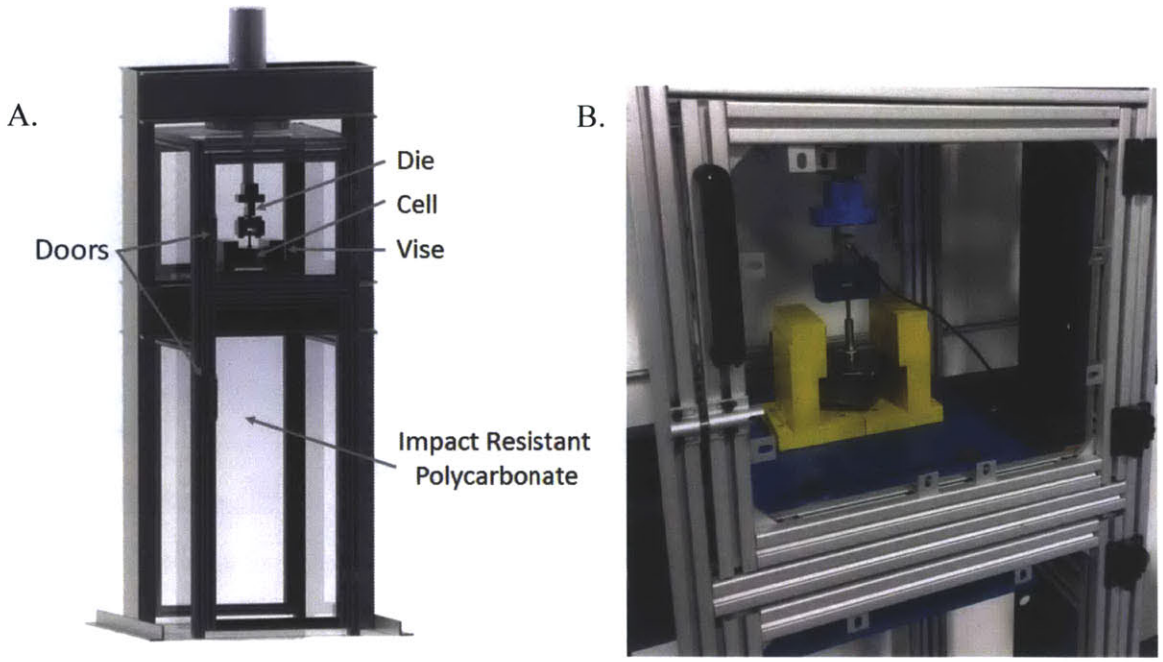


*Figure 34 - Press and Enclosure for Seal Removal A. Rendering of the Process Containment B. Implemented Design*

### 6.1.1 Safety

For the seal breaking step, the safety analysis showed that seal breaking was a fire, mechanical, and impact risk. The risks were considered substantial, which required engineered safety controls and containments. These engineering controls were directly implemented into the system.

The risk of a fire is low when exposing the active material to air due to its rate of reaction within air is slow. To deal with the chance of hydrogen gas, the installation of an inert gas drop next to the seal breaking was done to provide an inert gas blanket and dilution of hydrogen while the breaking and removal step is completed.

The risk of mechanical pressure comes from the pulling of the cell against the jig and the breaking of the seal with the double acting press. The mechanical pressure risk was reduced by placing the press within process containment.

The risk of impact is caused by the pulling of the seal, which can cause the ceramic to shatter, causing particles to fly across the room. To mitigate this risk, the containment is made with lockable doors of extruded aluminum and impact resistant polycarbonate.

### 6.1.2 Process Characterization and Testing

The characterization of the seal breaking and stem removal was carried out with a force measurement system to determine the actual breaking strength of the seal and the washer removal. The force measurement was carried out using the Mark 10 i5 with the MR01-2000 at sample rate of 20 samples per second. The data was read to a computer and captured in a Labview application. The cell used for this experiment was heat cycled five times but was not put through a charge and discharge cycle.

There were two peaks seen in the force verse time plot, Figure 35. The first peak is when the seal breaks. The second peak is where the washer is removed from the canister. The two peaks of the washer removal are hypothesized to be the force required to remove the seal from the electrolyte and to force require to spherically bend the washer for removal through the hole in the canister. Figure 35 shows the ceramic seal breaks at half of the force required to remove the washer from the canister. The washer force happens over several seconds because of the distance the stem must travel before it is placed under tension. Then it must travel through the stem hole which has a small length.

The forces required to break the ceramic are below the calculated breaking strength. This could be caused by the variability in ceramic strength which can vary in orders of magnitudes, improper joining of the metal and ceramic, or misalignment of the stem-ceramic-canister resulting in stress concentration on some parts of the seal causing failure. The seal breaking strength being lower than calculated results in the washers removal force being the highest force for the removal of the stem.

To test if the two peaks are the washer being removed from the electrolyte and the spherical bending of the washer, a control test of pulling just a washer through the seal hole should be completed.

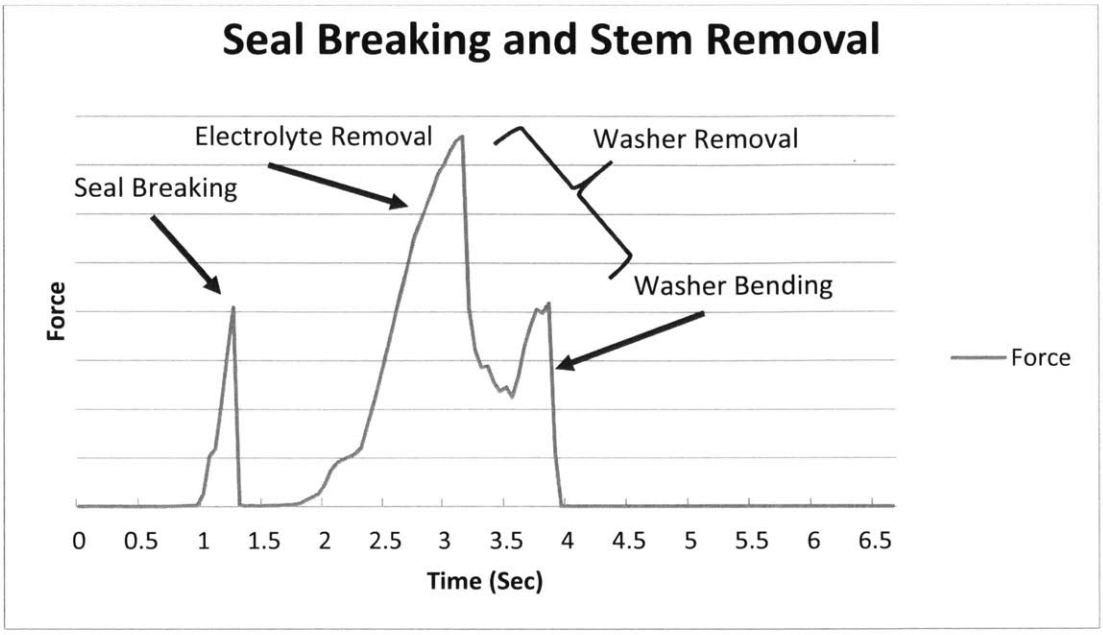


*Figure 35 – Seal Breaking and Stem Removal Force vs. Time Plot*[1]

## 6.2 Detailed Design of Cell Opening

After an extensive study of the long term cost, safety, and throughput, the cutting option suggested to Ambri is the semi-automated bandsaw. This type of bandsaw allows for the highest throughput with the lowest long-term cost per cell and has the highest safety capability with proper engineering controls. The bandsaw is to be used without cutting fluid in order to prevent the removal of oil from the cell in subsequent steps. Due to the safety evaluation, the bandsaw is suggested to be placed in process enclousure. Our ability to implement this process as described was affected by the limited amount of time and Ambri's requirement of a safe process.

The enclosure is suggested to have ventilation for the whole containment and at the source of particulate generation. The containment is to protect the user and factory from potentially hazardous particles formed during the cutting process. The enclosure was not designed or implemented because it is saw specific. The enclosure also should have an inert gas blanketing system, which will provide a constant flow of inert gas to prevent or extinguish a fire involving the reactive material by displacing the oxygen and humidity, Figure 36.

[1] Due to the proprietary nature of the batteries material composition and design, the y-axis scale has been removed.

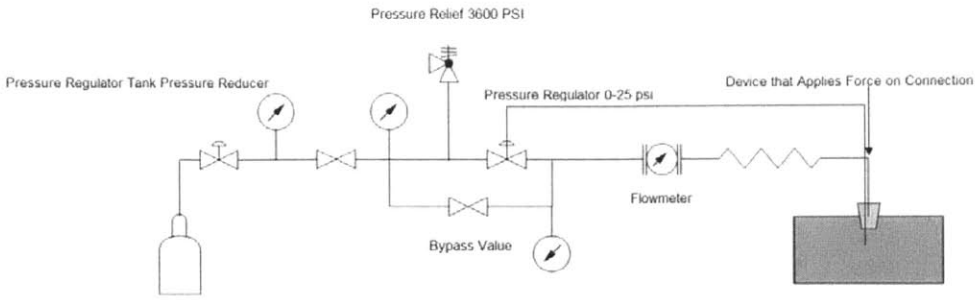


*Figure 36 – Inert Gas Dosing System for Cell Opening Process*

A cutting plan was developed in order to minimize hazardous particle generation caused by sawing. Since the cells are symmetrical within a defined tolerance, a jig is suggested to be installed which aligns the cell to be cut at .2 inches. Cutting the cell at .2 inches allows for the saw blade to not come in contact with the 63 percent of the materials types contained within the cell. Secondly, cutting at this distance allows for the removal of the radius. If the radius is not removed from the container, the die in the cell dissection step will not process the cells correctly. Lastly, the liner remains intact allowing for an inert gas blanket to remain over the active material preventing its oxidation.

### 6.2.1 Safety

Cell opening utilizes a commercial bandsaw, which has implemented safety controls; however, because it is being used to cut hazardous and reactive metals, additional safety measures need to be implemented. When the process was examined with safety analysis, the risks identified were air quality and fire. These risks were considered substantial and required engineered safety controls and containments.

The risk of a fire is low when exposing the active material to air because the rate of reaction of the active material within air is slow. Since the production of hydrogen is slow, meaning hydrogen levels can easily be diluted to level below the LEL, an inert gas drop was used to dilute the hydrogen and blanket the active material from ambient air. The safety system implemented can be seen in Figure 36. The main features of the inert gas blanket system are to put the inert gas over the active material through the seal hole. The small kerf of the saw results in the liner wall being intact after sawing, which prevents a large volume of inert gas being used to blanket the active material.

The risk of creating fine airborne material is minimized by using the proper blade; however, the chance of fine airborne material is still possible, which results in the need to place the saw within an externally ventilated containment. The containment prevents the hazardous material from becoming airborne in the operator's space.

### 6.2.2 Process Characterization and Testing

The process characterization and testing could not be completed at Ambri's Marlborough facility because no cell opening process was implemented during the course of this research work. Also, the saw at Ambri's Cambridge facility could not be operated dry without proper ventilation.

## 6.3 Detailed Design Cell Content Removal

The cell dissection process is the removal of the active material from within the battery. The input to this process is a canister with the seal and both sides removed. The part is then placed on the vise for the press to remove the content from the cell. The process step implemented at the Ambri facility also uses the Dake 25DA press to provide the force to remove the content from the canister. The final design and implemented system can be seen in Figure 37 and Figure 38.

Due to the limits in time, the new vise design was not able to be implemented at the Marlborough facility. The updated vise design has a hole between the two holders which enable the cell's contents to drop directly into the active material bucket. The design still uses overhangs to hold the cell while the die removes the content.

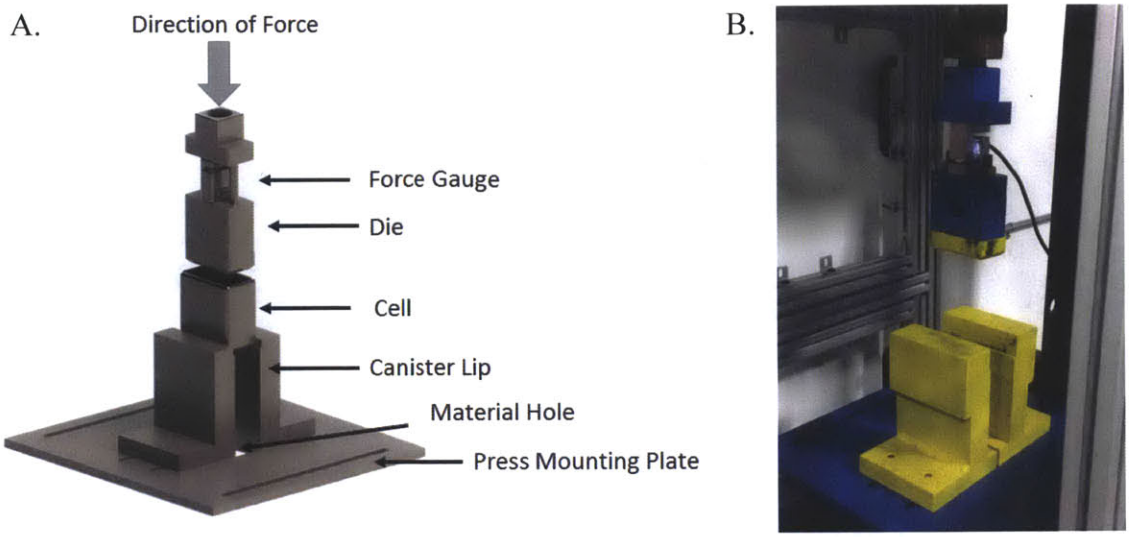


*Figure 37 - Final Content Removal Vise A. Rendering of optimized design B. Implemented design*

The best die design that was found during experimentation was used for the implemented process. The die was updated to enable to monitoring of the force required to remove the content from the cell.

In order to keep the operator safe during the removal of the active content, the press has an enclosure installed around it made of impact resistant polycarbonate which can be seen in Figure *38*. There are four locking doors on the enclosure which prevent the doors from opening if impacted by debris from the pressing of the active content. The doors also allow for easy maintenance, easy operation, and placement of the steel container. The door opens to the right in order to prevent the user from having his/her hands in the press during operation since the operator operates the machine from the right side.

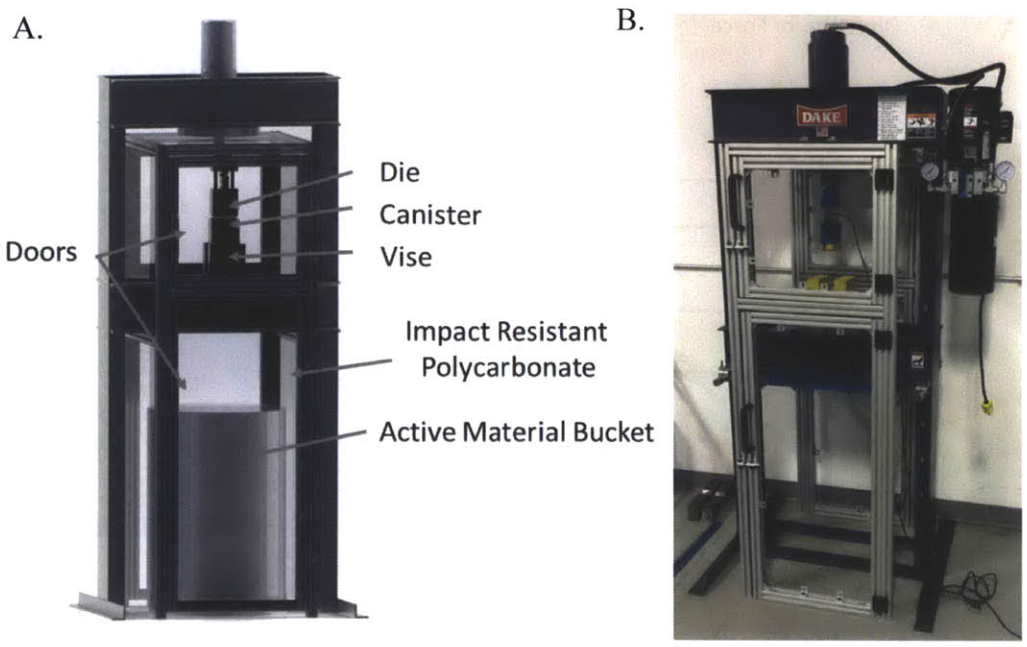


*Figure 38 - Press and Enclosure for Content Removal A. Rendering of the Final Design B. Implemented design*

### 6.3.1 Safety

The safety analysis completed for the content removal identified the risks as fire, mechanical, and impact risk. Engineering safety controls and containment were implemented because all risks were considered substantial.

The risk of a fire is low due to the lack of substantial heat generation around the active material. Also the rate at which the formation of explosive gas is produced when the active material is exposed to air is low. To deal with the chance of hydrogen gas, the installation of an inert gas purge into the removed seal port is suggested. This inhibits the formation of hydrogen gas in the cell as well as dilutes the hydrogen which reduces the chance of a fire.

The risk of mechanical pressure comes from the pushing canister up against the jig in order to remove the content. The operator's risk of getting hurt from the mechanical pressure was reduced by placing the press within the containment.

The risk of impact is caused by risk of the debris being caused by the pushing of the canister up against the jig. The containment is made of impact resistant polycarbonate and has locking doors to protect the user.

### 6.3.2 Process Characterization and Testing

The characterization of the force required to remove the content from the canister was completed with the Mark 10 5i force meter with the MR01-2000 force gauge. The Mark 10 was hooked up to a computer using a Labview application to collect the data at a rate of 20 samples per second. The cell that was tested was a cell which had been heat cycled 5 times but had not been through a charge and discharge cycle. The scale of Figure 35 and Figure 39are not the same. Figure 39's scale is around four times smaller than Figure 35.

The force versus time plot, Figure 39, shows the content removal force was significantly lower than the calculated force by about a factor of 100. This indicates the wetting of the materials to the canister is weaker than anticipated which enables the process to easily remove the crucible. The force is almost constant over time the stamp is pushing the content from the canister. This could have been caused by the interaction of the die and the canister wall and not the shear strength of the contents separation from the canister wall. This was also indicated by the removal of the paint from the die.

The force gauge did not go back to zero because the canister was still adhered to the die when the measurement was stopped.

In order to determine the actual force required to shear the active content from the canister, the die cannot touch the sides of the cell at any point during the experiment. Due to time constraints, this experiment was not able to be completed.

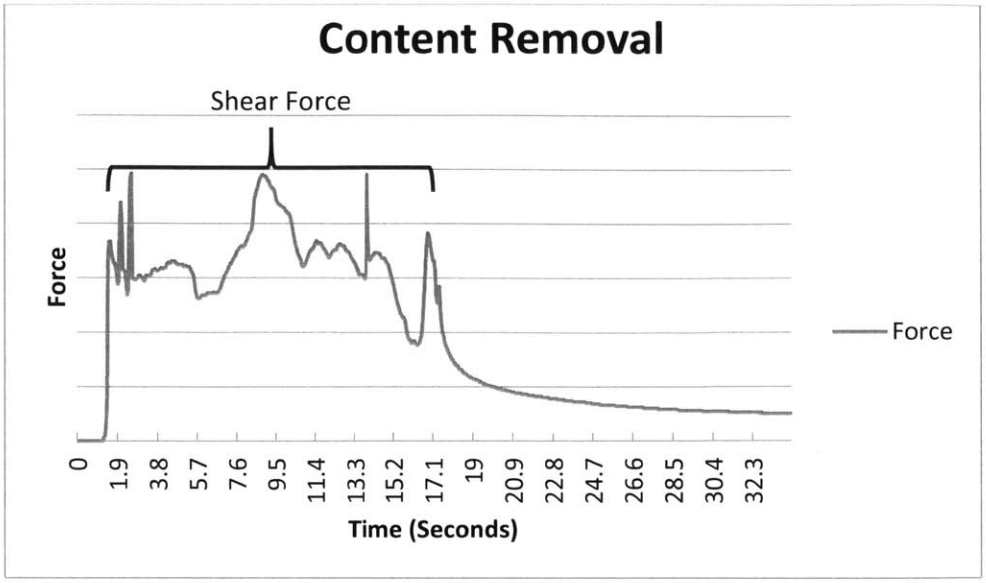


*Figure 39 - Force vs. Time Graph of the Content Removal Die*[2]

## 6.4 Detailed Design Aqueous Wash

The system was design to provide robust, reliable, and safe use; however, if the design is not used properly, the chemicals contained within can cause harm to the operator and/or factory. The design has numerous safety features which can prevent most failures from doing harm to the operator and/or factory, but these safety features need to be utilized and fully implemented. Due to the short time spent and other factors at Ambri, the MIT team was not able to fully implement all system features as intended by design.

A basic system description is the cells are placed into a cell holder which is placed inside of the reaction vessel. The cell holder allows for the cells to be placed in the proper orientation for a fast and controlled reaction. Once the cell is placed inside the reaction vessel, the airtight lid is installed and secured. The reaction liquid is then transferred from the storage tank to the reactor via a course filter and pump. Once the liquid is in the reactor, the liquid is circulated through the course and fine filter to remove particulates and heat exchanger to keep the reaction temperature as low as possible.

[2] Due to the proprietary nature of the batteries' material composition and design the y-axis scale has been removed.

### 6.4.1 System Design

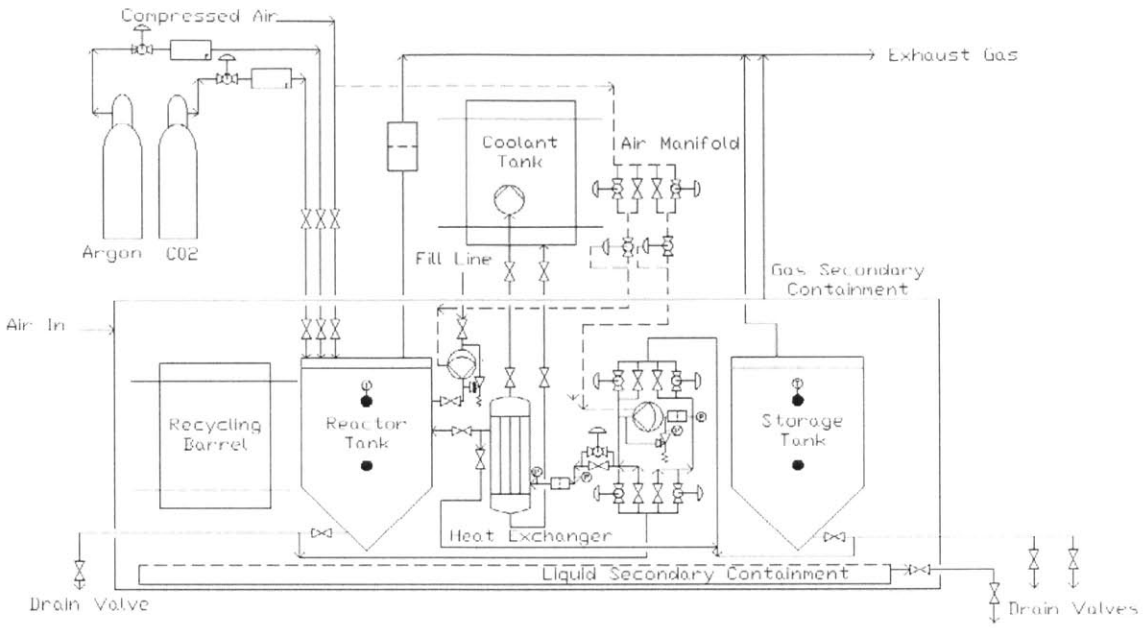


*Figure 40 - Aqueous Wash Pipe and Instrumentation Diagram*

The system is designed to operate off of one process pump. The pump selected is a positive displacement air operated PVDF Sotera SP100 pump with a maximum pressure of 100 psi and a maximum flow rate of 17.5 gallons per minute. The pump can be controlled either manually or automatically with the installed solenoid valve which controls the air supply to the pump. The pump speed is controlled through the modulation of the control air pressure which is accomplished with a pressure regulator. Since the pump is a positive displacement pump, pressure relief valves were installed to prevent over pressurization. A high flow rate is required for the evacuating of the reactor in case of emergency and the removal of heat during the process. The implementation of the process pump, relief valve, and air manifold can be seen in, Figure 41.

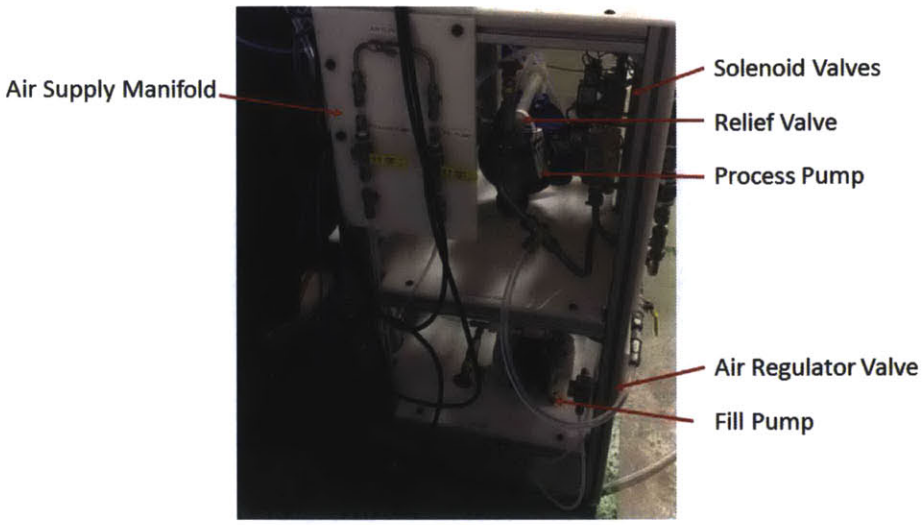


*Figure 41 - Side View of Implemented Process*

There are two neo logic filters installed within the system. The filters were selected based off of the system design temperature of 60$^{O}$C, max flow rate of 17.5 gpm and 7 gpm for the heat exchanger, and chemical resistivity. The filter has a body mode of 316 stainless steel and filters made of polyethylene. The course filter is 100 microns and the fine filter is 50 microns. These sizes were selected based on the anticipated particle size generated in the system. To determine when the filters have become clogged an inlet pressure gauge and outlet pressure gage was installed to monitor the differential pressure. Once, the differential pressure becomes above 10 or 15 psi the filters should be changed.

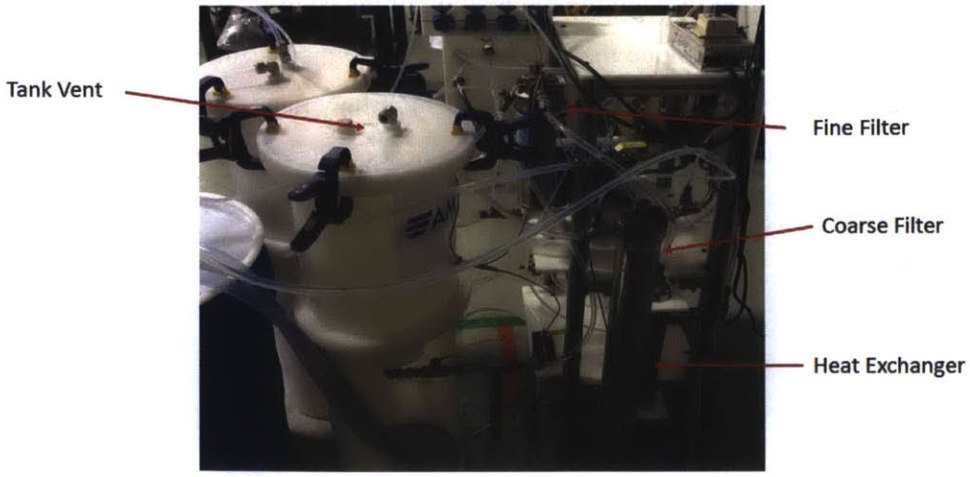


*Figure 42 - Back View of Implemented Process*

In order to run the system on one pump, a manifold was designed to reverse the flow from the tanks and circulate the flow through the heat exchanger, Figure 43. Only the addition of one valve is required for the heat exchanger, because it is circulating into either the storage tank or reactor. All solenoid valves installed in the system are of the fail close design, Figure 41. The system was designed with manually operated ball valves to allow for a manual operation mode. The pump manifold was placed on a HDPE sheet with the solenoid valves placed on the backside in order to reduce the visual clutter for the operator. The solenoid manifold is made out of 316 stainless steel tubing and PFA tubing.

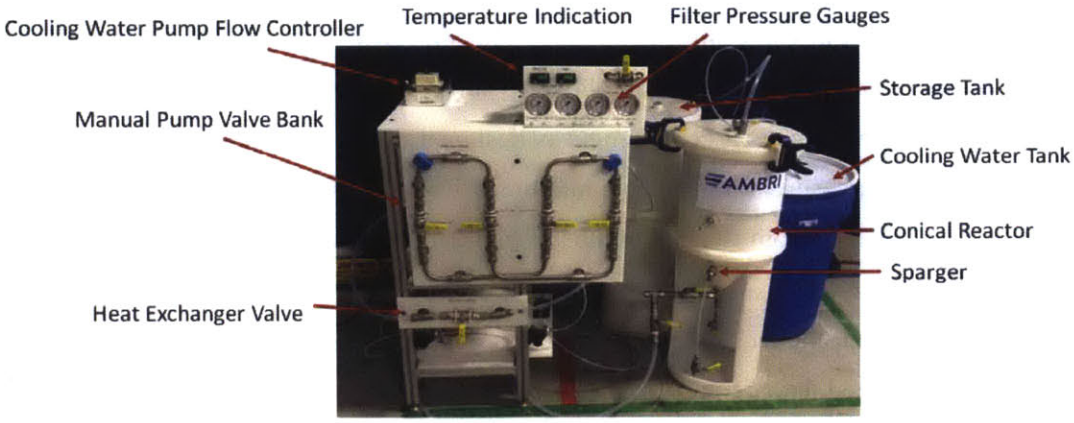


*Figure 43 - Implemented Process at Ambri in the Marlborough Facility*

A shell in tube heat exchanger made of 316 stainless steel and had a heat removal capacity of 164 kJ was used. The heat exchanger should have the fluid be in the counter flow configuration. This allows for the greatest heat transfer efficiency to be obtained due to it having a higher average temperature differential than a parallel flow heat exchanger [42]. The heat exchanger was connected to the 8020 process stand with water jet HDPE mounting brackets which were integrally supported by the shelves, Figure 42. The cooling liquid is circulated by a centrifugal pump capable of circulating 8.3 gallons per minute. The cooling water pump is controlled by varying the voltage to the Rules centrifugal pump. The cooling liquid needs to have a temperature differential in order to provide enough heat transfer to keep the reaction vessel below 60 °C. To create a temperature differential, it is suggested ice be placed within the cooling water tank to create at least a 10 °C temperature difference which was seen in the characterization. The cooling water tank has a 30-gallon water capacity. To prevent algae formation, the cooling water should be treated with 0.2-10 ppm chlorine with a pH of 7.4 [43].

A recycling barrel should be placed inside the containment to allow the transfer of the reacted cell remains to the recycling barrel without them leaving the liquid containment which prevents contamination of the factory.

### 6.4.2 Reactor Design

The reactor was designed to contain the violent reaction which occurs during the neutralization of the active material. The reaction vessel selected for the implementation was a conical reactor made of high density polyethylene, Figure 43. The conical reactor is easy to clean, and provides easy draining. From the study of the fluid flow through the reactor, the circulation inlet was placed as close to center as possible in order to have uniform flow over the cells. The cell arrangement to have uniform flow is seen in Figure 44. The porous cell containment need keeps the cells in the proper orientation. The cell containment is designed to have a bottom that swings open, allowing for the direct emptying of its contents into the recycling barrel. The containment must also prevent the reactive material from floating to the top in order to prevent off gas from being ignited.

In order to prevent the leakage of gas from the conical tanks, they have o-rings seals. The tank top and tank are placed under compression through the utilization of three robust plastic clamps. Plastic clamps were used they reduce the chance of failing due to corrosion.

The baffle installed in the reactor was seen in the CFD model to assist in maintaining a homogeneously mixed solution around the cells. The baffle also increases the residence time of the sparge gas which increases its ability to diffuse into the solution, allowing for more efficient use of the gas. The sparger is used to input the inert gas and $CO_2$ into the reactor to insure adequate mixing and distribution within the reactor.

The reactor is filled from the bottom in order to slowly submerge reactive material into the reaction solution. This helps prevent the reactive material from reacting without having adequate cooling ability to prevent the ignition of the off gas. The reactor is drained from the bottom to allow as much solution to be drained from the reactor as possible.

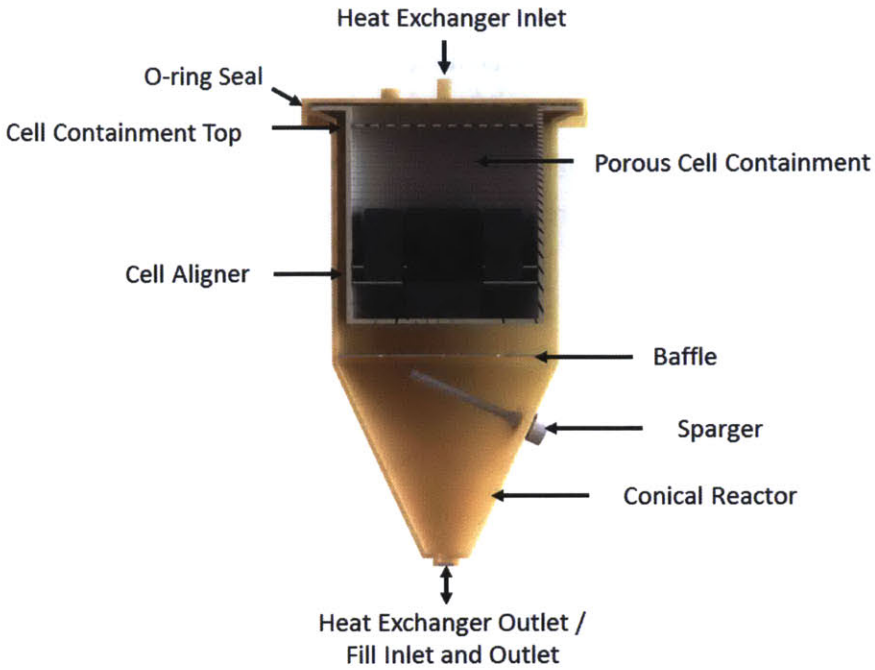


*Figure 44 - Conical Reactor Design*

### 6.4.3 Safety

The aqueous wash system has numerous safety concerns as the chemicals and reaction produce toxic gasses and hazardous aqueous solutions. The system was carefully designed in order to minimize the probability of a failure through proper design, material, and fitting selection. The safety precautions implemented and suggested are necessary in order to operate this process safely. Not only is it important to properly handle but also to properly store the chemicals that are produced.

Proper storage and handling of the chemicals and gas entails insuring the chemicals pose little to no harm to the operator. The chemical stability of the material was considered to ensure parts do not fail and cause harm to the operators. Safe handling also requires proper containment of the solution in case of a spill. This was accomplished by placing the system on a secondary liquid containment. The placement and movement of the reactive and reacted material was made ergonomic and safe with dull corners and safety protocols. The potentially wet reacted material is placed into the recycling barrel within the secondary containment to prevent leakage of the aqueous solution from the system. The reacted material should be dried with air to reduce dripping of the material once reacted and remove hazardous gasses from the reactor.

The gasses produced from each cell are both flammable and toxic, meaning the gasses must be properly handled to dilute and rendered inert for the environment and user. This was accomplished through the exhausting of the gasses through an induced draft ventilation system, inert gas dilution, and a charcoal filter. Leaking of the gas out of the airtight reactor was also considered to be hazardous to the user. This resulted in the process being placed inside a ventilated secondary containment.

In order to prevent a runaway reaction due to the formation of heat within the system, a heat exchanger was installed with a cooling water reservoir. If a runaway reaction does occur, removing the aqueous solution stops the reaction. This is accomplished with a pump that can empty the container within 30 seconds from when the temperature rises to the alarm set point.

The system has a valve bank which allows one pump to service the transferring of liquids between vessels and cooling of the liquid. The values which control transferring and cooling should be automated to decrease the risk of the operator not properly operating the system and causing harm to the operator or factory.

If a system failure does occur, it is of paramount importance that the operator is wearing proper safety equipment, because the solution contained within the system is dangerous to life and limb. Proper personal protective equipment includes, but is not limited to, safety glasses, face shield, liquid handling apron, lab coat, chemical resistant boots, and gloves.

### 6.4.4 Process Characterization and Testing

Process characterization and testing of the system before being placed into service is the upmost importance to ensure that it runs as designed and properly operates. Testing and commissioning of the aqueous wash requires additional wash personal protective equipment to insure the safety of those involved and the factory.

The first test run on the system was the circulation of water. This was to identify any leak in the system with a non-toxic substance. The water was circulated several times, then the outlet valves were throttled to test pressurize the system to its maximum operating pressure set by the pressure relief valve. Once all leaks were found and fixed, the system was allowed to move to the next phase of testing.

The next test that was conducted was the charging of the system with a partially saturated solution which provides slowing of the reaction of the reactive material. The solution was first mixed using a mono-hydate solid with a measured amount of water added. The pH of the solution was used to determine the molarity of the solution. Once the solution was mixed, a small pure sample of the reactive material was added to the system. This was done to insure the reaction could be safely handled within the reactor. This small scale reaction showed a temperature differential of $10^{o}C$ . The heat exchanger was able to reduce the reactor temperature by about $0.1^{o}C$ every 45 seconds of operation during the 25 minutes experiment. The rate of cooling seemed to decrease over the reaction time which was to be expected due to the non-isothermal cooling water tank and varying temperature difference.

To study the decrease in heat transfer with respect to the temperature differential between the reactor and cooling water tank an experiment was conducted. The experimental setup was the operation of the heat exchanger loop and cooling water loop without active material to eliminate the addition of heat energy in the system; however, due to the high ambient temperature of on average $27.7\ ^{o}C$ during the experiment a close to adiabatic process was not achieved. The heat transfer into the system is assumed to be not negligible due to the large amount of surface area for heat transfer to occur. Also, condensation was seen on the side of the cooling water tank, and heat exchanger indicating heat transfer between the system and surroundings. The experiment was conducted with the process pump running at 50 psi which is half the rated operating pressure. The heat exchanger was arranged in the parallel flow configuration, not the counter flow configuration. This means the heat exchanger efficiency in the counter flow arrangement will be increased significantly over the stated values. The heat exchanger loop had a partially saturated aqueous solution and the cooling water loop used water. The temperature for both tanks was recorded each minute.

The plot of the temperature of the tank over the 33-minute experiment is plotted in Figure 45. This plot shows that the rate of heat transfer was decreasing with respect to the temperature differential between the cooling loop and heat exchanger loop. The difference in rate of temperature change between the reactor and cooling tank is because of the difference in reactor volume to cooling water tank which is about 1:5. The linearity of the cooling water tank indicates the heat exchanger is operating in its designed range with an increase in temperature of $.2\ ^{o}C$ / min.

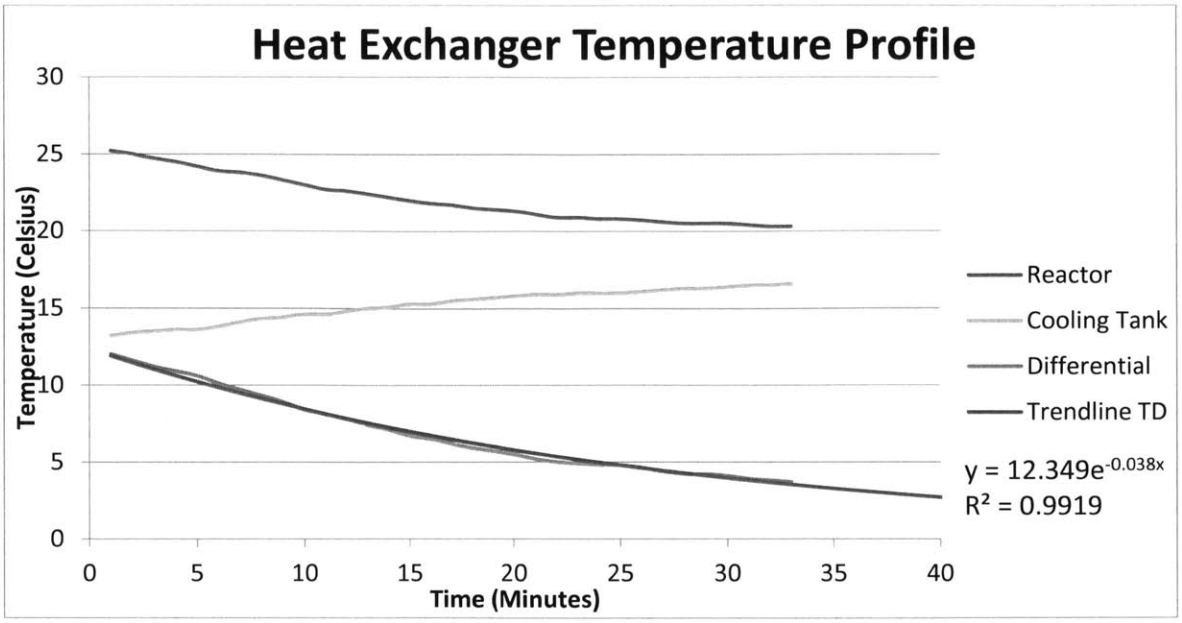


*Figure 45 - Temperature vs. Time Profile for Parallel Flow Heat Exchanger*

Due to the rate of heat transfer being proportional to the rate of temperature changem, which is related to the temperature difference between the two media, the temperature differential was calculated and an exponential regression was calculated, equation 16. The exponential function derived is

$$y = 12.349e^{-0.038x} \qquad (16)$$

Where $y$ is the temperature difference and $x$ is the time. The quality of fit was found using the coefficient of determination given by equation 17 [41].

$$R^2 = 1 - \frac{SS_{res}}{SS_{tot}} = .9919 \qquad (17)$$

Where $SS_{res}$ is the sum of squares of the residuals, and $SS_{tot}$ is the total sum of squares. Given the $R^2$ value is high the model adequately reflects the system trend. Using the temperature differential model, the rate of temperature change was calculated by taking the derivative of equation 15. The derived equation is provided in equation 18.

$$\frac{\Delta T}{\Delta t} = \frac{dy}{dx} = -0.047e^{-0.038x} \qquad (18)$$

Where $\Delta T$ is the change in temperature and $\Delta t$ is the change in time. Combining equation 15 and 17 allows for analytically solving for which temperature difference gives you the desired amount of heat transfer from the system, equation 91.

$$\frac{\Delta T}{\Delta t} = -0.047e^{\ln\frac{y}{12.349}} \qquad (19)$$

Figure 48 plots the cooling rate versus the temperature differential which graphically represents equation 16 and 18.

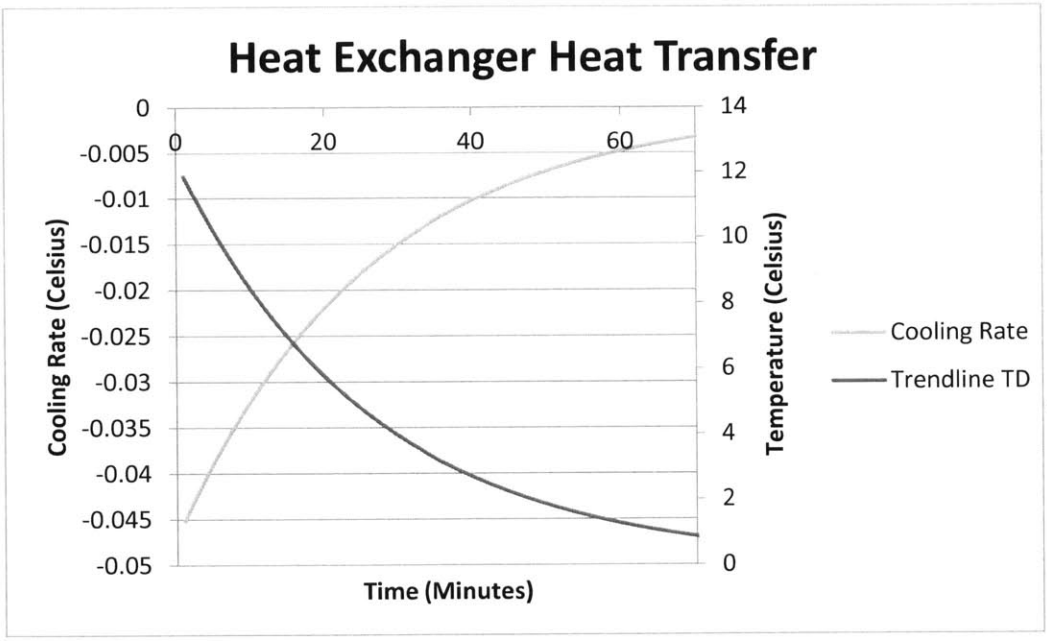


*Figure 46 – Parallel Flow Heat Exchanger Cooling Rate*

To determine the effect of no cooling of flow on the temperature, the equivalent of one cell's active material was reacted within the reaction vessel. Temperature data was taken every minute and was plotted in Figure 47. The ambient temperature of was 27.7 $^{O}$C, and during the experiment a close to adiabatic process can be assumed because no circulation took place. The reaction solution used was a partially saturated aqueous solution of the active material. The max temperature increase seen was 3 $^{O}$C. The temperature increased until the reaction was complete, at which point a slight temperature drop occurred due to the lack of mixing causing a temperature gradient in the reactor. The waviness in the data is hypothesized to be caused by the mass transfer limit being reached around the active material because of the lack of flow and the line's linear trend.

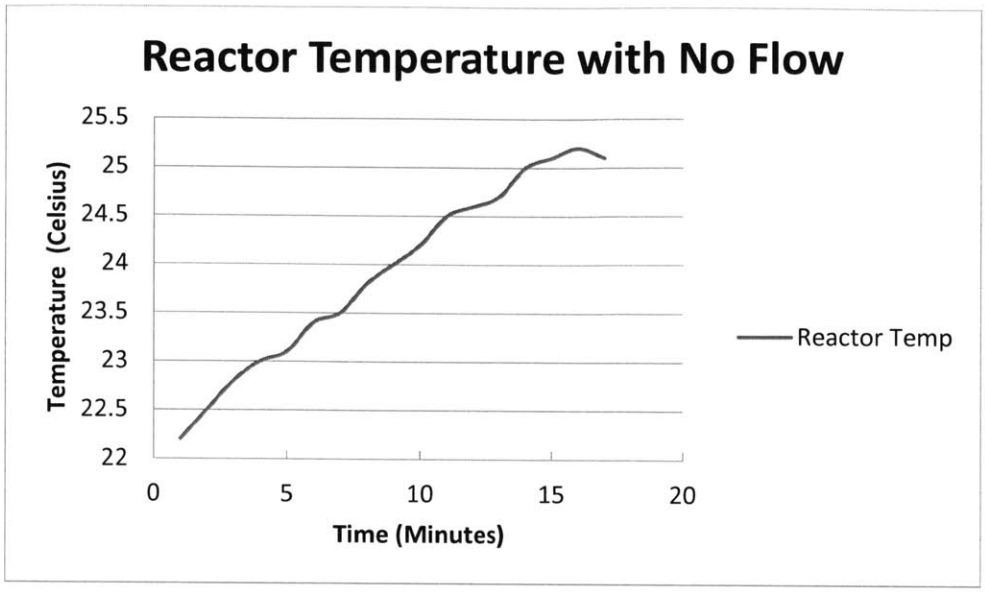


*Figure 47 - Reactor Temperature with No Flow*

The last experiment undertaken was the characterization of the system containing the equivalent of 5 cells of active material. The experiment was conducted with an aqueous solution containing a half saturated solution of active material. The solution contained no other common ions during this experiment. The ambient temperature was 27.7 $^{O}$C. The heat exchanger was in the parallel flow configuration. The process pump was operated at a pressure of 50 psi. Temperature data was collected for the reactor and cooling water tank in one minute increments, Figure 48.

The reactor temperature plot shows a parabolic shape which indicates the heat exchanger was not able to remove all of the heat of the reaction; however, the heat exchanger was able to limit the maximum temperature rise to 2.9 $^{O}$C which is within the acceptable limits temperature rise. The amount of heat released into the system is a function of multiple factors within the system making the rate of energy release hard to quantify analytically but was examined experimentally.

The data for the cooling water tank for the first two minutes indicates there was a temperature gradient with in the cooling water tank giving an artificially high reading. The temperature increase of the heat exchanger is more linear because the temperature differential stays within 1 $^{O}$C for the first 17 min of the process. A slight slope change be seen at 17 minutes which is expected because of the narrowing of the temperature differential. The linearity of the cooling water tank indicates the heat exchanger was able to on average increase the cooling water tanks temperature by .2 $^{O}$C / minute.

The temperature differential is always decreasing which indicates that the heat exchanger has not exceeded its capacity to cool the system. Once the addition of heat is no longer exceeding the rate of heat transfer to the cooling water tank - around 17 minutes, the temperature differential slope is seen to increase.

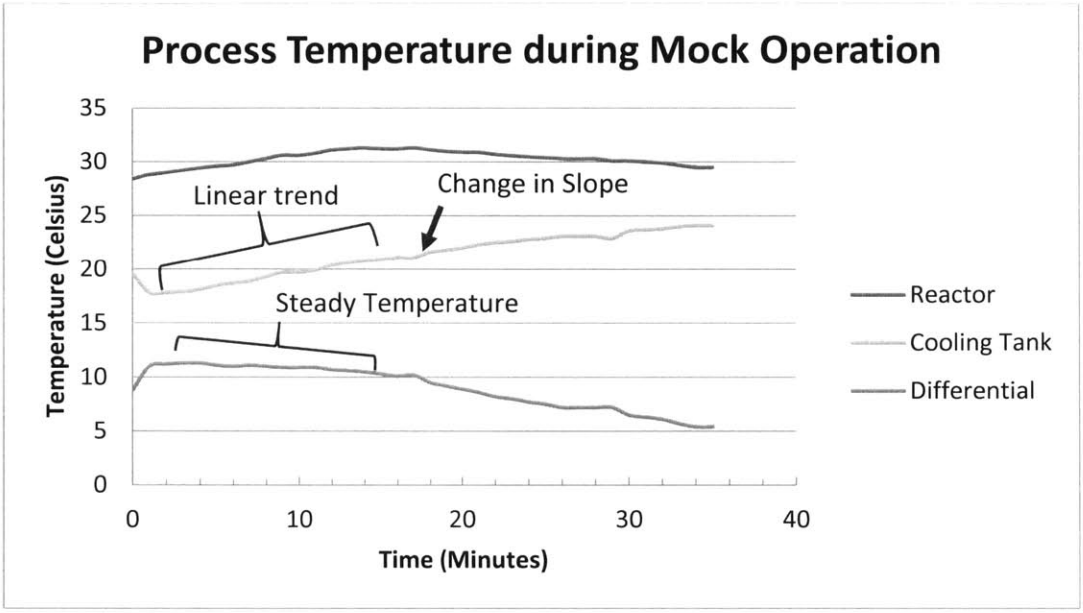


*Figure 48 - Temperature vs. Time Graph of Process Operation during Experiment*

The MIT team was not able to complete a more through characterization due to time and safety limitations.

## 6.5 Factory Layout

The placement of the process equipment is important to reducing operator fatigue, decrease factory contamination sources, and optimize material flow. The space dedicated to the recycling process is an 18 foot x 12 foot section. The footprint constraints and material flow path were both considered in the placement of the machines within the cell. In Figure 49 a rendering and schematic of the process layout is shown in order to provide a visualization of machines placement and material flow.

Given there is a dedicated piece of machinery for each of the process steps, the machines were placed in the order of the process steps outlined, Figure 31. In order to fit all the machinery within the allotted space, the machines were placed in a U configuration, resembling a Toyota production cell, which optimizes material flow and decreases operator fatigue. The only difference is an operator must use the bandsaw twice per cell cycle. Through the recycling process cell analysis, it can be seen the bottleneck is the aqueous wash system, which means an additional bandsaw is not required.

A.

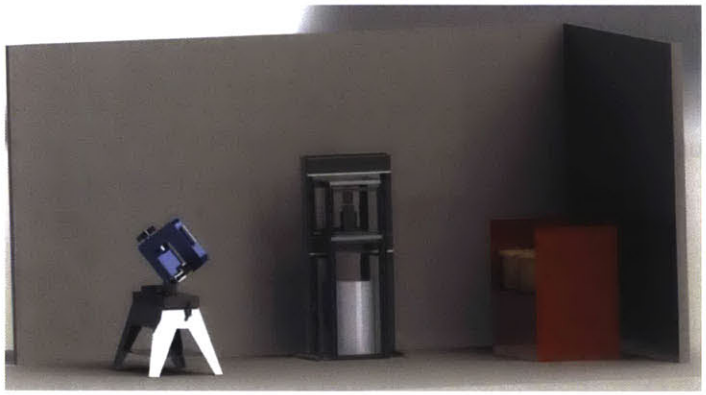

B.

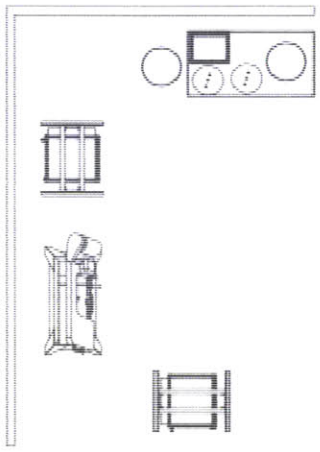

*Figure 49 - Factor Floor Layout A. Rendering of implemented process B. Schematic of future process*

## 6.6 Cost Analysis

To determine the economic viability of the developed process, a detailed cost analysis of the system was performed. A time study was completed to determine the labor cost of the different systems. Disposal, scrap metal, commodity, and wholesale prices were used to determine cost of operating the system. The goal of our system was to operate at a minimum of 5 cells per 8 hour working day; however, the throughput is 40 cells per working day as long as the water temperature of the aqueous wash system is controlled.

When Ambri starts production of its cells, the only means of disposal is through incineration because the research and development process can no longer be used. The cost model shows that significant saves can be achieved through the utilization of the developed process.

The current Ambri research and development system removes the active material from the cell and disposes of the stainless steel canister as hazardous waste and active material as hazardous waste that must be incinerated. Removing the active material allows for the steel canister to be disposed of as less hazardous waste, which reduces the cost of disposal for fifty percent of the weight by two orders of magnitude. There is an increase in the labor required to open the cells.

The implemented process at Ambri removes or converts all hazardous material from the cell, allowing them to be recycled or disposed of cheaply. The content from the stainless steel container is removed, allowing it to be recycled. The active material then reacted which produces an aqueous solution, which is two orders of magnitude less expensive to dispose of. Then the cathode material can be recycled a scrap metal and the remaining content can be disposed of for little to no cost.

The future process can take the aqueous solution produced by the active material and turn it into a reusable commodity. The commodities that can be recovered will be of high purity and command a high price in the market. At this point, the process will be able to help pay for the direct labor required to separate the components, and if a high enough price for the commodities produced can be commanded, then the process could even break even. The analysis was completed assuming Ambri can only get fifty percent of the commodity price or the bulk wholesale price. With the implemented recycling process Ambri can recover $1/20^{th}$ of the cost of the cell by recycling. The recovered cost comes from the sale of the scrap metal generated during recycling and is debited in the cost comparison model to the direct labor cost.

Given the model parameters, the relative cost break down is given for the four processes relative to the incineration cost is graphed in Figure 50. The current research and development process is a 48% cost savings. The implemented process is an 83% cost savings. The future recycling process could operate will below 8% of the incineration cost and has the potential to generate money for Ambri.

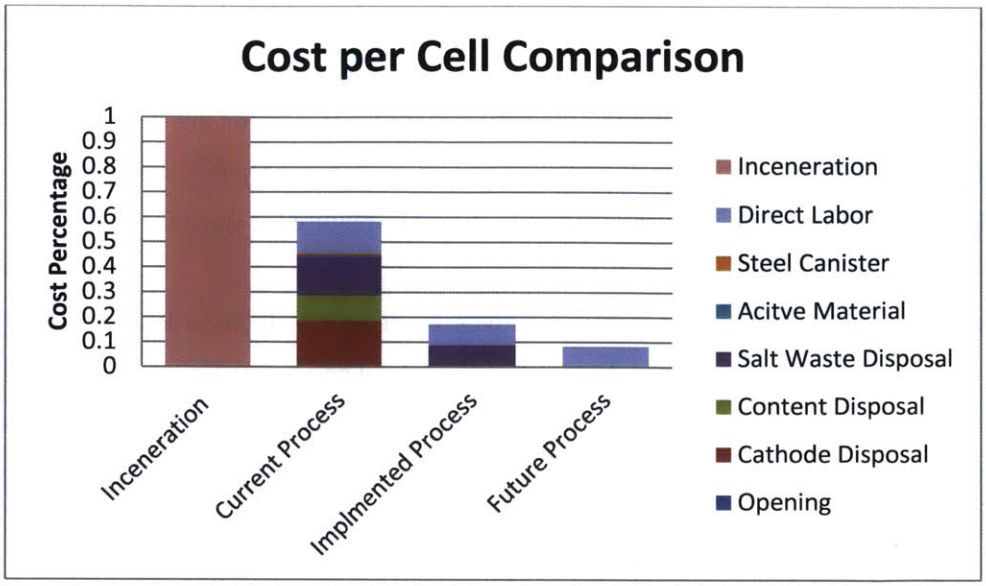


*Figure 50 - Cost per Cell Comparison between the Four Recycling Processes*[3]

By taking a look at the implemented process cost breakdown, the cost is overwhelmingly dominated by two factors the direct labor at 49% of the cost and salt waste disposal at 49.5% of the cost. Figure 51 shows that in order to bring costs down, further process development needs to focus on bringing down direct labor costs and minimize or eliminating the salt waste disposal cost. This graph also shows that the implemented process minimized high-cost waste streams but even the low cost waste streams dominate the cost of recycling each cell.

[3] The cost per cell is displayed as a percentage due to the proprietary nature of AMBRI's cell composition and recycling costs.

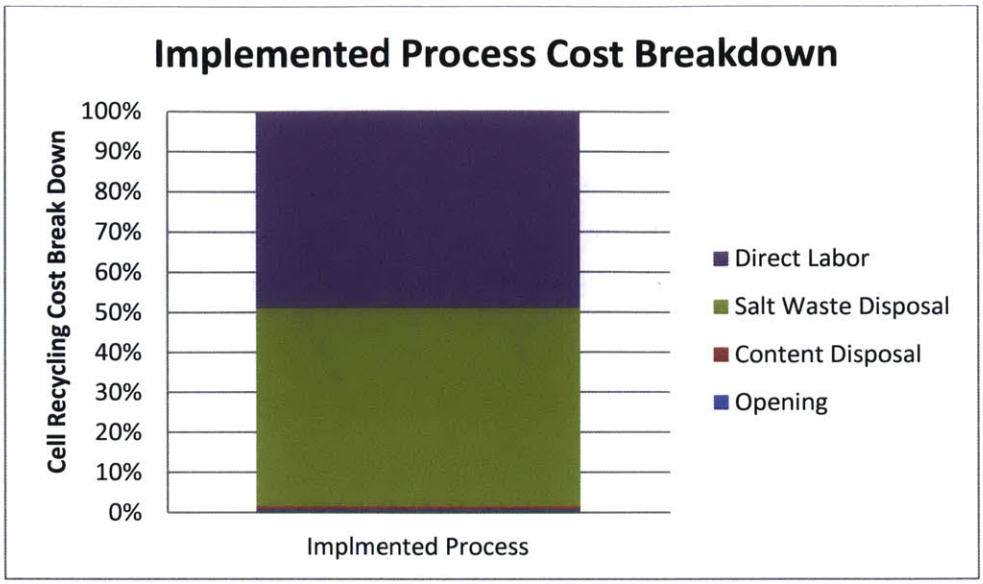


*Figure 51 - Implemented Process Cost Breakdown*[4]

The cost savings Ambri can achieve through the utilization of the recycling process was calculated using the recycling cost determined in the cost comparison model, Figure 50. The process has the ability to recycle 40 cells per working day on average. In 2014, there are 251 working days. This results in the implemented process having a throughput of 10,040 cells per year. If the process was operated for one year at capacity, a cost savings of around one million dollars over incineration or a cost savings of around five hundred thousand dollar over the current research and development process would be realized by Ambri.

# 7. Recommendations, Future Work, and Conclusion

## 7.1 Recommendations

Through the MIT and Ambri collaboration a liquid metal battery recycling process was developed which exceeded the initial requirements. The process is designed to be modular and flexible in order to handle new process chemistries and cell designs. This design allowed the process to be implemented within the budget and timeline specified; however, this design allows for the process to be upgraded allowing increased flexibility, throughput, efficiency, safety, and decreased cost.

[4] The cost per cell is displayed as a percentage due to the proprietary nature of Ambri's cell composition and recycling costs.

Due to time constrains, not all process steps could be fully implemented as envisioned. The recommendations are feasible and should be implemented in the immediate or near future to improve the implemented system's safety, flexibility, and throughput. Full process characterization was also not completed to the level require for a complete process understanding. The characterization recommendations are suggested to be completed in the near term in order to develop a more fundamental understanding of how the cells react in the recycling environment under all conditions.

### 7.1.1 Process Improvements

Process improvements are suggested in order to increase the recycling process' capabilities and increase Ambri's knowledge of the system. Most suggestions centered on the final implementation of the liquid metal battery recycling process. The implementation of the suggestions will allow for the recycling process to be implemented to operate as designed and safely.

### 7.1.2 Seal Breaking and Stem Removal

The automation of the press is recommended in order to provided one or more safety interlocks to prevent the operator from having his/her hand caught between the press and to insure the process containment is being properly utilized. This can be accomplished with a simple microcontroller, and hydraulic solenoid valve.

The seal breaking process step currently relies on a cell feature which has an unknown life in the seal and battery design. This mandates a change of the system to a force application method that can grab onto the stem and pull it out. The suggested method of grabbing the stem is with vee block wedge grips with the appropriate force ability. Wedge grips take two forms: pneumatic/hydraulic and manual. The investment in the automatic wedge grips is suggested because it drops the time per cell and is a more repeatable application of force. The wedge grip options found that fit Ambri's application are from Instron, MTS Systems Corporation, and TestResources. The quotes or datasheet is provided for these options in the appendix.

The seal breaking and stem removal process has the ability to monitor the breaking strength of the cells overtime and off the production line. Currently, there are no standards for the breaking strength of the seal and it is suggested that a specification be set in order to monitor the seal overtime.

### 7.1.3 Cell Content Removal

The content removal press should also have process automation in order to provided one or more safety interlocks to prevent the operator from having his/her hand pinched and to insure proper utilization of the process containment. The press automation provides the operator with a safer working environment.

The die design for the content removal system can be further improved to remove more of the material that adheres to the sides of the canister wall. The removal of this material will improve the quality of the scrap metal allowing Ambri to get a higher price for the scrap metal produced in this process step. This could be accomplished with a thin piece of spring steel acting as a scraper on the side walls.

The implemented die design has the ability to collect data on force required to remove the content from the canister. There should be quality control standards implemented in order to utilize this new cell monitoring capability.

### 7.1.4 Aqueous Wash

The aqueous wash system also needs to have its safety improved before it can be utilized as an industrial process. The gas secondary containment is suggested to prevent the release of flammable and hazardous gasses into the operator's space and factory floor. The gas containment needs to have the air pulled from the containment, not pushed into the containment, as this prevents pushing the gas out of the inevitable small holes. The containment's sides are suggested to be made out of acrylic side panels. This allows for the visual monitoring of the process, and acrylic is chemically resistant to the solutions within the system. The structure is suggested to be made out of 8020 6061 aluminum for easy assembly and modification.

The liquid secondary containment should be capable of holding a minimum of 20 gallons, which is the maximum volume the system can hold. The material selected needs to be chemically compatible with aqueous solution inside the system. The suggested material is polyethylene. The liquid containment should be fully enclosed within the gas containment. This is illustrated in Figure 40.

To improve the aqueous wash systems usability and safety further, the implementation of the planned process automation should be undertaken. The system is outfitted with normally closed solenoid valves with bypass valves which allows for manual operation. The implementation would allow for the solution to be transferred from the tank to reactor. In addition, the implementation of a control system the process could be controlled with automatic set points, and alarms. This functionality would allow the system to detect reactions that are out of control and respond by flooding the system with argon and pumping down the reactor in order to stop the reaction. A control system improves the system usability by an operator.

The other major process improvement that should be undertaken is the processing of the aqueous solution as this is 49.5% of the cell recycling cost. Currently, the system is capable of controlling the pH which causes the precipitation of a salt. This allows for the electrolyte salt saturation limit to be reached instead of hydroxide solution limit. Once the electrolyte salt saturation limit is reached valuable salts can be formed by bubbling $CO_2$ through the solution until a pH of 7 is reached. With the heating of the solution, valuable salt will precipitate out of solution and with filtration can be collected and sold. If it proves more economical, Ambri could add a more reactive carbonate into solution to precipitate out more of the valuable salt. The remaining salts can be recrystallized through the use of an evaporative recrystallization process utilizing solar energy. Depending on the purity and composition of the salts, Ambri could sell the salts or purify and put the salts back into the system. The salts composition can be characterized with a capillary electrophoresis to determine the best option.

### 7.1.5 Characterization

The implemented system that has been developed handles the cells without oil, at ambient temperature, and minimizes inert gas usage. To safely move this process forward and achieve the highest throughput and lowest cost, further scientific characterization on all process steps needs to be undertaken.

During the seal breaking, the cell's active components can be exposed to a non-inert environment for the first time since manufacturing; however, if the reason for recycling is a failed seal, the content of the cell has had long term exposure to the environment. It is important that cells of both types have their composition and off gasses monitored during seal breaking to insure no unexpected gasses are produced. This characterization should be done on cells which have undergone different

numbers of charge and discharge cycles. The gasses collected from the battery should be analyzed with gas chromatography - mass spectrometry.

In order for open cells to be placed in a buffer both unopened and opened cells need to be need to be tested and characterized for hydrogen and toxic gas production due to seal being removed and the active material being exposed to the environment. The experiment suggested is to take several cycled cells and expose them to a known atmosphere with 100% humidity. The flow rate across the cell should be varied between cells. The experiment should be conducted for no less than 1 hour at 30 degrees Celsius. The analytical method to determine the gas composition of the gases vented from the cell is gas chromatography - mass spectrometry. Until this is completed proper personal protective equipment and the amount of time the cell spends out of ventilated process containments should be limited.

The cell opening process step needs to undergo active material and gas monitoring to insure the active material is not heated and gasses are not produced during cutting. It is strongly suggested that the cutting method which has a directed chip stream be employed as the particles produced can be hazardous for the operator to inhale or touch. Until a study of the particulates formed by the cutting method is completed, the operator should wear proper respiratory protection as well as any additional protective equipment required.

The recycling process also needs to be characterized under the laws and regulations which govern the recycling processes in Massachusetts and the United States of America. The Ambri process was designed in order to meet requirements as interpreted by the MIT team, but a thorough analysis needs to be completed by a third party recycling process law firm who understands the current laws governing recycling processes.

Once the process is fully implemented, the entire process needs to undergo an accurate time study. A time study will determine the amount of direct labor per cell. The time study also provides insights on where future development needs to occur in order to bring direct labor costs down through the identification of bottlenecks. An accurate study of the working process will also provide data for the determination of the feasibility for process scale up.

## 7.2 Future Work

Through the course of the engagement between MIT and Ambri, the focus was the implementation of a recycling system which had potential for scale up; however, the detailed economic analysis of sale up and feasibility study was not completed. For this analysis, all recycling options and related costs should be reconsidered for the final commercialized cell chemistry and design.

As seen in the cost analysis of the recycling processes, Section 6.6, the direct labor costs per cell is going to be the highest cost of the disposal process once the waste streams are fully minimized. In order to bring down the direct labor costs, it is suggested Ambri explore the possibility of implementing a robotic arm into the system. The implementation of a robotic arm and fully automating the system allows for a decreased safety risk for Ambri employees because they would no longer be exposing their people to the hazards of the active materials and for a decrease in direct labor per cell required because the robot handles the work. The process layout could easily be modified to accommodate a robot due to its layout already being in rectangular. The process lends itself to automation because of its high repeatability and eventually higher throughput requirements.

Due to the mass of the batteries, it is important to consider the possibility of a mobile recycling process which could recycle the batteries at the decommissioning site. The ability to bring the recycling process to the decommissioning site would reduce the transportation costs because the recycling process would weigh less than large installation of liquid metal batteries. The main obstacle identified is the contracting with local metal and salt recyclers. Mobile recycling has been successful in the paper recycling industry.

Once the final battery chemistry is commercialized with a large installed capacity, a closed-loop recycling process and network should be developed. A good model for this system is the lead-acid battery recycling network which is very efficient at recovering and purifying the metals for re-entry into the battery production process. Through careful process design and implementation, it is hypothesized that similar results could be achieved with liquid metal batteries due the use of mostly elemental, ionic, and bi-alloyed materials.

## 7.3 Conclusion

The design, implementation, and characterization of a liquid metal battery recycling process was achieved in the timeline specified; however, the implementation of the process improvements

outlined in the recommendations section will greatly improve the through-put, process safety, and process service lifetime. The future work section outlines the areas of interest that should be researched in order to scale up the process in the years to come.

The recycling process was determined through a study of current recycling process implemented in lead-acid, and lithium ion battery industries. The research showed a combination of physical separation and hydrometallurgy has been implemented as successful recycling processes in both industries and appears to be well suited for liquid metal battery recycling. Through the direct observation of the current Ambri research and development process, the new implemented recycling process had four process steps implemented which are, as follows: seal breaking and stem removal, cell opening, content removal, and the aqueous wash.

The design of the system was initially founded on the fundamental properties of the materials, and chemistry of the batteries to be recycled. Once the fundamental characteristics were determined materials were selected and designs were drafted for experimentation. The designs for experimentation were used to determine actual forces, usability of the design, and optimize for throughput, safety, and reliability. Through the experimentation and process failure mode and effects analysis, the final designs were determined for implementation.

The implementation of the liquid metal battery recycling process took place during the summer of 2014 in Marlborough, Massachusetts. The implementation consisted of redesigning the experimental setups for higher throughputs, usability by operators, increasing safety, and preventing factor contamination. The implementation consisted of sourcing parts which were capable of handling the alkaline solution developed in the process which could be obtained in the short timeline. The implementation also consisted of building the apparatuses which were to be used in the pilot recycling plant.

Once the implementation was complete, a characterization of the system was carried out; however, due to time and safety constrains a full characterization was not able to be completed. The characterization of the seal showed the forces were a fraction of the theoretical calculation, and the cycle time is adequate for high throughputs. The characterization of the content removal showed the forces required were easily exceeded with the press. The characterization of the aqueous wash system showed the ability of the system to cool the reaction adequately. The testing also showed a highly controlled reaction rate with adequate heat removal capability and flow rate. The

characterization also showed the process is capable of having a throughput of 40 cells per day. The process throughput if operated for one year at capacity corresponds to a cost savings of one million dollars for Ambri when compared to the cost of incineration.

The design, implementation, and characterization were completed on a short timeline which resulted in the inability to implement and characterize all designed features. The suggested design features and experiments not implemented or carried out were presented, described, and laid out for Ambri's Marlborough Team to implement. With the completion and implementation of the essential process safety features, the recycling process will achieve 8 times Ambri's initial desire throughput.

# Sources Cited


[1] Ambri, 2014, "2014 Brochure," http://www.ambri.com/storage/documents/ambri_2014_progress_update.pdf.

[2] Narain, V., 2013, "Global Industrial Batteries Market," http://www.frost.com.libproxy.mit.edu.

[3] ABB Inc., 2010, "Energy Efficiency in the Power Grid," https://www.nema.org/Products/Documents/TDEnergyEff.pdf.

[4] Imre, G., Johnson, M., and Vetrano, J., 2013, "Grid Energy Storage," U.S. Department of Energy.

[5] Pike Research, 2014, " Energy Storage on the Grid," http://www.navigantresearch.com/research/energy-storage-on-the-grid.

[6] David, B., Kim, H., Sirk, A., and Sadoway, D., 2012, "Magnesium–Antimony Liquid Metal Battery for Stationary Energy Storage," Journal of the American Chemical Society 134, no. 4 : 1895–97. doi:10.1021/ja209759s.

[7] Ambri, 2014, "2014 Progress Update," http://www.ambri.com/storage/documents/2014-Brochure-v3.pdf.

[8] Thomas, R., 2010, "Linden's Handbook of Batteries 4th Edition," McGraw Hill Professional.

[9] University of Cambridge, 2014, "DoITPoMS - TLP Library Batteries - Lead/acid Batteries," http://www.doitpoms.ac.uk/tlplib/ batteries/batteries_lead_acid.php.

[10] Denise Crocce Romano, E., Bernardes, A., and Soares Tenório, J., 2004, "An Overview on the Current Processes for the Recycling of Batteries," Journal of Power Sources 135, no. 1–2: 311–19. doi:10.1016/j.jpowsour.2004.03.083.

[11] Ozawa, K., 1994, "Lithium-ion rechargeable batteries with LiCoO2 and carbon electrodes: the LiCoO2/C system," Solid State Ionics, 69(3-4), 212–221. doi:10.1016/0167-2738(94)90411-1.

[12] Jinqiu, X., Thomas, H., Francis, W., Lum, K., Wang, J., and Liang, B., 2008, "A Review of Processes and Technologies for the Recycling of Lithium-Ion Secondary Batteries," Journal of Power Sources 177, no. 2:512–27. doi:10.1016/j.jpowsour.2007.11.074.

[13] Bullock, K.,1994, "Lead/acid Batteries," Journal of Power Sources 51, no. 1–2: 1–17. doi:10.1016/0378-7753(94)01952-5.

[14] U.S. Environmental Protection Agency, 2012,"Common Wastes & Materials: Batteries," http://www.epa.gov/osw/conserve/materials/battery.htm.

[15] Battery Solutions Inc., 2014, "End Sites Recycling Processes," http://www.batteryrecycling.com/battery+recycling+process.

[16] Tarascon, J., M., and Armand, M., 2001, "Issues and Challenges Facing Rechargeable Lithium Batteries," Nature 414, no. 6861: 359–67. doi:10.1038/35104644.

[17] Voelcker, J., "Lithium Batteries Take to the Road - IEEE Spectrum," http://spectrum.ieee.org/transportation/advanced-cars/lithium-batteries-take-to-the-road.

[18] Georgi-Maschler, T., Friedrich, B., Weyhe, R., Heegn, H., and Rutz., M., 2012, "Development of a Recycling Process for Li-Ion Batteries," Journal of Power Sources 207 : 173–82. doi:10.1016/j.jpowsour.2012.01.152.

[19] Office, European Patent, 2012, "Method for Recycling Batteries," http://www.epo.org/learning-events/european-inventor/finalists/2012/tedjar.html.

[20] Michael, L., 2001, "Recycling of Lithium Ion Cells and Batteries." Journal of Power Sources 97–98. Proceedings of the 10th International Meeting on Lithium Batteries : 736–38. doi:10.1016/S0378-7753(01)00600-0.

[21] Armand, M., and Tarascon, J., M., 2008, "Building better batteries," Nature, 451(7179), 652–7. doi:10.1038/451652a.

[22] Peterson, S. , B., Apt, J., and Whitacre, J. , F., 2010, " Lithium-ion battery cell degradation resulting from realistic vehicle and vehicle-to-grid utilization," Journal of Power Sources, 195(8), 2385–2392. doi:10.1016/j.jpowsour.2009.10.010.

[23] Hoyer, C., Kieckhäfer, K., and Spengler, T. , S., 2011, "Glocalized Solutions for Sustainability in Manufacturing," doi:10.1007/978-3-642-19692-8.

[24] Visvanathan, C., 1996, " Hazardous waste disposal. Resources, Conservation and Recycling,"16(1-4), 201–212. doi:10.1016/0921-3449(95)00057-7.

[25] US EPA, OSWER., 2014, "Basic Information: Overviews & Factsheets," http://www.epa.gov/osw/nonhaz/municipal/wte/basic.htm.

[26] Environmental Technology Council, 2000, "High Temperature Incineration," http://www.etc.org/advanced-technologies/high-temperature-incineration.aspx.

[27] EPA, Office of Solid Waste & Emergency Response, 2012, "A Citizen ' s Guide to Incineration," EPA 542-F-12-010.

[28] Juvinall, R. C., and Marshek, K.M., 2012, "Machine Component Design," Fifth Edition, Wiley.

[29] Ramakrishnan, S., and Rogozinski, M., 1997,"Properties of Electric Arc Plasma for Metal Cutting," J.Phys. D: Appl. Phys. 30 636-644.

[30] Deshpande, P. C., Tilwankar, A. K., and Asolekar, S. R., 2012, "A novel approach to estimating potential maximum heavy metal exposure to ship recycling yard workers in Alang, India," The Science of the Total Environment, 438, 304–11. doi:10.1016/j.scitotenv.2012.08.048.

[31] Vyas, A., and Shaw, M. C., 1999, "Mechanics of saw-tooth chip formation in metal cutting," Journal of Manufacturing Science and Engineering, 121(2), 163-172.

[32] Atkins, P., and Jones, L, 2012, "Chemical Principles," Sixth Edition, W.H. Freeman.

[33] Herbert H. Uhlig et al., 2011, "Uhilg's Corrosion Handbook," Third Edition. The Electrochemical Society, Wiley.

[34] Special Metals, 2014, "Nickel 200 Datasheet," http://www.specialmetals.com.

[35] Meade, C., and Jeanloz, ,R., 1988,"Yield Strength of B1 and B2 Phases of NaCl," Journal of Geophysical Research VOL. 93 NO. B4 PAGES 3270-3274.

[36] Chemical Resistance Guide, 1998, Metal Finishing, 96(10), 72. doi:10.1016/S0026-0576(98)80804-0.

[37] Cole-Parmer, 2014, "Chemical Compatibility Database from Cole-Parmer," http://www.coleparmer.com/Chemical-Resistance.

[38] Airgas Inc., 2013, " Hydrogen [Material Safety Data Sheet]," http://www.airgas.com/documents/pdf/001026.pdf.

[39] Mohamed, B.D., 2009, "Failure Mode and Effect Analysis," Handbook of Maintenance Management and Engineering, 75–90. Springer London,, http://dx.doi.org/10.1007/978-1-84882-472-0_4.

[40] Hagelüken, C., 2005, "Recycling of electronic scrap at Umicore's integrated metals smelter and refinery," Proceedings of EMC, 1–16.

[41] Montgomery, D.C., 2009, "Introduction to Statistical Quality Control," Sixth Edition. Wiley.

[42] Shah, R.K., and Sekulic, D.P. , 2003, "Fundamentals of Heat Exchanger Design," Wiley.

[43] Hamilton, J., 1993, "Method to prevent algae growth in pools and spas," Patent Retrieved from http://www.google.com/patents/US5254526.

## Appendix A: Datasheets

1. Dake 25DA
2. Lenox Blade Selection
3. Mark 10 5i
4. Mark 10 Force Measurement Sensor
5. Sotera Pump SP100
6. ARO Pump PD01
7. NeoLogic Solutions Filter
8. Omega DPi32

# FORCE 25DA - Specifications

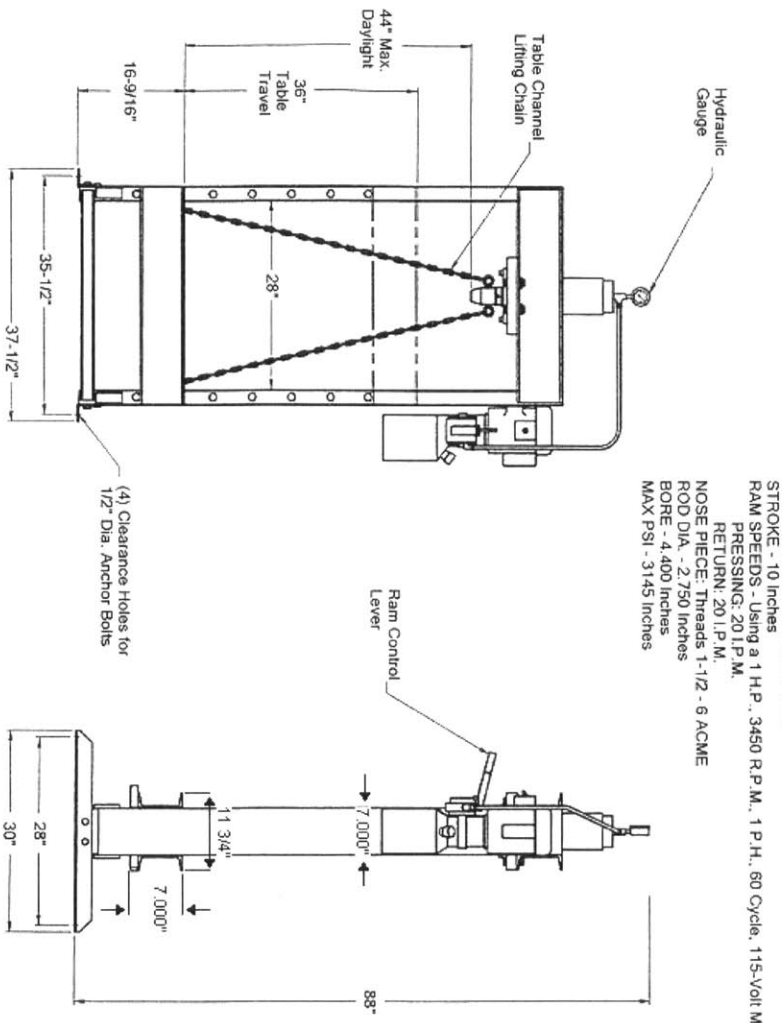


CAPACITY - PRESSING: 25-Tons
STROKE - 10 Inches
RAM SPEEDS - Using a 1 H.P., 3450 R.P.M., 1 P.H., 60 Cycle, 115-Volt Motor
PRESSING: 20 I.P.M.
RETURN: 20 I.P.M.
NOSE PIECE: Threads 1-1/2 - 6 ACME
ROD DIA. - 2.750 Inches
BORE - 4.400 Inches
MAX PSI - 3145 Inches

## INPUTS

| | |
|---|---|
| **MACHINE** | DAITO GA-330 |
| **MATERIAL** | 409 |
| **DIMENSIONS** | RECTANGLETUBE |
| A - (in) | 4 |
| B - (in) | 4 |
| C - (in) | 0.125 |
| **VISING** | SINGLE |
| #Total | 1 |
| # High (rows) | 1 |
| # Wide (Pieces-bottom row) | 1 |
| **CONDITIONS** | LIFE, DRY |

## RECOMMENDATIONS

| | |
|---|---|
| **BLADE** | **RX+ X 13'6" X 1-1/4 X 0.042 X 5/8** |
| BLADE TYPE | RX+ |
| WIDTH | 1-1/4 |
| THICKNESS | 0.0420 |
| TPI | 5/8 |
| LENGTH | 13ft 6in |
| Material Number | 93031RPB134115 |
| **BAND SPEED** | **70** |
| **FEED RATE** | **1.06** |
| AVERAGE CHIP LOAD | 0.00021 |
| CUTTING RATE | 0.46 in²/min |
| **CUT TIME** | **00:04:14** |

## NOTES

Material entered as 45 HRc.

All calculations are based on sawblade potential and results may vary with actual conditions

SAWCALC Version 1.0 Web
© LENOX, Newell Rubbermaid

# Data Sheet

## Digital Force Gauges **M5-1000 / M5-2000**



### Focus on Engineering: Reversible Housing

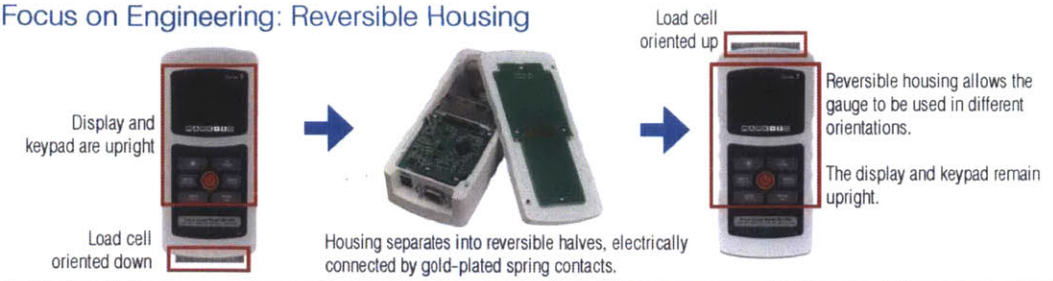


## Specifications

| | |
|---|---|
| Capacity x Resolution: | **M5-1000:** 1000 x 0.5 lbF, 16000 x 5 ozF, 500 x 0.2 kgF, 5000 x 2 N, 5 x 0.002 kN<br>**M5-2000:** 2000 x 1 lbF, 32000 x 20 ozF, 1000 x 0.5 kgF, 10000 x 5 N, 10 x 0.005 kN |
| Accuracy: | ±0.1% of full scale |
| Sampling Rate: | 7,000 Hz |
| Power: | AC or rechargeable battery. Multi-step low battery indicator is displayed, gauge shuts off automatically when power is too low. |
| Battery life: | **Backlight on:** up to 7 hours of continuous use / **Backlight off:** up to 24 hours of continuous use |
| Outputs: | **USB / RS-232:** Configurable up to 115,200 baud. Includes Gauge Control Language 2 for full computer control.<br>**Mitutoyo (Digimatic):** Serial BCD suitable for all Mitutoyo SPC-compatible devices.<br>**Analog:** ±1 VCD, ±0.25% of full scale at capacity,<br>**General purpose:** Three open drain outputs, one input.<br>**Set points:** Three open drain lines. |
| Configurable settings: | Digital filters, outputs, automatic output (via USB/RS-232), automatic shutoff, default settings, averaging mode, external trigger, passwords, key tones, audio alarms, backlight, calibration |
| Safe overload: | 150% of full scale (display shows "OVER" at 110% and above) |
| Weight: | 1.8 lb [0.82 kg] |
| Load cell deflection: | 0.015 [0.38] at full scale |
| Environmental requirements: | 40 - 100°F, max. 96% humidity, non-condensating |
| Included items: | Carrying case with chisel, cone, V-groove, hook (M5-1000 only), flat, extension rod, universal voltage AC adapter, battery, quick-start guide, USB cable, resource CD (USB driver, MESUR™ Lite software, MESUR™gauge DEMO software, and user's guide), and NIST-traceable certificate of calibration with data. |
| Warranty: | 3 years (see individual statement for further details) |

The gauges include a 110V AC adapter.

Specify suffix 'E' for euro plug (220V), 'U' for UK plug (220V), or 'A' for Australian plug (220V).

Ex.
M5-1000E, M5-2000A

## Dimensions in [mm]

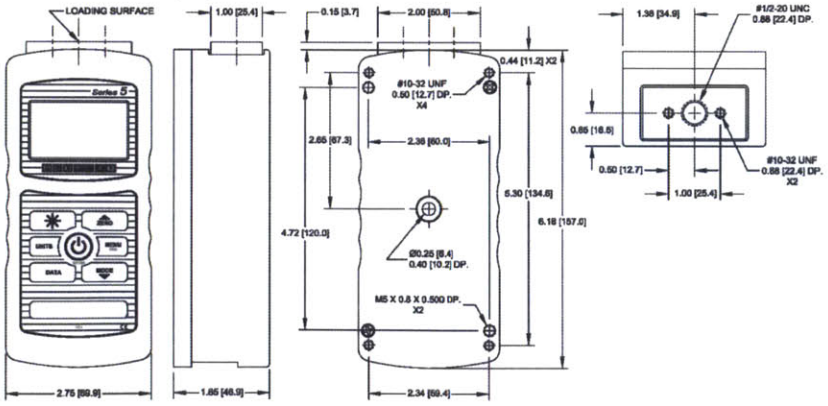


MARK-10

**Mark-10 Corporation** ■ www.mark-10.com ■ info@mark-10.com
Toll-free: 888-MARK-TEN ■ Tel: 631-842-9200 ■ Fax: 631-842-9201

3 YEAR WARRANTY

# Data Sheet Plug and Test™ Force Sensors **Series R01**

32-1130 REV 2


Series R01 rugged smart sensors are designed for measuring tension and compression force, with applications in virtually every industry. Durable S-Beam design with threaded holes on two sides allows for many configurations. The sensor can be integrated into an existing system or mounted to a Mark-10 test stand. A shortened cable is available for mounting to an ESM1500LC test stand*. Capacities available from 50 to 10,000 lbF [250 N to 50 kN]. Compatible with Mark-10 indicators (sold separately) through unique Plug & Test™ technology.

## Specifications

| | |
|---|---|
| Accuracy: | ±0.15% of full scale + indicator |
| Safe Overload: | 150% of full scale |
| Weight: | 1.9 to 3.0 lb [0.9 to 1.4 kg], depending on model |

## Dimensions in [mm]

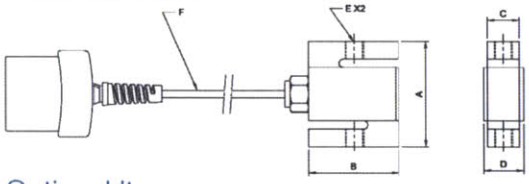


## Optional Items

| | |
|---|---|
| AC1018 | Mounting kit, Series R01/R03 to test stand (not required for ESM1500) |

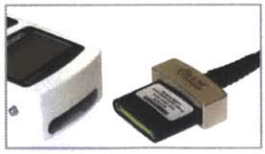

< Unique Plug & Test™ technology allows for interchangeable sensors to be used with any Mark-10 indicator. All calibration and configuration data is saved in the smart connector.

< The Plug & Test™ connector locks into the receptacle in the indicator when fully inserted. Dual buttons on the indicator housing release the connector for easy removal. Gold plated spring contacts ensure long lasting and reliable connection.

^ Optional AC1018 mounting kit adapts a Series R01 sensor to a Mark-10 test stand.

^ Series R01 sensor with shortened cable is shown mounted to an ESM1500LC test stand.*

| Model No. | A | B | C | D | E | F |
|---|---|---|---|---|---|---|
| MR01-50* | 2.40 [61.0] | 2.00 [50.8] | 0.46 [11.7] | 0.65 [16.5] | 1/4-28 UNF | MR01-XXXXX: 20 ft [6 m] MR01-XXXX-1* 7.5 in [191 mm]* |
| MR01-100* | | | | | | |
| MR01-200* | | | | | | |
| MR01-500* | | | 0.71 [18.0] | 0.90 [22.9] | 1/2-20 UNF | |
| MR01-1000* | | | | | | |
| MR01-2000* | | | | | | |
| MR01-5000 | 3.90 [99.1] | 3.00 [76.2] | 0.96 [24.4] | 1.15 [29.2] | 3/4-16 UNF | |
| MR01-10000 | | | | | | |

## Capacity x Resolution

| Model No. | With Models 7i & 5i indicators | | | | | | With Model 3i indicator | | | |
|---|---|---|---|---|---|---|---|---|---|---|
| | lbF | ozF | gF | kgF | N | kN | lbF | kgF | N | kN |
| MR01-50* | 50 x 0.02 | 800 x 0.5 | 25000 x 10 | 25 x 0.01 | 250 x 0.1 | - | 50 x 0.05 | 25 x 0.02 | 250 x 0.2 | - |
| MR01-100* | 100 x 0.05 | 1600 x 1 | 50000 x 20 | 50 x 0.02 | 500 x 0.2 | - | 100 x 0.1 | 50 x 0.05 | 500 x 0.5 | - |
| MR01-200* | 200 x 0.1 | 3200 x 2 | - | 100 x 0.05 | 1000 x 0.5 | 1 x 0.0005 | 200 x 0.2 | 100 x 0.1 | 1000 x 1 | - |
| MR01-500* | 500 x 0.2 | 8000 x 5 | - | 250 x 0.1 | 2500 x 1 | 2.5 x 0.001 | 500 x 0.5 | 250 x 0.2 | 2500 x 2 | - |
| MR01-1000* | 1000 x 0.5 | 16000 x 10 | - | 500 x 0.2 | 5000 x 2 | 5 x 0.002 | 1000 x 1 | 500 x 0.5 | 5000 x 5 | - |
| MR01-2000* | 2000 x 1 | 32000 x 20 | - | 1000 x 0.5 | 10000 x 5 | 10 x 0.005 | 2000 x 2 | 1000 x 1 | 10000 x 10 | - |
| MR01-5000 | 5000 x 2 | - | - | 2500 x 1 | 25000 x 10 | 25 x 0.01 | 5000 x 5 | 2500 x 2 | - | 25 x 0.02 |
| MR01-10000 | 10000 x 5 | - | - | 5000 x 2 | 50000 x 25 | 50 x 0.02 | 10000 x 10 | 5000 x 5 | - | 50 x 0.05 |

* Add suffix "-1" for shortened cable, for use on the ESM1500LC test stand. Ex: MR01-1000-1. "-1" sensors include hardware for mounting to the ESM1500LC's crosshead.

MARK-10 **Mark-10 Corporation** ■ www.mark-10.com ■ info@mark-10.com
Toll-free: 888-MARK-TEN ■ Tel: 631-842-9200 ■ Fax: 631-842-9201

3 YEAR WARRANTY

SOTERA SYSTEMS

# 1/2" Air Operated Diaphragm Pump S & E Data Sheet

Model SP100-05X-XX-XXX-X

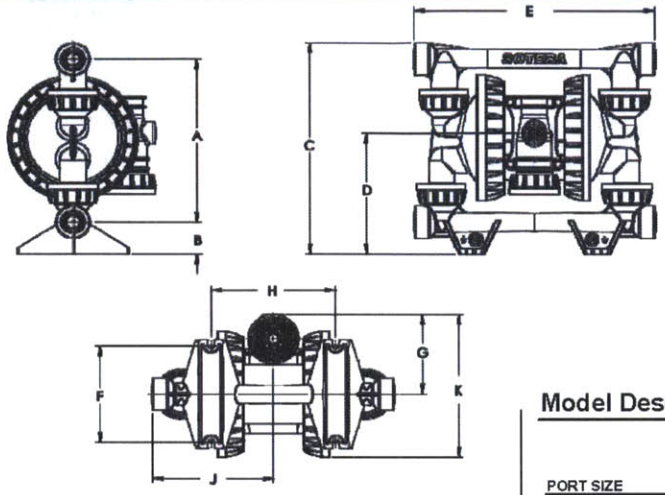


| Dimension | Inches | Metric |
|---|---|---|
| A | 8.245" | 209.42 mm |
| B | 1.625" | 41.28 mm |
| C | 10.70" | 271.78 mm |
| D | 6.123" | 155.524 mm |
| E | 12.000" | 304.80 mm |
| F | 4.875" | 123.825 mm |
| G | 4.031" | 102.387 mm |
| H | 6.250" | 158.75 mm |
| J | 6.000" | 152.40 mm |
| K | 7.206" | 183.032 mm |

## Pump Technical Data

**Pump Type:** Non-Metallic Air Operated Double Diaphragm

**Models:** See Model Description Chart for "-XXX"

**Construction Materials:** See Model Description Charts

**Maximum Air Inlet Pressure:** 100 p.s.i.g. (6.9 bar)

**Maximum Material Inlet Pressure:** 10 p.s.i.g. (.69 bar)

**Maximum Outlet Pressure:** 100 p.s.i.g. (6.9 bar)

**Air Consumption (@ 40p.s.i):** 0.65 c.f.m. / gallon (approx.)

**Maximum Flow Rate (flooded inlet):** 17.5 g.p.m. (66.23 l.p.m.)

**Displacement / Cycle @ 100p.s.i.g.**: 0.036 gal. (0.14 lit.)

**Maximum Particle Size:** 3/32" dia. (2.4 mm)

**Maximum Temperature Limits (diaphragm / ball / seat material):**

Acetal ..... 10° to 180° F (-12° to 82° C)

Hytrel® ..... -20° to 150° F (-29° to 66° C)

PVDF ..... 10° to 200° F (-12° to 93° C)

Polypropylene ..... 35° to 175° F (2° to 79° C)

Santoprene® ..... -40° to 225° F (-40° to 107° C)

PTFE ..... 40° to 225° F (4° to 107° C)

**Dimensional Data (box):** 11-3/4"(H) x 14-1/4" (W) x 9-1/8" (D)

**Noise Level:** 75.0 db (A) (@ 70 p.s.i., 60 c.p.m.)

**Weight Information:**

| Pump Material | Pump Weight lbs | Pump Weight Kg | Shipping Weight lbs | Shipping Weight Kg |
|---|---|---|---|---|
| Polypropylene | 5.7 | 2.6 | 7.2 | 3.3 |
| PVDF | 7.2 | 3.3 | 8.7 | 4.0 |
| Groundable Acetal | 6.8 | 3.1 | 8.3 | 3.8 |

## Model Description Information

**SP100 - 05 X - XX - XXX - X**

**PORT SIZE**

**FLUID CONNECTION**
- N - 1/2-14 NPTF-1
- B - Rp 1/2 (BSPP)

**DRIVE MATERIAL OF CONSTRUCTION**
- P- POLYPROPYLENE
- C - GROUNDABLE NYLON

**WET-END MATERIAL OF CONSTRUCTION**
- P - POLYPROPYLENE
- D - GROUNDABLE ACETAL
- F - PVDF

**DIAPHRAGM**
- S - SANTOPRENE®
- H - HYTREL®
- T - PTFE WITH SANTOPRENE® BACKER

**BALLS**
- S - SANTOPRENE®
- H - HYTREL®
- T - PTFE

**SEATS**
- S - SANTOPRENE®
- H - HYTREL®
- P - PP (w/PTFE seal)
- F-PVDF (w/PTFE seal)

**OPTIONS**

**FLUID SECTION SERVICE KIT** — KIT S05 X X X
- DIAPHRAGM
- BALLS
- SEATS

Tuthill

Tuthill Transfer Systems
Fort Wayne, Indiana
(800) 634-2605
www.tuthill.com

## SP100-05X-XX-XXX

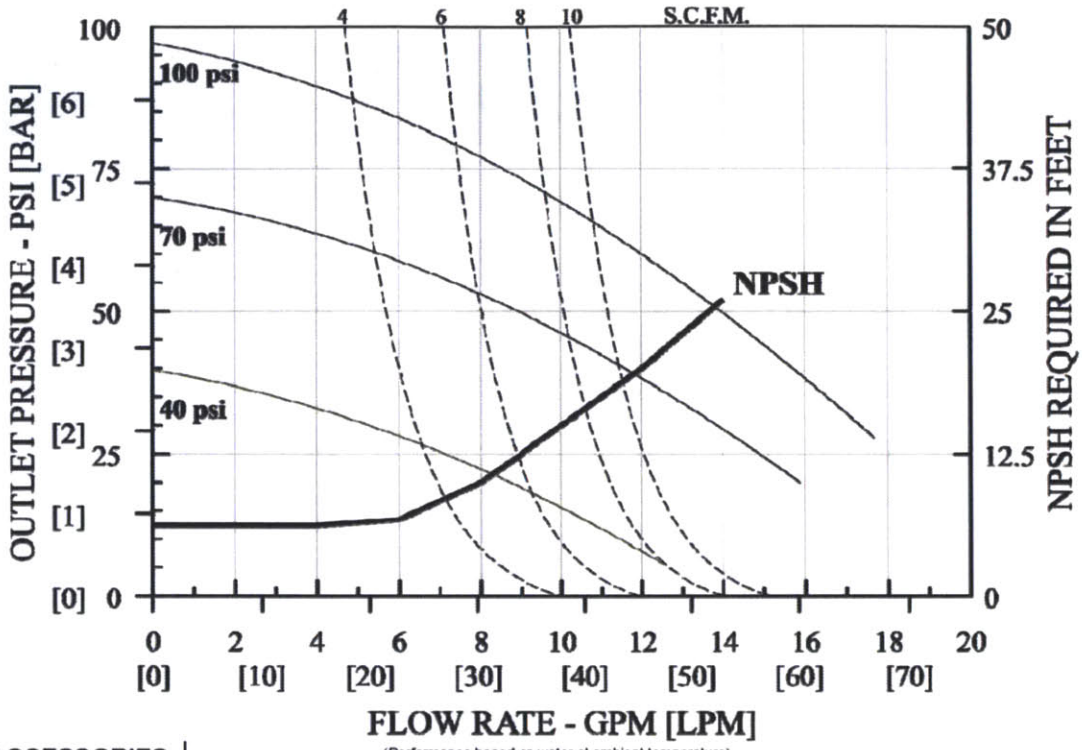


(Performance based on water at ambient temperature)

## ACCESSORIES

The following accessories are available to customize your SP100 AOD Pump.

Contact your Sotera Representative if you have questions, or would like to order any of the accessories listed below.

| Part # | Accessory | Description |
|---|---|---|
| KITS05WMA | Wall Mount Bracket | Stainless steel bracket for wall mount applications of the SP100 AOD Pump. |
| KITS05FRH | Filter / Regulator Kit | Air line filter, regulator, and hose |
| KITS05MUF | Muffler | Muffler for air exhaust |
| KITS05WCH | Assembly Wrench | Special service tool for use on manifold and fluid retainer rings |
| KIT180MAMPS | Tote Plate (for IBC tote) | Tote plate, attaching hardware |

Visit us on the web at:

# www.sotera.com

Learn more about Tuthill Corporation and our family of high quality, value minded products at:

www.tuthill.com

SOTERA SYSTEMS
Sotera Systems
8825 Aviation Drive
Fort Wayne, IN 46809
1-800-834-2695

Tuthill

# SALES & ENGINEERING DATA

| | |
|---|---|
| RATIO SERIES: | 1:1 |
| FLUID PSIG RANGE: | 10 - 125 |

## PX01X-XXX-XXX-AXXX
### 1/4" DIAPHRAGM PUMP

RELEASED: 3-7-13
REVISED: 7-14-14
(REV. C)

## DIMENSIONAL DATA

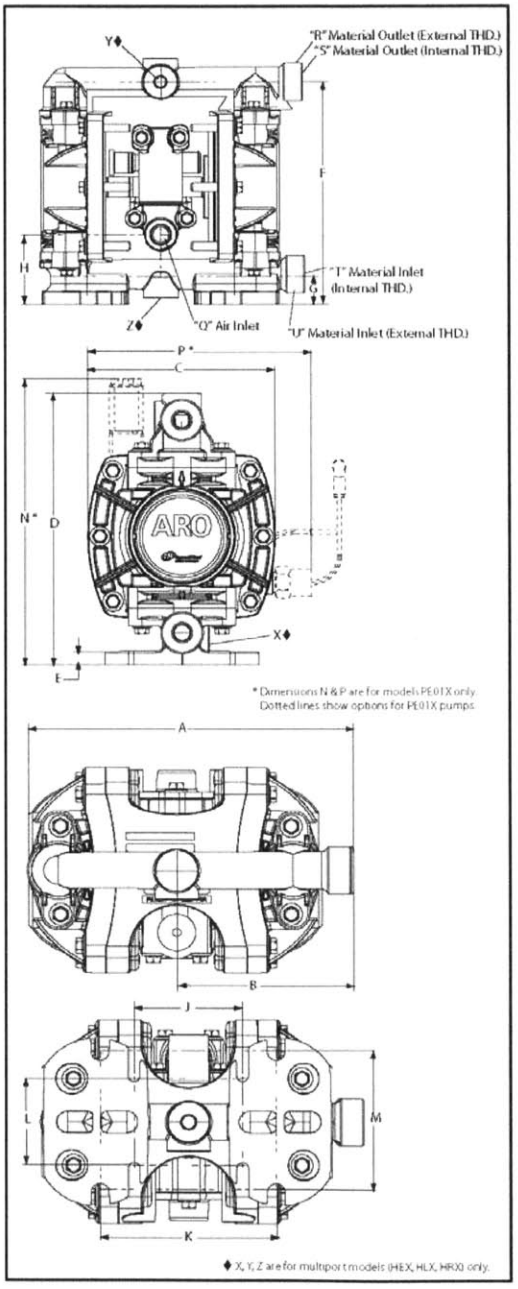


* Dimensions N & P are for models PE01X only. Dotted lines show options for PE01X pumps.

♦ X, Y, Z are for multiport models (HEX, HLX, HRX) only.

## SPECIFICATIONS

**Model Series** PD01X-XXX-XXX-AXXXX, PE01X-XXX-XXX-AXXX
**Pump Type**.. Non-Metallic Air Operated Double Diaphragm
**Ratio**..... 1:1
**Air Inlet**..... Q - 1/4 - 18 PTF SAE Short
**Weight**..... Polypropylene..... 2.86 lbs (1.30 kgs)
PVDF..... 3.88 lbs (1.76 kgs)
Acetal..... 3.52 lbs (1.60 kgs)

## PERFORMANCE

**Maximum Air Inlet Pressure**..... 125 psig (8.6 bar)
**Minimum Air Inlet Pressure**..... 10 psig (0.69 bar)
**Maximum Outlet Pressure**..... 125 psig (8.6 bar)
**Maximum Flow Rate**..... 5.3 gpm (20 lpm)
**Maximum Material Inlet Pressure**.... 10 psig (0.69 bar)
**Displacement / Cycle @ 125 psig**.... 0.019 gal / 0.072 ltrs
**Maximum Particle Size**..... 1/16" dia.(1.6 mm)
**Maximum Temperature Limits (diaphragm / ball / seat material)**
Acetal..... 10° to 180° F (-12° to 82° C)
E.P.R. / EPDM..... -60° to 280° F (-51° to 138° C)
Kynar® PVDF..... 10° to 200° F (-12° to 93° C)
Hytrel®..... -20° to 150° F (-29° to 66° C)
Neoprene..... 0° to 200° F (-18° to 93° C)
Nitrile®..... 10° to 180° F (-12° to 82° C)
Polypropylene..... 35° to 175° F (2° to 79° C)
Viton®..... -40° to 350° F (-40° to 177° C)
Santoprene®..... -40° to 225° F (-40° to 107° C)
PTFE..... 40° to 225° F (4° to 107° C)
**Noise Level** @ 70 psig, 60 cpm..... 62.3 dB(A)①

① The pump sound pressure levels published here have been updated to an Equivalent Continuous Sound Level ($L_{Aeq}$) to meet the intent of ANSI S1.13-2005, CAGI-PNEUROP S5.1.

Mounting Adapter Plate Optional Accessory Kit (24123879) available. Please contact your nearest **ARO / Ingersoll Rand** customer service or distributor for details.

### DIMENSIONS

Dimensions shown are for reference only, they are displayed in inches and millimeters (mm).

| | | | |
|---|---|---|---|
| A - 7.2" (182 mm) | H - 1.9" (48.6 mm) | Q - 1/4 - 18 PTF SAE Short | Z - 1/4 - 18 PTF SAE Short |
| B - 3.9" (100.0 mm) | J - 2.4" (61 mm) | R - 3/4-14 NPTF | |
| C - 4.6" (117.0 mm) | K - 3.9" (99 mm) | S - 1/4 NPTF / BSPT Hybrid* | |
| D - 6.8" (173.0 mm) | L - 2.1" (53 mm) | T - 1/4 NPTF / BSPT Hybrid* | |
| E - 0.3" (8.8 mm) | M - 3.2" (81 mm) | U - 3/4-14 NPTF | |
| F - 6.1" (156 mm) | N - 7.2" (184 mm) | X - 1/4-18 NPTF / BSPT Hybrid | |
| G - 0.8" (20.7 mm) | P - 5.6" (142.2 mm) | Y - 1/4 NPTF / BSPT Hybrid | |

* Multiport Options Discharge Manifold has (2) and Inlet Manifold has (3).


INGERSOLL RAND COMPANY LTD
209 NORTH MAIN STREET – BRYAN, OHIO 43506
✆ (800) 495-0276 • FAX (800) 892-6276
ingersollrandproducts.com




CCN 80448087

ARO Ingersoll Rand.

## PERFORMANCE CURVES

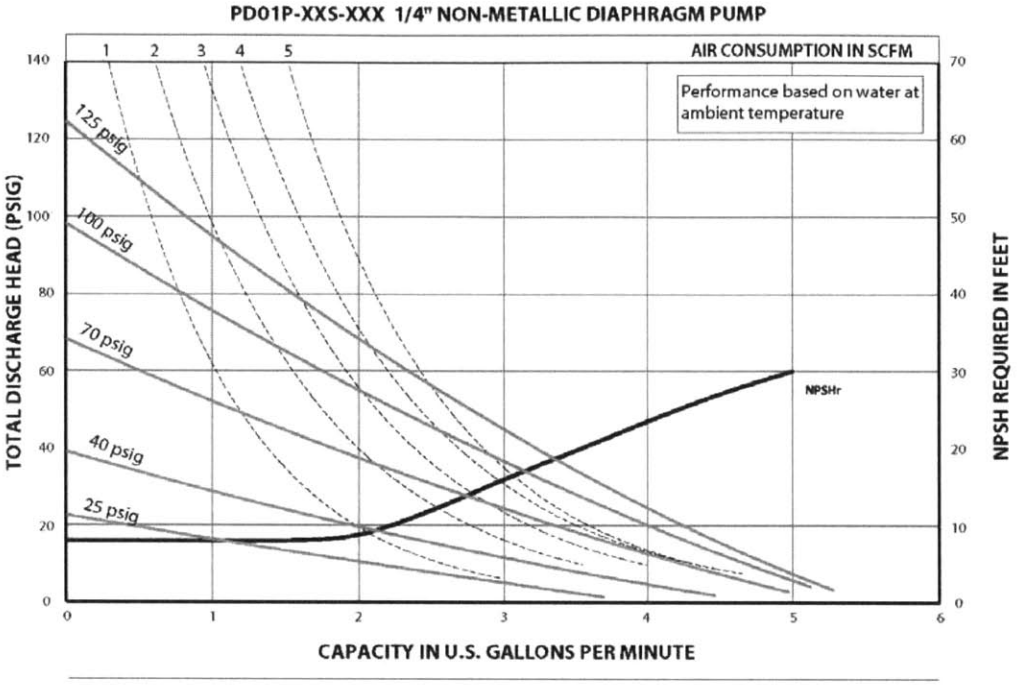


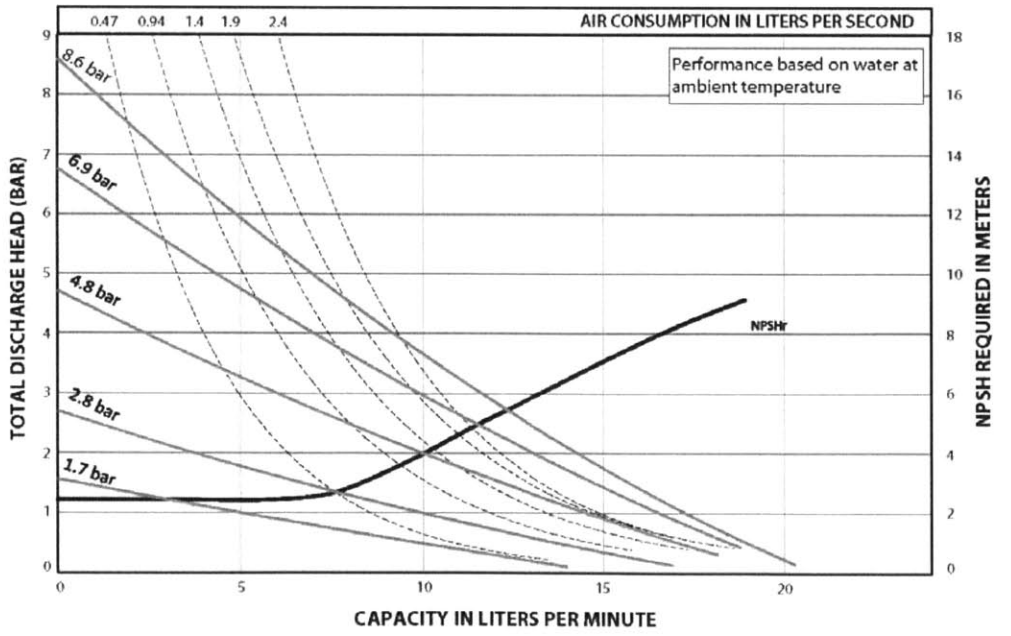

## PERFORMANCE CURVES

### PE01X-XXX-XXX SOLENOID-CONTROLLED TIME-BASED FLOW RATE

OPERATING CONDITION: 70 PSI AIR PRESSURE, 30 PSI FLUID BACKPRESSURE

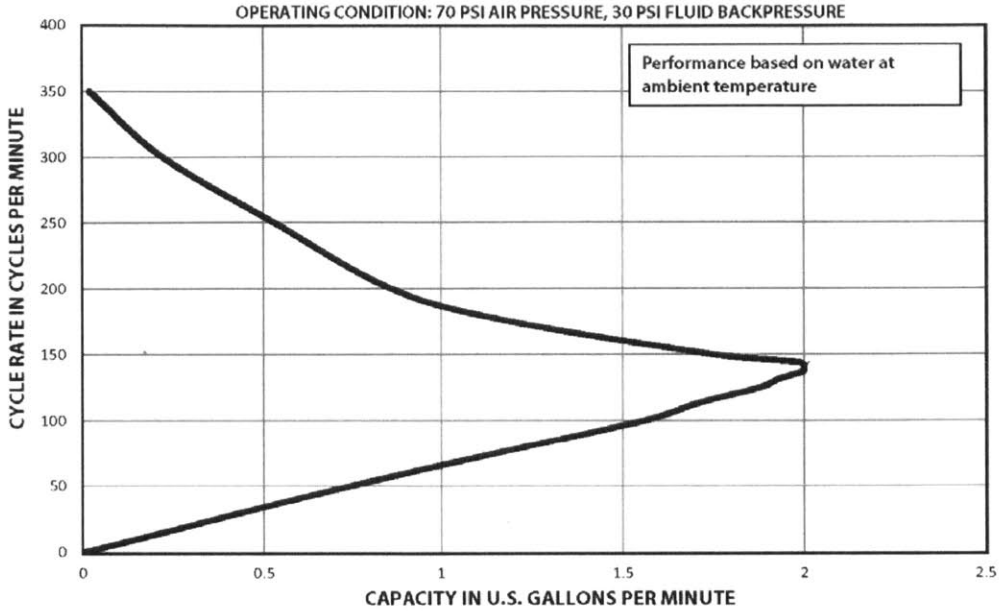


OPERATING CONDITION: 4.8 BAR AIR PRESSURE, 2.1 BAR FLUID BACKPRESSURE

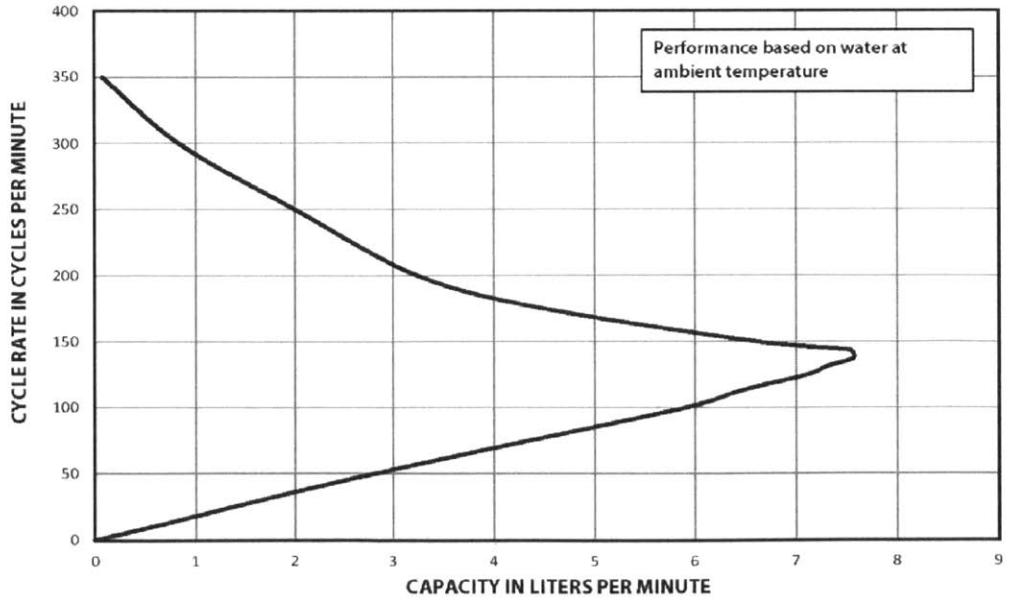

# SFN Series

## Single Filter Housings
## Bolt and Nut Closure

neo-PURE™

*Residential / Commercial / Industrial Filtration Applications*

## Applications

- Water
- Food and Beverage
- Electronics
- Coolants
- Oil / Gas
- Paints / Inks / Coatings
- Paper and Pulp
- Chemicals
- Desalination Prefiltration
- Cooling Tower Filtration

USA MADE

## Standard Features

- Manufactured in USA
- Designed for commercial or industrial filter applications
- Heavy-duty 304L or 316L stainless steel construction for maximum durability and corrosion resistance
- Bolt and nut closure allow for quick cartridge change-outs (T-handle optional) and inline connections for easy installation
- Uses double open-end (DOE) cartridges
- Available with 1/4", 3/8", 1/2", 3/4", and 1" connections
- Both ends of cartridge have knife-edge seals to help eliminate potential bypass

## Specifications, Operating Parameters and Options

**Maximum Operating Pressure**
250 psig (17 bar) @ 275°F (135°C)

**Connections**
Inlet/Outlet: 1/2", 3/4", or 1" FNPT
Optional: 1" RF flange, BSP or 1" sanitary ferrules
Drain Ports: 1/8" FNPT

**Materials of Construction**
Head: 304L, 316L or Brass Nickel-Plated
Shell/Connections: 304L or 316L stainless steel
Drain: Stainless steel plug

**Gaskets**
Standard: Buna N (FDA grade)
Optional: EPR, silicone, Teflon, Viton, neoprene, vellumoid

**Finish**
Polycoat on exterior surfaces

**Options**
1/4" gauge ports In/Out
Tee handle
Variable seal (spring loaded)
Vent screw outlet

| MODEL | QUANTITY (LENGTH) OF CARTRIDGES | RATED FLOW CAPACITY* GPM (LPM) | MAXIMUM DIAMETER CARTRIDGE | DRAIN SIZE | STANDARD | | SPRING LOADED | |
|---|---|---|---|---|---|---|---|---|
| | | | | | A | B | A | B |
| SFN-x | 1 (4-7/8") | 3.5 (13.2) | 2-3/4" | 1/8" | 8-7/8" (22.5) | 6-15/16" (17.6) | 9-1/2" (24.1) | 7-9/16" (19.2) |
| SFN-1 | 1 (9-3/4") | 7 (26.5) | 2-3/4" | 1/8" | 13-3/4" (34.9) | 11-13/16" (33.0) | 14-3/8" (36.5) | 12-7/16" (31.6) |
| SFN-2 | 1 (20") | 14 (53.0) | 2-3/4" | 1/8" | 23-7/8" (60.6) | 21-15/16" (55.7) | 24-1/2" (62.2) | 22-9/16" (57.3) |
| SFN-3 | 1 (30") | 21 (79.5) | 2-3/4" | 1/8" | 33-7/8" (86.0) | 31-15/16" (81.1) | 34-1/2" (87.6) | 32-9/16" (82.7) |

* Based upon 7 gpm per 10" length with a 25 micron wound cartridge at 2 PSID clean and viscosity of 1 cps. Flow rates are approximate. Actual flow rates are based upon fluid, viscosity, cartridge type, micron ratings and other factors.

## Dimensions

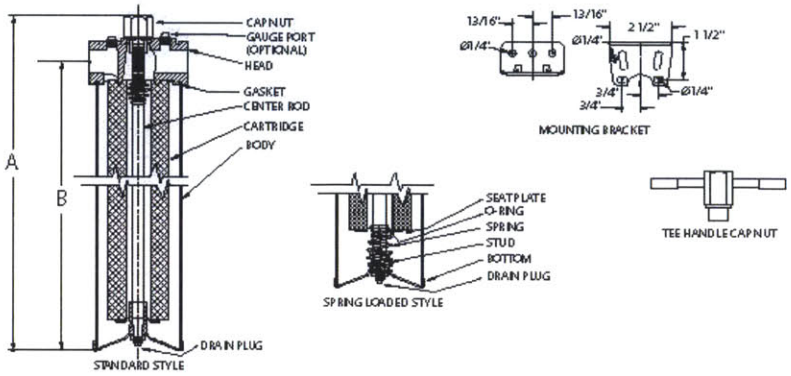


## Ordering Guide (Example: SFN-1B-316L4-FL-T-S)

| SFN | – | 1B | – | 316L | 4 | – | FL | – | T | – | S |
|---|---|---|---|---|---|---|---|---|---|---|---|

| MODEL | CARTRIDGE LENGTH | MATERIAL | INLET/ OUTLET SIZE | CONNECTION TYPE | OPTIONS | GASKET |
|---|---|---|---|---|---|---|
| SFN = 304L Stainless Steel Head Nut Double Open End | 1 = 9-3/4" | Blank = 304L (standard) | 4 = 1/2" | Blank = FNPT (standard) | Blank = None (standard) | Blank = Buna N (standard) |
| SFBH = Brass Nickel-Plated Head Nut Double Open End | 1B = 10" (9-7/8" MB and SV) | 316L = 316L | 6 = 3/4" | FL = Flange 1" only | GP = 1/4" gauge ports IN/OUT | E = EPR |
| | 2 = 20" | | S = 1" | BP = BSP | T = Tee handle | S = Silicone |
| | 2B = 19-1/2" | | | TC = Ferrules 1" only | DSG = Variable seal (spring loaded) | T = Teflon |
| | 3 = 30" | | | | V = Vent screw outlet | N = Neoprene |
| | 3B = 29-1/4" | | | | | Vell = Vellumoid |
| | x = 4-7/8" available | | | | | |

## Cartridge Options

Available in 9-3/4", 20" and 30" Lengths


**Meltblown Sediment Cartridges**

For more information, see **MB Series Brochure**



**String Wound Cartridges**

For more information, see **WPP Series Brochure**

**Pleated Filter Cartridges**

NeoLogic SOLUTIONS Filtration Division
9450 SW Gemini Dr, ECM #83358, Beaverton, OR 97008
Tel 855-896-3525 | Fax 855-409-9622
www.neologicsolutions.com
email: info@neologicsolutions.com
STUART, FL | BEAVERTON, OR | GREENVILLE, SC | SAN DIEGO, CA

Questions?
Ask one of our Service Representatives:
Mon-Fri 8a-8p, Sat 8:30a-4:30p EST

*We ship 6 days a week!* FedEx

# Temperature, Process and Strain Meters

MONOGRAM

i.Series


DPi32, shown smaller than actual size.

DPi16, shown smaller than actual size.

DPi8, shown smaller than actual size.

## DPi Series

5 YEAR WARRANTY

- Universal Inputs
- User-Friendly, Simple to Configure
- High Quality
- Powerful Features
- Extended 5-Year Warranty
- Free Software
- Totally Programmable Color Displays
- High Accuracy: 0.5°C (±0.9°F), 0.03% Reading
- Both RS232 and RS485 MODBUS®, Selectable from Menu Available
- Built-In Excitation
- Embedded Internet Connectivity Optional
- RS232 and RS485 Serial Communications Optional
- Temperature Stability ±0.04°C/°C RTD and ±0.05°C/°C Thermocouple @ 25°C (77°F)
- AC or DC Powered Units
- Ratiometric Mode for Strain Gages
- Programmable Digital Filter

The OMEGA® iSeries is a family of microprocessor-based instruments offered in three true DIN sizes with NEMA 4 (IP65) rated front bezels. All of the instruments share the same set-up and configuration menu and method of operation, a tremendous time saver for integration of a large system. The iSeries family includes extremely accurate digital panel meters "DPi" and single loop PID controllers "CNi" that are simple to configure and use, while providing tremendous versatility and a wealth of powerful features.

The DPi Series covers a broad selection of transducer and transmitter inputs with 2 input models.

The Universal temperature and process instrument (DPi models) handles 10 common types of thermocouples, multiple RTDs and several process (DC) voltage and current ranges. This model also features built-in excitation, 24 Vdc @ 25 mA. With its wide choice of signal inputs, this model is an excellent choice for measuring or controlling temperature with a thermocouple, RTD, or 4 to 20 mA transmitter.

The strain and process instruments (DPiS models) measure inputs from load cells, pressure transducers, and most any strain gage sensor as well as process voltage and current ranges. The DPiS has built-in 5 or 10 Vdc excitation for bridge transducers, 5 Vdc @ 40 mA or 10 Vdc @ 60 mA (any excitation voltage between 5 and 24 Vdc is available by special order). This DPiS model supports 4- and 6-wire bridge communications, ratiometric measurements. The DPiS features fast and easy "in process" calibration/scaling of the signal inputs to any engineering units. This model also features 10-point linearization which allows the user to linearize the signal input from extremely nonlinear transducers of all kinds.

### Programmable Color Display

The DPi Series are ⅛, ¼ and ½ DIN digital panel meter featuring the big iSeries color-changing display. The digits are twice the size of typical ⅛ DIN panel meters. The iSeries meters feature the only LED displays that can be programmed to change color between **GREEN**, **AMBER**, and **RED**.

Embedded internet and serial communications featuring optional "embedded Internet" (specify "-EIT" option) the iSeries are the first instruments of their kind that connect directly to an Ethernet network and transmit data in standard TCP/IP packets, or even serve Web pages over a LAN or the Internet. The iSeries are also available with serial communications. With the "-C24" option, the user can select from the pushbutton menu between RS232, RS422, and RS485, with straightforward ASCII commands or MODBUS.


**Dimensions: mm (inch)**

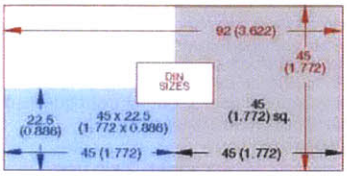


## Options

| Ordering Suffix | Description |
|---|---|
| **Network Options** | |
| -EIT | Ethernet with embedded internet |
| -C24 | Isolated RS232 and RS485, 300 to 19.2 KB |
| -C4EIT | Ethernet with embedded Web server + isolated RS485/422 hub for up to 31 devices |
| -DC | 12 to 36 Vdc*, 24 Vac (standard power input: 90 to 240 Vac/dc, 50 to 400 Hz) |
| **Factory Setup** | |
| -FS | Factory setup and configuration |
| -FS(RTD-1N) | Customized DPiS model for MIL-T-7990B nickel RTD input, 0 to 200°C (32 to 392°F) |
| -FS(RTD-2N) | Customized DPiS for MIL-T-7990B nickel RTD input, -40 to 300°C (-40 to 572°F) |
| **Software (Requires Network Option)** | |
| OPC-SERVER LICENSE | OPC server/driver software license |

***Note: "-DC", "-C24" and "-C4EIT" not available with excitation. Models "-EIT" and "-C4EIT" are only offered on DPi8 and DPiS8 models. * 20 to 36 Vdc for DPi8A, DPi16A, -C4EIT or -EIT.***

***Ordering Examples: DPi8A, 1/8 DIN meter with isolated scalable analog retransmission of process value. DPi8C, 1/8 DIN temp/process meter in compact case, DPi32, 1/32 DIN temp/process monitor.***

## *iSeries Controllers Also Available!*

*CNi Series Models with Control and Alarm Outputs, Visit omega.com*


**CNi16D, shown actual size. Visit omega.com/cni16_series**

| Input Type | | Range | Accuracy |
|---|---|---|---|
| **Universal Strain/Process Input Models** | | | |
| Process Voltage | | 0 to 100 mV, 0 to 1V, ±100 mV, 0 to 10V | 0.03% rdg |
| Process Current | | 0 to 20 mA (4 to 20 mA) | 0.03% rdg |
| **Universal Temperature/Process Input Models** | | | |
| J | Iron-Constantan | -210 to 760°C (-346 to 1400°F) | 0.4°C (0.7°F) |
| K | CHROMEGA®-ALOMEGA® | -270 to -160°C (-454 to -256°F)<br>-160 to 1372°C (-256 to 2502°F) | 1.0°C (1.8°F)<br>0.4°C (0.7°F) |
| T | Copper-Constantan | -270 to -190°C (-454 to -310°F)<br>-190 to 400°C (-310 to 752°F) | 1.0°C (1.8°F)<br>0.4°C (0.7°F) |
| E | CHROMEGA®-Constantan | -270 to -220°C (-454 to -364°F)<br>-220 to 1000°C (-364 to 1832°F) | 1.0°C (1.8°F)<br>0.4°C (0.7°F) |
| R | Pt - Pt/13%Rh | -50 to 40°C (-58 to 104°F)<br>40 to 1768°C (104 to 3214°F) | 1.0°C (1.8°F)<br>0.5°C (0.9°F) |
| S | Pt - Pt/10%Rh | -50 to 100°C (-58 to 212°F)<br>100 to 1768°C (212 to 3214°F) | 1.0°C (1.8°F)<br>0.5°C (0.9°F) |
| B | Pt/30%Rh - Pt6%Rh | 100 to 640°C (212 to 1184°F)<br>640 to 1820°C (1184 to 3308°F) | 1.0°C (1.8°F)<br>0.5°C (0.9°F) |
| C | W/5%Re - W/26%Re | 0 to 2320°C (32 to 4208°F) | 0.4°C (0.7°F) |
| N | OMEGALLOY® Nicrosil-Nisil | -250 to -100°C (-418 to -148°F)<br>-100 to 1300°C (-148 to 2372°F) | 1.0°C (1.8°F)<br>0.4°C (0.7°F) |
| L | J DIN | -200 to 900°C (-328 to 1652°F) | 0.4°C (0.7°F) |
| RTD | Pt, 0.00385, 100, 500, 1000 Ω | -200 to 900°C (-328 to 1652°F) | 0.4°C (0.7°F) |
| RTD | Pt, 0.00392, 100, 500, 1000 Ω | -200 to 850°C (-328 to 1562°F) | 0.4°C (0.7°F) |
| RTD-1N | (Nickel MIL-T-7990B) (FS required) | 0 to 200°C (32 to 392°F) | 0.1°C (0.2°F) |
| RTD-2N | (Nickel MIL-T-7990B) (FS required) | -40 to 300°C (-40 to 572°F) | 0.3°C (0.5°F) |
| Process Voltage | | 0 to 100 mV, 0 to 1V, 0 to 10V | 0.03% rdg |
| Process Current | | 0 to 20 mA (4 to 20 mA) | 0.03% rdg |

## To Order *Visit omega.com/dpi_series for Pricing and Details*

| Model No. | Size/Cutout | Input Type | Other Features |
|---|---|---|---|
| DPi8 | 1/8 DIN | Temperature/process | — |
| DPi8A | 1/8 DIN | Temperature/process | Analog output |
| DPiS8 | 1/8 DIN | Strain/process | — |
| DPi16 | 1/16 DIN | Temperature/process | — |
| DPi16A | 1/16 DIN | Temperature/process | Analog output |
| DPiS16 | 1/16 DIN | Strain/process | — |
| DPi32 | 1/32 DIN | Temperature/process | — |
| DPiS32 | 1/32 DIN | Strain/process | — |
| DPi8C | 1/8 DIN | Temperature/process | Compact depth |
| DPiS8C | 1/8 DIN | Strain/process | Compact depth |

*Comes complete with operator's manual.*

## Accessory

| Model No. | Description |
|---|---|
| DPP-5 | 1/8 DIN panel punch |

M

# i.Series Common Specifications (All i/8, i/16, i/32 DIN)

## Universal Temperature and Process Input (DPi/CNi Models)

**Accuracy:** ±0.5°C temp; 0.03% rdg
**Resolution:** 1°/0.1°; 10 µV process
**Temperature Stability:**
**RTD:** 0.04°C/°C
**TC @ 25°C (77°F):** 0.05°C/°C
**Cold Junction Compensation**
**Process:** 50 ppm/°C
**NMRR:** 60 dB
**CMRR:** 120 dB
**A/D Conversion:** Dual slope
**Reading Rate:** 3 samples/s
**Digital Filter:** Programmable
**Display:** 4-digit 9-segment LED 10.2 mm (0.40"); i32, i16, i16D, i8DV 21 mm (0.83"); i8 10.2 mm (0.40") and 21 mm (0.83"); i8DH **RED**, **GREEN**, and **AMBER** programmable colors for process variable, setpoint and temperature units
**Input Types:** Thermocouple, RTD, analog voltage, analog current
**Thermocouple Lead Resistance:** 100 Ω max
**Thermocouple Types (ITS 90):** J, K, T, E, R, S, B, C, N, L (J DIN)
**RTD Input (ITS 68):** 100/500/1000 Ω Pt sensor, 2-, 3- or 4-wire; 0.00385 or 0.00392 curve
**Voltage Input:** 0 to 100 mV, 0 to 1V, 0 to 10 Vdc
**Input Impedance:** 10 MΩ for 100 mV 1 MΩ for 1 or 10 Vdc
**Current Input:** 0 to 20 mA (5 Ω load)
**Configuration:** Single-ended
**Polarity:** Unipolar
**Step Response:** 0.7 sec for 99.9%
**Decimal Selection:**
**Temperature:** None, 0.1
**Process:** None, 0.1, 0.01 or 0.001
**Setpoint Adjustment:** -1999 to 9999 counts
**Span Adjustment:** 0.001 to 9999 counts
**Offset Adjustment:** -1999 to 9999
**Excitation (Not Included with Communication):** 24 Vdc @ 25 mA (not available for low-power option)

## Universal Strain and Process Input (DPiS/CNiS Models)

**Accuracy:** 0.03% reading
**Resolution:** 10/1µV
**Temperature Stability:** 50 ppm/°C
**NMRR:** 60 dB
**CMRR:** 120 dB
**A/D Conversion:** Dual slope
**Reading Rate:** 3 samples/s
**Digital Filter:** Programmable
**Input Types:** Analog voltage and current
**Voltage Input:** 0 to 100 mVdc, -100 mVdc to 1 Vdc, 0 to 10 Vdc
**Input Impedance:** 10 MΩ for 100 mV; 1 MΩ for 1V or 10 Vdc
**Current Input:** 0 to 20 mA (5 Ω load)
**Linearization Points:** Up to 10
**Configuration:** Single-ended
**Polarity:** Unipolar
**Step Response:** 0.7 sec for 99.9%
**Decimal Selection:** None, 0.1, 0.01 or 0.001
**Setpoint Adjustment:** -1999 to 9999 counts
**Span Adjustment:** 0.001 to 9999 counts
**Offset Adjustment:** -1999 to 9999
**Excitation (Optional In Place Of Communication):** 5 Vdc @ 40 mA; 10 Vdc @ 60 mA

## Control

**Action:** Reverse (heat) or direct (cool)
**Modes:** Time and amplitude proportional control; selectable manual or auto PID, proportional, proportional with integral, proportional with derivative and anti-reset Windup, and on/off
**Rate:** 0 to 399.9 s
**Reset:** 0 to 3999 s
**Cycle Time:** 1 to 199 s; set to 0 for on/off
**Gain:** 0.5 to 100% of span; setpoints 1 or 2
**Damping:** 0000 to 0008
**Soak:** 00.00 to 99.59 (HH:MM), or OFF
**Ramp to Setpoint:** 00.00 to 99.59 (HH:MM), or OFF
**Auto Tune:** Operator initiated from front panel

## Control Output 1 and 2

**Relay:** 250 Vac or 30 Vdc @ 3 A (resistive load); configurable for on/off, PID and ramp and soak
**Output 1:** SPDT, can be configured as alarm 1 output
**Output 2:** SPDT, can be configured as alarm 2 output
**SSR:** 20 to 265 Vac @ 0.05 to 0.5 A (resistive load); continuous
**DC Pulse:** Non-isolated; 10 Vdc @ 20 mA
**Analog Output (Output 1 Only):** Non-isolated, proportional 0 to 10 Vdc or 0 to 20 mA; 500 Ω max

## Output 3 Retransmission

**Isolated Analog Voltage and Current**
**Current:** 10 V max @ 20 mA output
**Voltage:** 20 mA max for 0 to 10 V output

## Network and Communications

**Ethernet:** Standards compliance IEEE 802.3 10 Base-T
**Supported Protocols:** TCP/IP, ARP, HTTPGET
**RS232/RS422/RS485:** Selectable from menu; both ASCII and MODBUS protocol selectable from menu; programmable 300 to 19.2 Kb; complete programmable setup capability; program to transmit current display, alarm status, min/max, actual measured input value and status
**RS485:** Addressable from 0 to 199
**Connection:** Screw terminals

## Alarm 1 and 2 (Programmable)

**Type:** Same as output 1 and 2
**Operation:** High/low, above/below, band, latch/unlatch, normally open/normally closed and process/deviation; front panel configurations
**Analog Output (Programmable):** Non-isolated, retransmission 0 to 10 Vdc or 0 to 20 mA, 500 Ω max (output 1 only); accuracy is ± 1% of FS when following conditions are satisfied: input is not scaled below 1% of input FS, analog output is not scaled below 3% of output FS

## General

**Power:** 90 to 240 Vac ±10%, 50 to 400 Hz*, 110 to 375 Vdc, equivalent voltage
**Low Voltage Power Option:** 24 Vac**, 12 to 36 Vdc for DPi/CNi/DPiS/CNiS; 20 to 36 Vdc for dual display, ethernet and isolated analog output from qualified safety approved source

## Isolation

**Power to Input/Output:** 2300 Vac per 1 minute test
**For Low Voltage Power Option:** 1500 Vac per 1 minute test
**Power to Relay/SSR Output:** 2300 Vac per 1 minute test
**Relay/SSR to Relay/SSR Output:** 2300 Vac per 1 minute test
**RS232/485 to Input/Output:** 500 Vac per 1 minute test
**Environmental Conditions:**
**All Models:** 0 to 55°C (32 to 131°F) 90% RH non-condensing
**Dual Display Models:** 0 to 50°C (32 to 122°F), 90% RH non-condensing (for UL only)
**Protection:**
**DPi/CNi/DPiS/CNiS32, i16, i16D, i8C:** NEMA 4X/Type 4 (IP65) front bezel
**DPi/CNi8, CNi8DH, i8DV:** NEMA 1/Type 1 front bezel
**Approvals:** UL, C-UL, CE per EN61010- 1:2001, FM (temperature units only)
**Dimensions**
**i/8 Series:** 48 H x 96 W x 127 mm D (1.89 x 3.78 x 5")
**i/16 Series:** 48 H x 48 W x 127 mm D (1.89 x 1.89 x 5")
**i/32 Series:** 25.4 H x 48 W x 127 mm D (1.0 x 1.89 x 5")
**Panel Cutout**
**i/8 Series:** 45 H x 92 mm W (1.772 x 3.622"), ⅛ DIN
**i/16 Series:** 45 mm (1.772") square, ¹⁄₁₆ DIN
**i/32 Series:** 22.5 H x 45 mm W (0.886 x 1.772"), ¹⁄₃₂ DIN
**Weight**
**i/8 Series:** 295 g (0.65 lb)
**i/16 Series:** 159 g (0.35 lb)
**i/32 Series:** 127 g (0.28 lb)

** No CE compliance above 60 Hz.*
*** Units can be powered safely with 24 Vac power, but no certification for CE/UL are claimed.*

## Appendix B: Quotes

1. Baileigh BS-260SA
2. Boyd Coating Research PTFE
3. Precision Coating PFA Green
4. Instron Manual Wedge Grips and Pneumatic Wedge Grips

1625 Dufek Drive
PO Box 531
Manitowoc, WI 54221-0531
Phone: (920) 684-4990
Fax: (920) 684-3944
Email: sales@baileighindustrial.com
Website: www.baileighindustrial.com

# Quote

021035



**BILL TO:**

DT3
DALE THOMAS
143 ALBANY ST APT 210
CAMBRIDGE, MA 02139

**SHIP TO:**

DT3
DALE THOMAS
143 ALBANY ST APT 210
CAMBRIDGE, MA 02139

## Notes

Customer MUST have Fork Lift & Loading Dock to get off truck
Customer must be delivering to Commercial/Business Address
-PLEASE notify us if we need to change & get new freight rate

| Sales Rep | Payment Terms | FOB Point | Shipping Terms | Carrier | Date |
|---|---|---|---|---|---|
| EBRESKE | PREPAYMENT | Origin | Prepaid & Billed | FEDEX FRT PRIO | 07/30/2014 |
| | | | | | (VALID FOR 30 DAYS) |

| QTY | Unit Price | Part Number | Description | B.C.D | Ext. Price |
|---|---|---|---|---|---|
| 1 | $7,395.00 | BS-260SA | 220 Volt Single Phase Dual Mitering Semi-Automatic Metal Cutting Band Saw. 1" Blade Width. *IN STOCK* | | $7,395.00 |

Authorization _____ Date: _____
By signing this document or providing payment, signee accepts all Baileigh Industrial Inc. terms and conditions, see attached or http://metal.baileighindustrial.com/terms-ofsale/

| | |
|---|---|
| Subtotal | $7,395.00 |
| Shipping & Handling | $406.00 |
| Misc. | $0.00 |
| T/D | <$0.00> |
| Sales Tax | $0.00 |
| **TOTAL** | $7,801.00 |

Boyd Coatings Research Co.,Inc
51 Parmenter Road
Hudson, MA 01749-3213
USA

Ph: 978-562-7561
Fax: 978-562-9622

# Quote

Number: 1114282 Date: 07-May-14

To

MIT-cam
70 Vassar Street
Bldg. 37, Room 276
Cambridge, MA 02139-4309
USA

Ph: 617-252-1736

Quote To

Dale Thomas
Massachusetts Institute of Technology
Laboratory for Manufacturing and Productivity
70 Vassar St Room 35-233
Cambridge, MA 02139
USA

| Terms | Ship Via | Salesperson |
|---|---|---|
| Per Credit Terms Established | | |

| Quantity | Description | Unit Price | Amount |
|---|---|---|---|
| | Reference: MIT<br>PLEASE REFERENCE OUR QUOTATION NUMBER ON ALL CORRESPONDENCE& ORDERS.<br>Please see the attached Terms & Conditions which are part of this Quotation. | | |
| 1 | Line: 001 Expiration Date: 06-Jul-14<br>Part: Rev:<br>TANK<br>12.5" x 15.5" Deep<br>$839.43 each piece<br>Each | $839.43 | |
| 1 | Line: 002 Expiration Date: 06-Jul-14<br>Part: Rev:<br>NRE CHARGE<br>ONLY APPLIES TO FIRST RUN<br>Each | $100.00 | |
| | SUMMARY OF CHARGES:<br>- $100.00 NRE Charge quoted above applies on first run only and is in addition to any minimum charges.<br><br>BCR PROCESS:<br>- Incoming inspection<br>- Rigging / Special Handling<br>- Surface preparation / masking<br>- Apply coating<br>- Testing<br>- Final Inspection<br><br>LEAD TIME:<br>- The actual lead-time will be determined at the time of your order.<br>- Standard process lead-time is ten (10) business days.<br>- An additional three (3) business days are required for first time orders due to our engineering review process.<br><br>BCR NOTES / EXCEPTIONS:<br>- Due to high temperature process, stainless parts may show discoloration.<br>- Quotation based on our standard application process & testing.<br>- The OD should be in tolerance based on process selected, but no verification measurements are quoted. | | |

PRECISION COATING
A Katahdin Company.

Date: 5/5/2014
Page: 1 of 3

| QUOTED TO: |
|---|
| Laboratory for Manufacturing and Productivity at MIT<br>77 Massachusetts Ave<br>35-231<br>Cambridge, MA 02139<br><br>Attention: Martin Feldman<br>Email: feldmann@mit.edu<br>Phone: |

| QUOTE DETAILS | | Quote Number: 014202 |
|---|---|---|
| Part Name: | **5 Gallon Pressure Pot** | Part #: **5 Gallon Pressure Pot** |
| Coating: | PFA Green | |
| Processing Instructions: | Mask exterior. Coat inside bucket and lid, approximate thickness .0010" to .0030" per surface. No after coating dimensions to be met. | |
| Pricing: | 1 pieces: $850.000 each<br>**Setup Charge: $300.00 per shipment under $3000** | |
| Other: | Pricing is valid for all quantities. | |
| Delivery: | 2 - 3 weeks | |
| Terms: | Visa/Mastercard/AMEX or COD on 1st order; Net 30 upon credit approval | |
| Expiration: | This quote expires on **8/3/2014** | |

If you need any further information, please contact me directly.

All the best,

Jim Kaemmerlen
Precision Coating Co., Inc.

63 Sprague Street | Hyde Park, MA 02136 | p: (781) 329-1420 | f: (781) 329-3618 | www.precisioncoating.com

Instron
825 University Avenue - Norwood, MA 02062-2643
Tel: 781-828-2500 Fax: 781-575-5725 www.instron.com

# QUOTATION

**Quote To:**
Dale Thomas
Massachusetts Institute of Technology
Mechanical Engineering Dept
77 Mass Avenue, Room E25-406
Cambridge, MA 02139
Tel: (207)659-4206
Fax:

cc:

Date: 06/03/2014
Quote# **INSQ98913**

**Reply To:**
Dave Johnson

Instron
825 University Avenue
Norwood, MA 02062-2643
Tel: 781-575-5320
Fax: 781-575-5725
Email: **david_johnson@instron.com**

**We are pleased to submit the following quotation for your consideration.**

| Qty. | Part Number | Price |
|---|---|---|

**Manual Wedge Action**

1 **2716-002**
Wedge Action Grips, Capacity: 100 kN (20,000 lb, 10,000 kg).
Maximum specimen size is face determined.
Temperature Range: -73 °C to 250 °C (-100 °F to 480 °F)
Upper and lower fittings: Type Dm (1.25 in connection with 1/2 in clevis pin).
Requires 25 mm wide (1 in.) faces.
Removable handles.

1 **2703-004**
Faces, Vee Serrated. Specimen diameter range: 7 to 12.7 mm (9/32 - 1/2 in.) 16 teeth per inch. Straight serrations.

| | |
|---|---|
| SubTotal | **$11,765** |
| Less University Discount | **-$1,764** |
| Total | **$10,000** |

**Pneumatic Wedge Action**

1 **2716-111**
Pneumatic Wedge Action Grips. Capacity: 100 kN (20,000 lb, 10,000 kg).
Upper and lower fittings: Type Dm (1.25 in connection with 1/2 in clevis pin).
Maximum specimen thickness: 40 mm (flat).
Maximum specimen width: 75 mm (flat).
Maximum specimen diameter: 50 mm (round).
Clamping length: 70 mm.
Temperature range: ambient only.
Requires faces.
Includes an air distribution kit with both, 1/4 NPTM (7/16-20), and 1/4 inch hose barb end

| Qty. | Part Number | Price |
|---|---|---|

connections.
An Automatic Air Control Kit or Footswitch is recommended.

1 **2703-182**
Faces, Vee Serrated. Specimen thickness range: 6-17.8 mm.
For 2716-110, 111, 120, 121 Pneumatic Wedge Action Grips. Set of four.

| | |
|---|---|
| SubTotal | **$21,631** |
| Less University Discount | **-$3,244** |
| 1 Total: | **$18,387** |

DELIVERY
4 to 6 weeks from receipt of order, subject to prior orders.

TERMS
Net 30 days from Invoice Date, subject to credit approval.

DELIVERY: Ex-Works
SHIP VIA: Most economical way
FREIGHT: Prepaid and Add

*** PRICES FIRM FOR 60 DAYS ***

WARRANTY: All Instron testing instruments are warranted against defects in material and workmanship for a period of one (1) year from the date of delivery or fifteen (15) months from the date of shipment, whichever comes first. All equipment purchased from Instron but not installed by Instron Service Personnel or Instron authorized representative shall be warranted against defects in material and workmanship for a period of one (1) year from the date of delivery.

All Purchase Orders may be mailed to:
Instron, a division of ITW, Inc.
825 University Avenue
Norwood, MA 02062-2643

Or e-mailed to: info@instron.com

Or faxed to: (781) 575-5725, ATTN: Order Admin.

We accept Visa, MasterCard, and American Express
Prices above are for U.S. destination. Warranty and service commitments only apply to instrumentation installed in the U.S.